Detectors

- Interaction of Charged Particles and Radiation with Matter
  - Ionization loss of charged particles
  - Coulomb scattering
  - Radiation loss by electrons
  - Radiation loss by muons
  - Absorption of γ -rays in Matter
- Detectors of Single Charged Particles
  - Proportional counters, Spark and streamer chambers, Drift chambers, Scintillation counters, Cerenkov counters, Solid-state counters,
  - Bubble chambers
- Shower Detectors and Calorimeters
  - Electromagnetic-shower detectors
  - Hadron-shower detectors

- References: Donald H. Perkins, Introduction to High Energy Physics, Fourth Edition

Interaction of Charged Particles and Radiation with Matter

- Ionization loss of charged particles
  - charged particles, passing through matter, lose energy primarily through scattering on the electrons in the medium
- Coulomb scattering
  - in scattering off the Coulomb field of the nucleus, the charged particle loses less energy, but suffers a large transverse deflection
- Radiation loss by electrons
  - in addition to losing energy through ionization (above), electrons lose significant energy through radiation

Ionization Loss of Charged Particles

- Charged particles, passing through matter, lose energy primarily through scattering on the electrons in the medium
- This process results in the Bethe-Bloch formula

$$\frac{dE}{dx} = \frac{4\pi N_0 z^2 \alpha^2}{m v^2} \frac{Z}{A} \left\{ \ln\left[\frac{2 m v^2}{I(1-\beta^2)} \right] - \beta^2 \right\}$$

incident particle: ze, p, v, M
target Ze, A, m, I, x in g/cm^2

- $I \approx 10$ eV Z (see next page)
- dE/dx
  - is independent of the mass M of the particle
  - varies as $1/v^2$ at non-relativistic velocities
  - increase logrithmically beyond minimum at $E \approx 3Mc^2$
  - depends weakly on the medium since $Z/A \approx 0.5$ for most media
  - $\approx 1 - 1.5$ MeV cm^2 /g or 0.1 - 0.15 MeV m^2 /kg

Ionization Energy

Excitation energies (divided by *Z*). Those based on measurement are shown by points with error flags; the interpolated values are simply joined. The open point is for liquid H_2; the black point at 19.2 eV is for H_2 gas. Also shown are curves based on two approximate formulae. (from PDG)

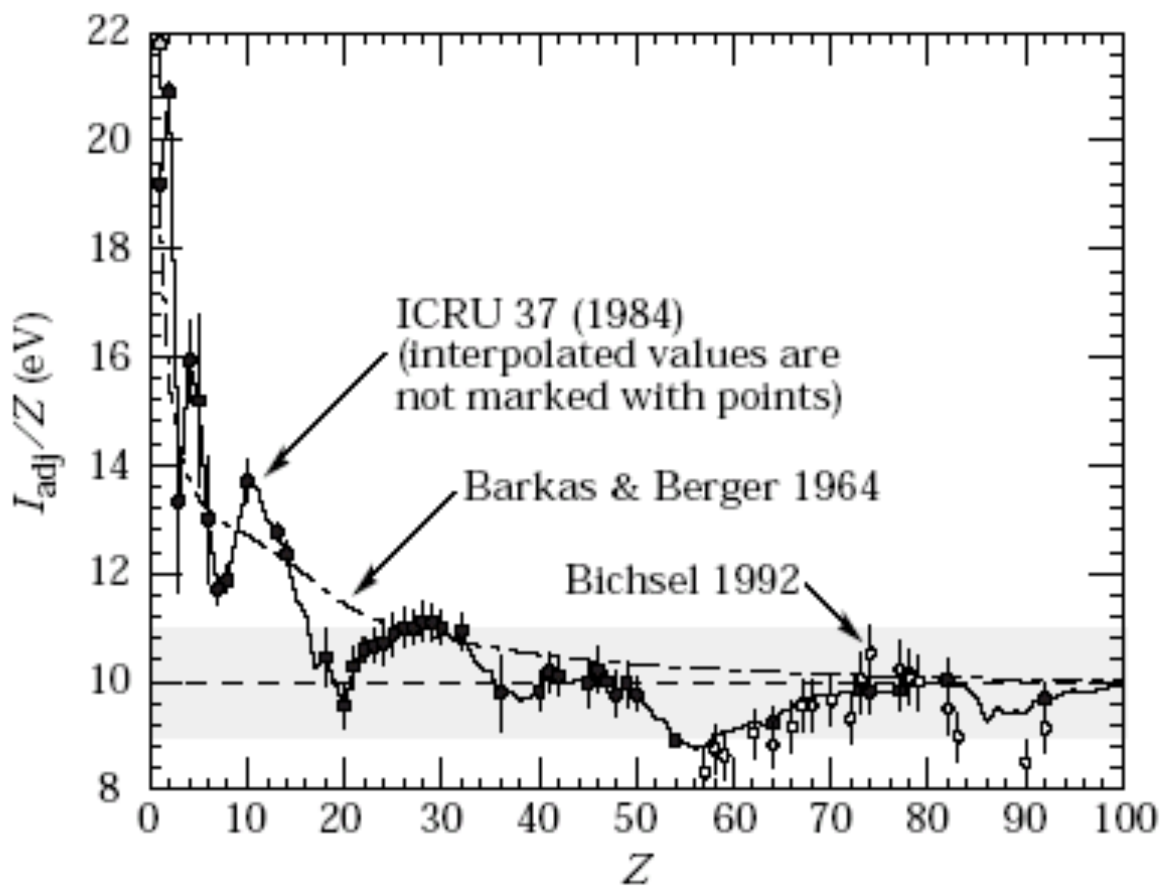

PDG

Ionization Loss of Charged Particles

- The Bethe-Bloch formula

$$\frac{dE}{dx} = \frac{4\pi N_0 z^2 \alpha^2}{mv^2} \frac{Z}{A} \left\{ \ln\left[\frac{2mv^2}{I(1-\beta^2)}\right] - \beta^2 \right\}$$

emerges from Rutherford scattering (moving electron, stationary target atom)

$$\frac{d\sigma}{dq^2} = \frac{4\pi\alpha^2 z^2}{v^2 q^4}$$

- For a massive nucleus, these is no energy transfer
- In the rest frame of the electron, the electron acquires a recoil energy T, where $q^2 = 2mT$

$$\frac{d\sigma}{dT} = \frac{2\pi\alpha^2 z^2}{mv^2} \frac{1}{T^2}$$

Ionization Loss of Charged Particles

- Now, consider the number of such scatters in the energy range $T \rightarrow T + dT$, in traversing dx, for a medium of atomic number Z

$$dN = \frac{2\pi N_0 \alpha^2 z^2}{mv^2} \frac{Z}{A} \frac{dT}{T^2} dx$$

- So ionization energy loss is

$$\frac{dE}{dx} = \int T \frac{dN}{dx} = \frac{2\pi N_0 \alpha^2 z^2}{mv^2} \frac{Z}{A} \ln \frac{T_{\max}}{T_{\min}}$$

  – the maximum energy loss is

$$T_{\max} = \frac{2mv^2 E^2}{M^2 + m^2 + 2mE} \approx \frac{2mv^2}{1 - \beta^2} \quad \text{at low energy}$$

  – and the minimum is I, the mean ionization potential

Ionization Loss of Charged Particles

$$\frac{dE}{dx} = \int T \frac{dN}{dx} = \frac{2\pi N_0 \alpha^2 z^2}{m v^2} \frac{Z}{A} \ln \frac{T_{max}}{T_{min}}$$

- Insert T_{max} and T_{min}, and add a factor of 2 which accounts for effects such as atomic excitation, and Bethe-Bloch equation is found (after proper relativistic treatment)

$$\frac{dE}{dx} = \frac{4\pi N_0 z^2 \alpha^2}{m v^2} \frac{Z}{A} \left\{ \ln \left[\frac{2 m v^2}{I(1-\beta^2)} \right] - \beta^2 \right\}$$

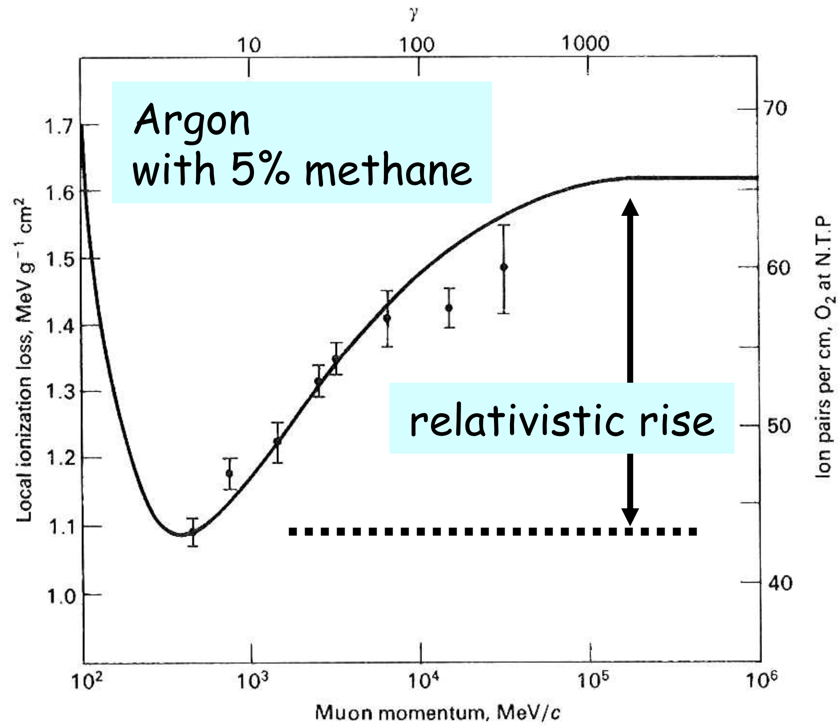

Ionization Loss of Charged Particles

- Relativistic rise
  - transverse electric field rises with γ, resulting from more distant collisions
  - polarization effects cut off rise
  - polarization effects are stronger in solids than gas
    - gas: rise ~ 1.5
    - solid: rise ~ 1.1

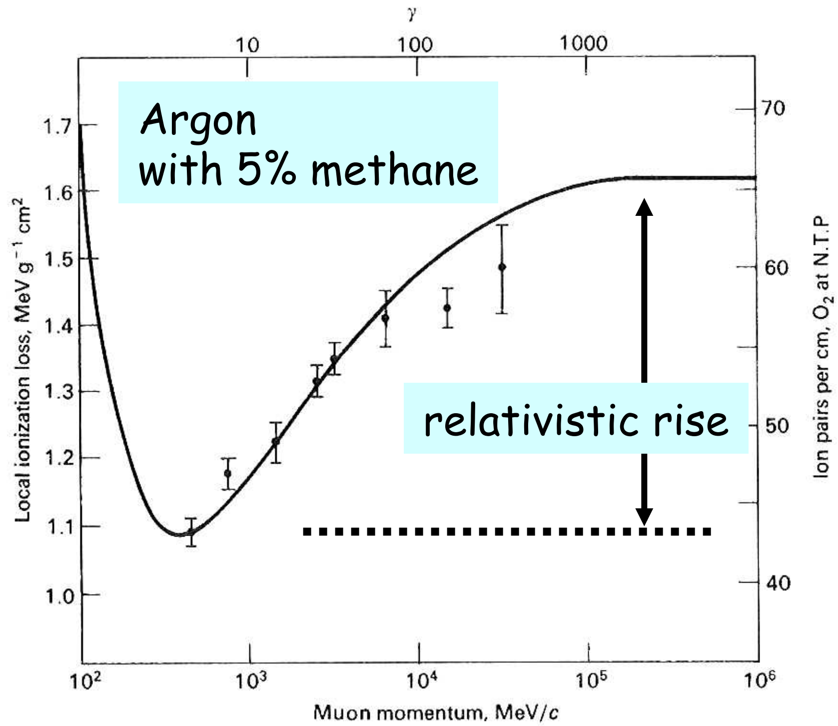

Ionization Loss of Charged Particles

- Ion pairs
  - Landau distribution
    - large fluctuations in energy loss
    - higher energy electrons (δ rays)
  - Number of pairs depends on energy required to produce pair in medium
    - helium: 40 eV
    - argon: 26 eV
    - semi-cond: 3 eV

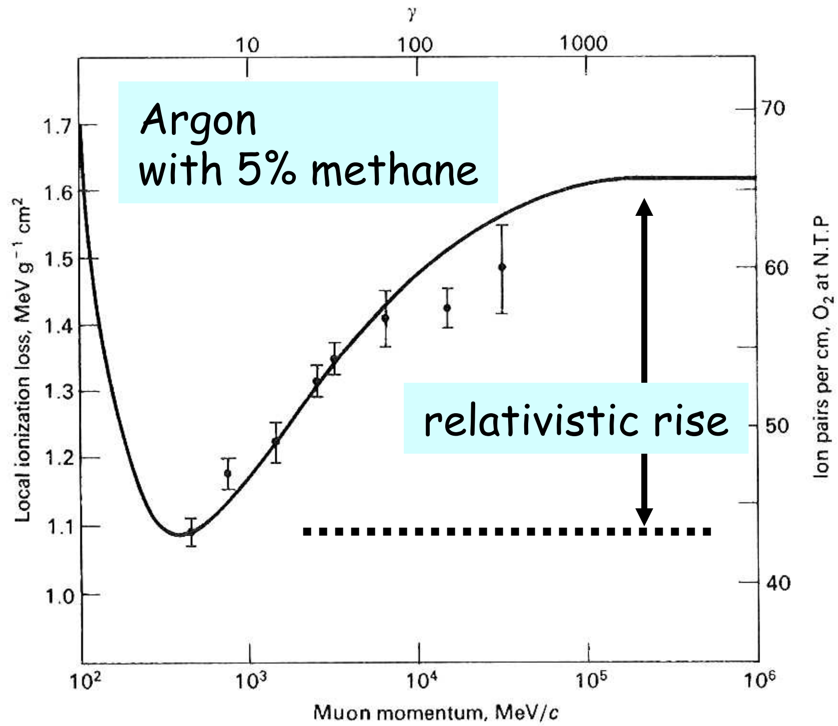

Ionization Loss of Charged Particles

- Measured ionization energy loss of electrons, muons, pions, kaons, protons and deuterons in the PEP4/9-TPC

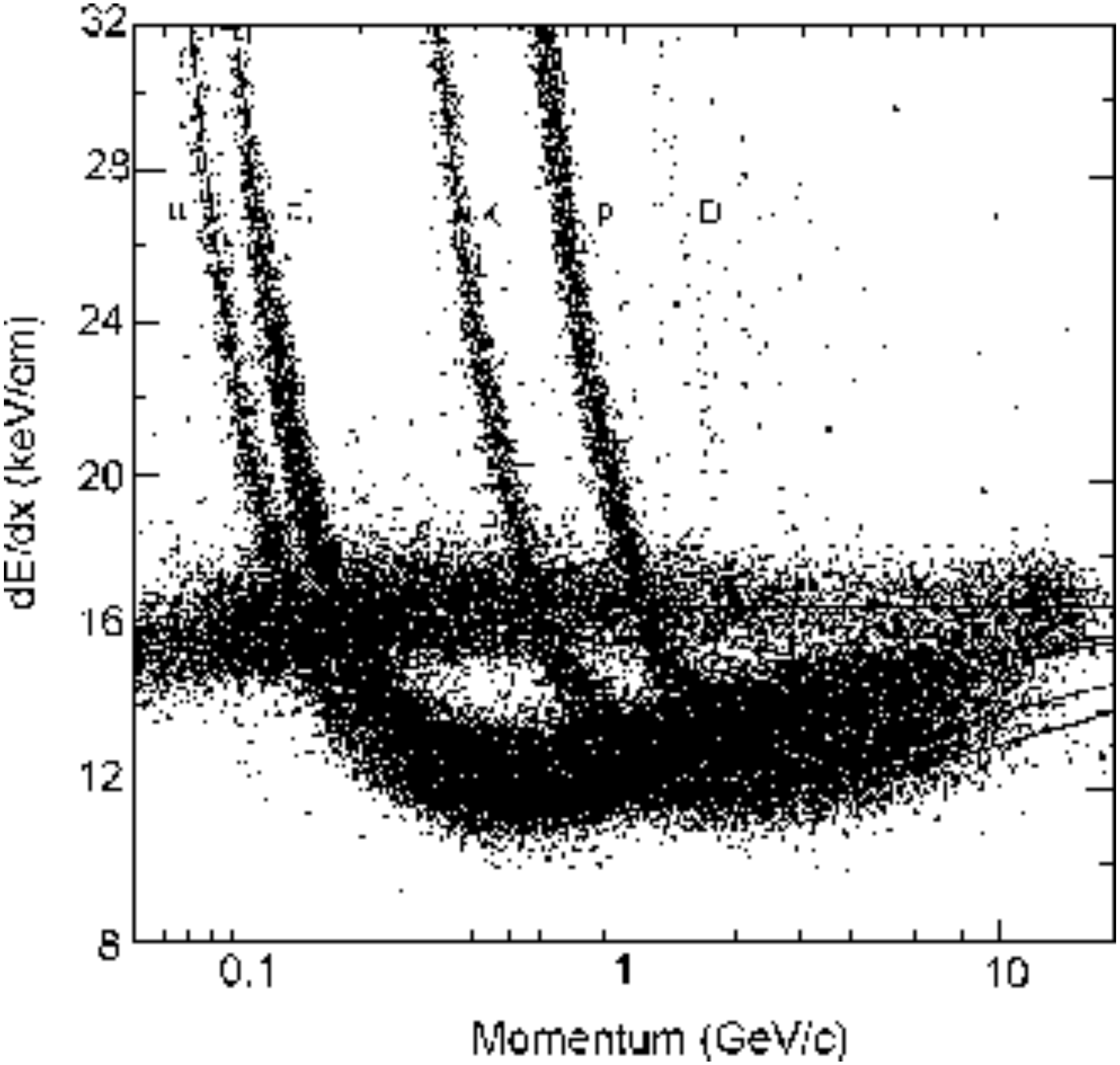

Landau Distribution

- The Bethe-Bloch formula describes the average energy loss of charged particles. The fluctuation of the energy loss around the mean is described by an asymmetric distribution, the Landau distribution. An approximation is

$$\Omega(\lambda) = \frac{1}{\sqrt{2\pi}} \exp\left\{-\frac{1}{2}(\lambda + e^{-\lambda})\right\}$$

- The high energy tail can complicate mass determination.

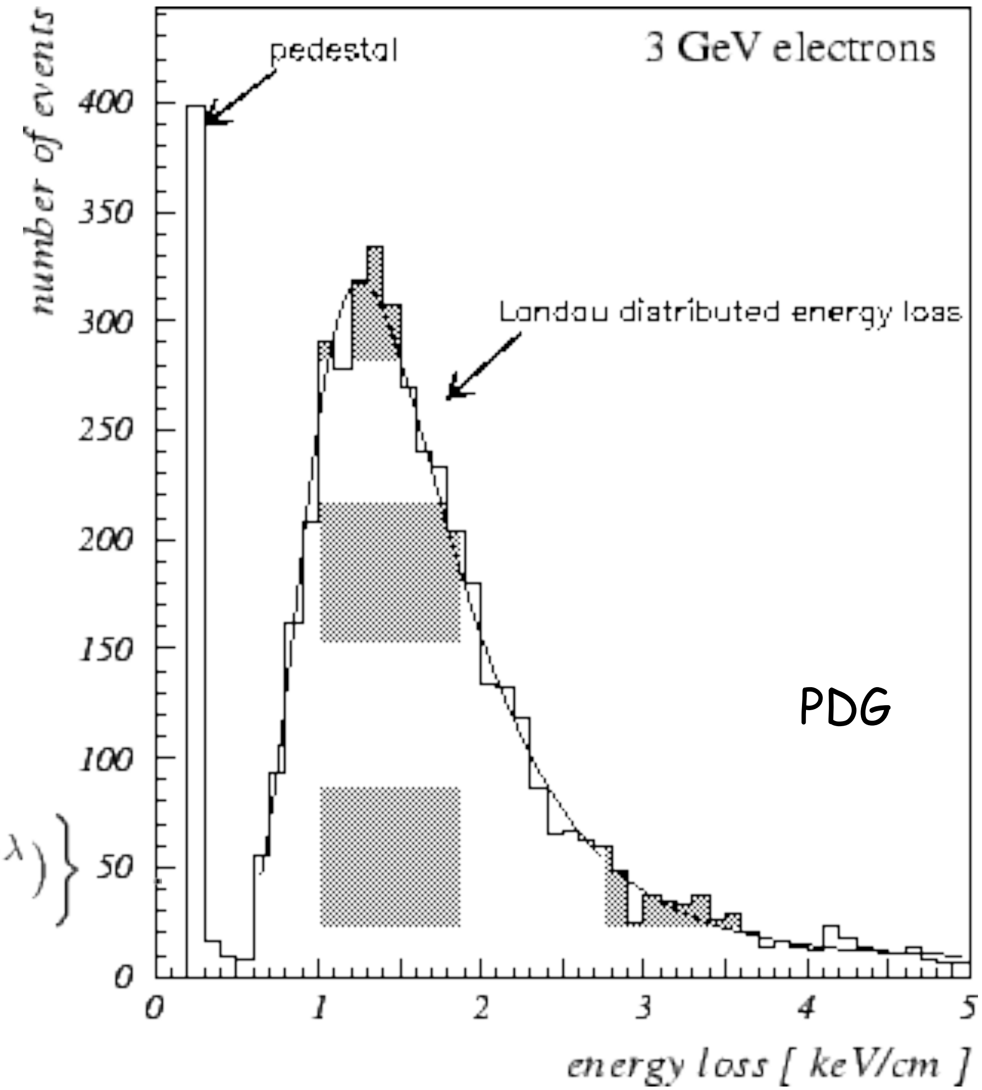

Bethe-Bloch Equation with Density Corrections

$$-\frac{dE}{dx} = Kz^2\frac{Z}{A}\frac{1}{\beta^2}\left[\frac{1}{2}\ln\frac{2m_ec^2\beta^2\gamma^2T_{\text{max}}}{I^2} - \beta^2 - \frac{\delta}{2}\right]$$

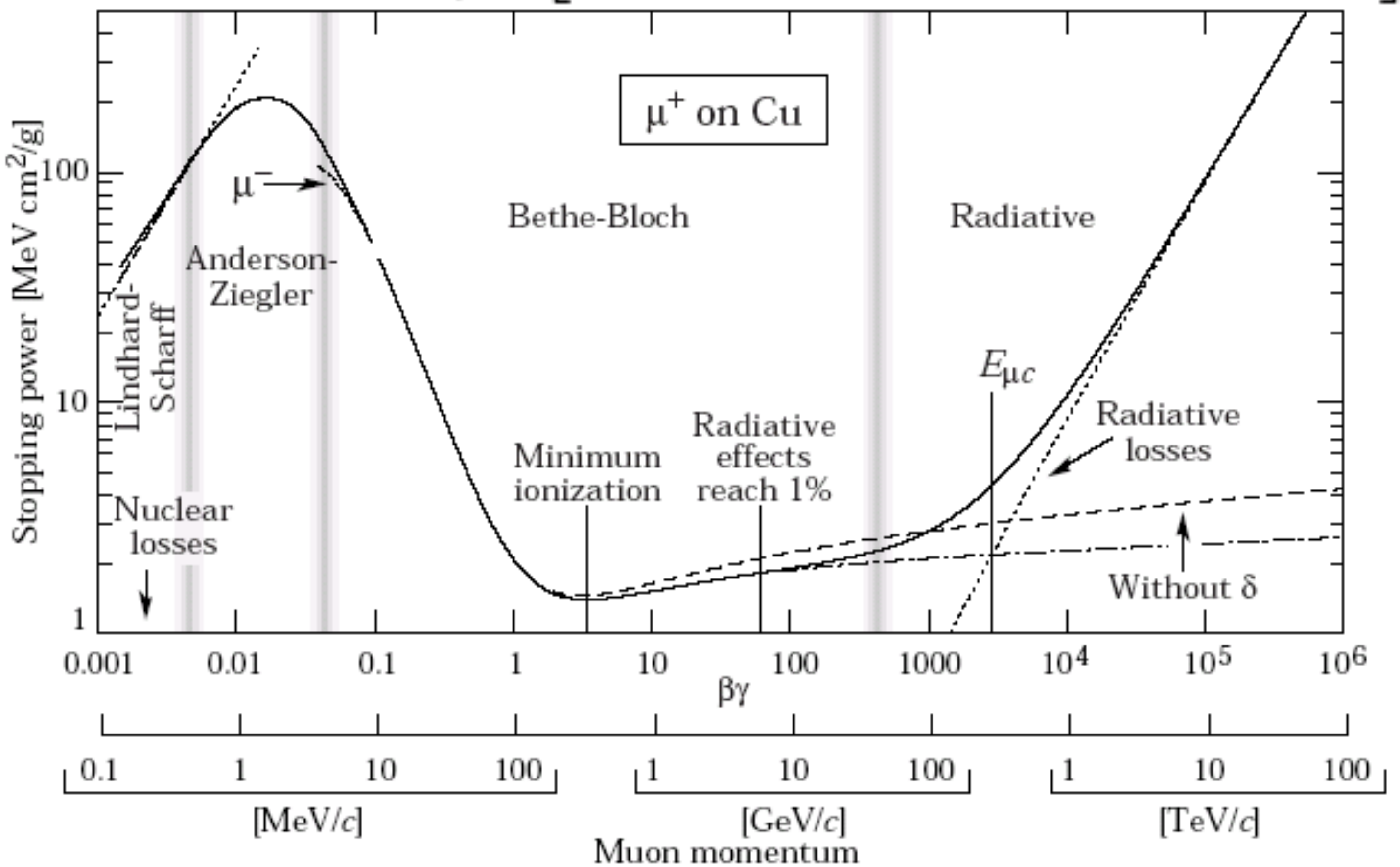

PDG

Coulomb scattering

- In scattering off the Coulomb field of the nucleus, the charged particle loses less energy than in scattering from the electrons, since the energy loss formula ~ 1/m

$$\frac{dE}{dx} = \frac{4\pi N_0 z^2\alpha^2}{mv^2}\frac{Z}{A}\left\{\ln\left[\frac{2mv^2}{I(1-\beta^2)}\right]-\beta^2\right\}$$

- but suffers a larger transverse deflection in scattering from the nucleus than the electrons

$$\frac{d\sigma(\theta)}{d\Omega} = \frac{1}{4}\left(\frac{Zz\alpha}{pv}\right)^2 \frac{1}{\sin^4(\theta/2)}$$

incident particle: ze, p, v
target Ze

Coulomb scattering

- In passing through a layer of material, many scatters occur, resulting in a net angle of multiple scattering which approximates a Gaussian distribution

$$P(\phi)d\phi = \frac{2\phi}{\langle\phi^2\rangle}\exp\left(\frac{-\phi^2}{\langle\phi^2\rangle}\right)d\phi$$

- The rms deflection in distance t depends on the medium

$$\phi_{\rm rms} = \langle\phi^2\rangle^{1/2} = \frac{zE_s}{pv}\sqrt{\frac{t}{X_0}}$$

$$E_s = \sqrt{4\pi \times 137}\ \ mc^2 = 21\ \text{MeV}$$

$$\frac{1}{X_0} = 4Z^2\left(\frac{N_0}{A}\right)\alpha^3\left(\frac{\hbar c}{mc^2}\right)^2 \ln\left(\frac{183}{Z^{1/3}}\right)$$

- X_0 is called the *radiation length*

Coulomb scattering

$$\phi_{\text{rms}} = \langle \phi^2 \rangle^{1/2} = \frac{zE_s}{pv}\sqrt{\frac{t}{X_0}} \quad ; \quad E_s = 21\text{ MeV}$$

Element	Z	E_c, MeV	X_0, g cm^{-2}
hydrogen	1	340	63.1
helium	2	220	94.3
carbon	6	103	42.7
aluminium	11	47	24.0
iron	26	24	13.8
lead	82	6.9	6.4

- Measured along one axis (say the x axis), the rms angular deflection is 1/√2 the above expression

Coulomb scattering

$$\phi_{\rm rms} = \langle \phi^2 \rangle^{1/2} = \frac{zE_s}{pv}\sqrt{\frac{t}{X_0}} \quad ; \quad E_s = 21\ \text{MeV}$$

- Multiple coulomb scattering limits the precision of determining the direction of a particle

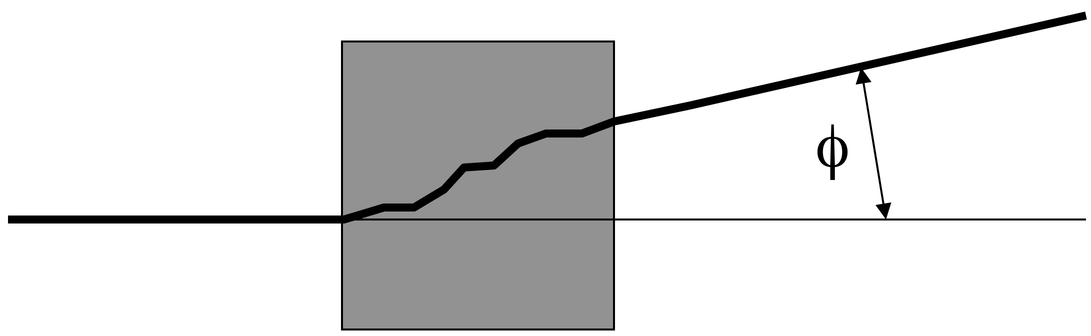

Coulomb scattering

$$\phi_{rms} = \langle \phi^2 \rangle^{1/2} = \frac{zE_s}{pv}\sqrt{\frac{t}{X_0}} \quad ; \quad E_s = 21 \text{ MeV}$$

- Consider the measurement of the curvature of a particle's path in a magnetic field
- Radius of curvature of the track (ρ) is given by expression

  p c = B e ρ

  p(GeV/c) = 0.3 B(Tesla) ρ (meters)

  - or in terms of deflection in distance s: $\phi_{mag} = s/\rho = 0.3\ s\ B / p$
- At the same time, the direction of the track is altered by mulitple Coulomb scattering

$$\phi_{scat} = \frac{0.021}{\sqrt{2}}\frac{1}{p\beta c}\sqrt{\frac{s}{X_0}}$$

so
$$\frac{\phi_{scat}}{\phi_{mag}} = \frac{0.05}{B\beta\sqrt{X_0 s}}$$

Iron, X_0= 0.02 m

s	ϕ_{scat}/ϕ_{mag}
1 m	0.25
6 m	0.10

Radiation loss by electrons

- In addition to losing energy through ionization (above), electrons lose significant energy through radiation
- This loss results principally through collisions with the nucleus, and therefore is parametrized by the same length as Coulomb scattering, the radiation length (X_0)
- In interacting with the electric field of a nucleus, an electron will radiate photons, in a process known as bremsstrahlung ("braking radiation")
  - photon energy spectrum dE'/E'
  - total loss in distance dx $$\left(\frac{dE}{dx}\right)_{\text{rad}} = -\frac{E}{X_0}$$
  - integration easily shows the energy surviving after a thickness x

$$\langle E \rangle = E_0 \exp\left(-\frac{x}{X_0}\right)$$

Radiation loss by electrons

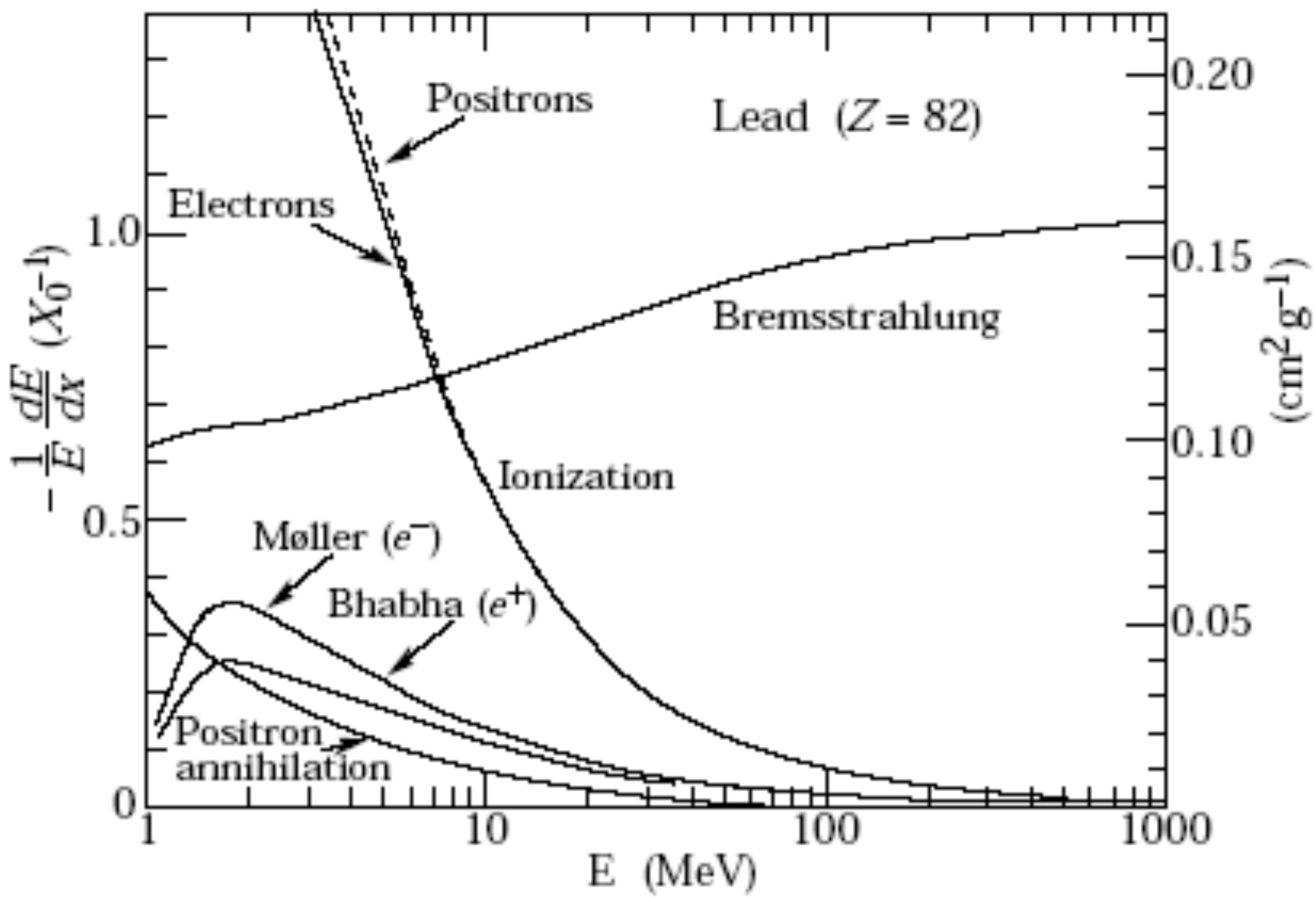

PDG

Radiation loss by electrons

- Critical Energy (E_c)
  - so the energy loss by electron has two components

$$\frac{dE}{dx} = \left(\frac{dE}{dx}\right)_{\text{ion}} + \left(\frac{dE}{dx}\right)_{\text{rad}}$$

  - the ionization loss for high energy electrons is approximately constant
  - however, the energy loss by radiation is proportional to E
  - the critical energy (E_c) is defined as that energy where these two mechanisms are equal
  - for Z > 5 $\quad E_c \simeq \frac{600}{Z}$ MeV

Element	Z	E_c, MeV
hydrogen	1	340
helium	2	220
carbon	6	103
aluminium	11	47
iron	26	24
lead	82	6.9

Radiation loss by electrons

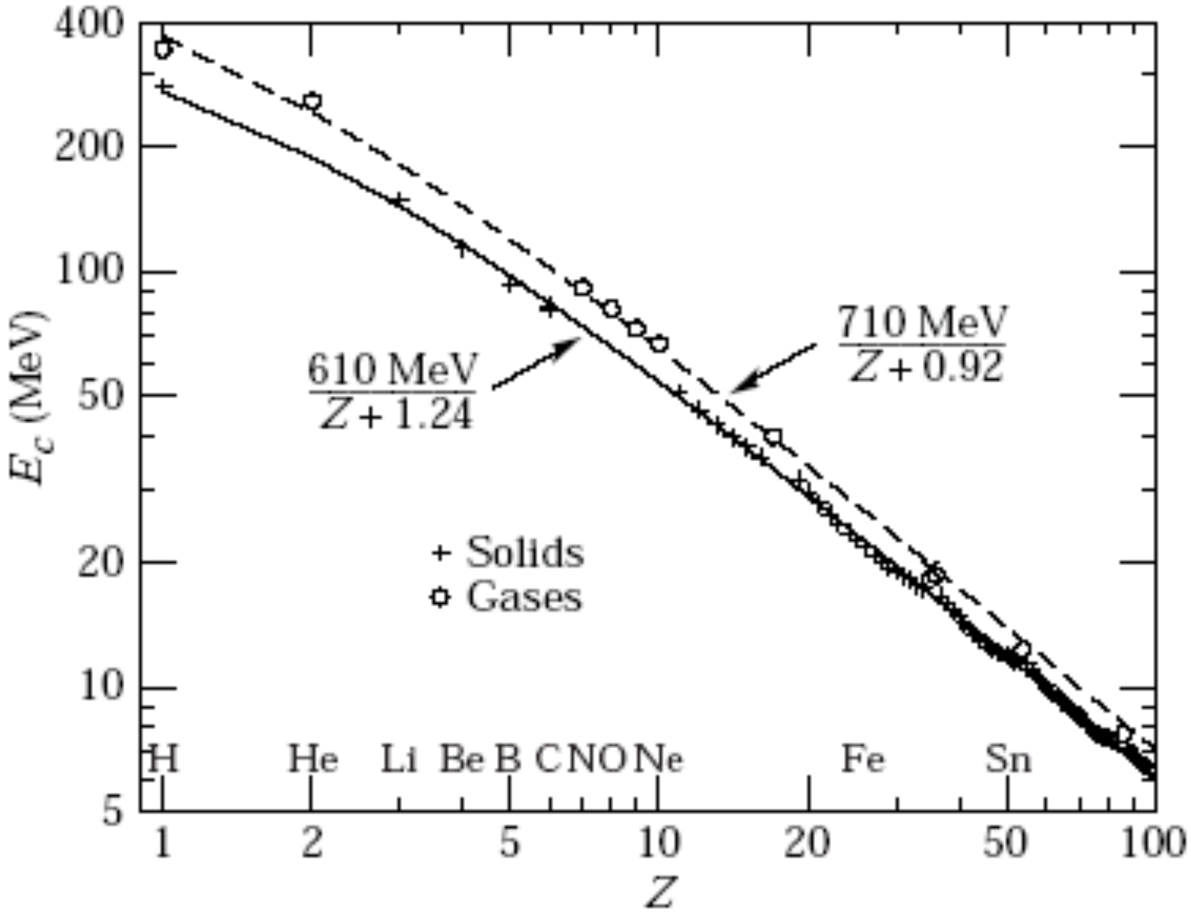

PDG

Radiation loss by muons

- For muons with energies above a few hundred GeV, bremsstrahlung and direct *e+e-* production dominate ionization losses especially in heavy materials.

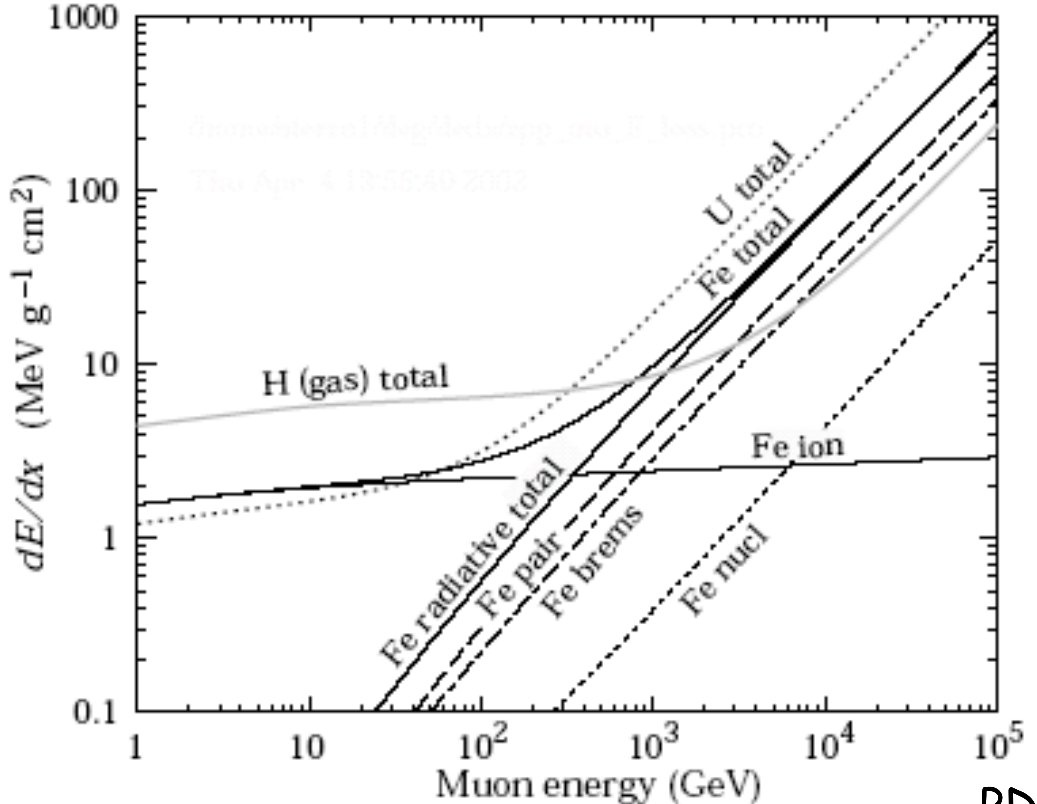

PDG

Absorption of γ -rays in Matter

- γ -rays are attenuated through three types of processes:
  - Photoelectric effect

    $\sigma \sim 1/E^3$
  - Compton scattering

    $\sigma \sim 1/E$
  - Pair production

    $\sigma \sim$ constant

    above threshold

- Above ~10 MeV,
  pair production dominant,
  and attenutaion energy
  independent

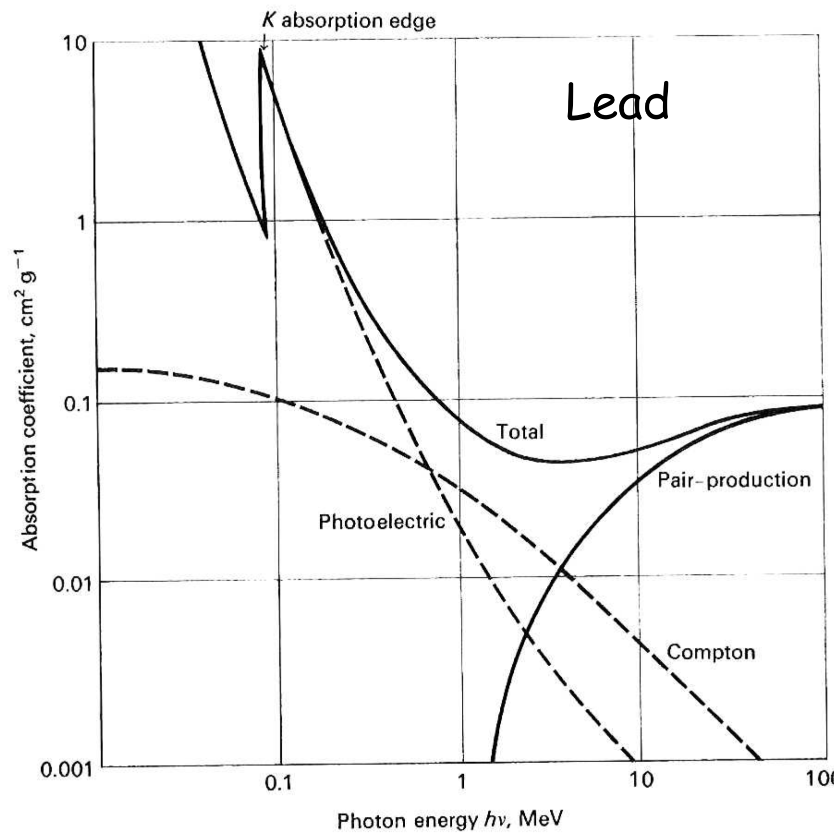

Absorption of γ -rays in Matter

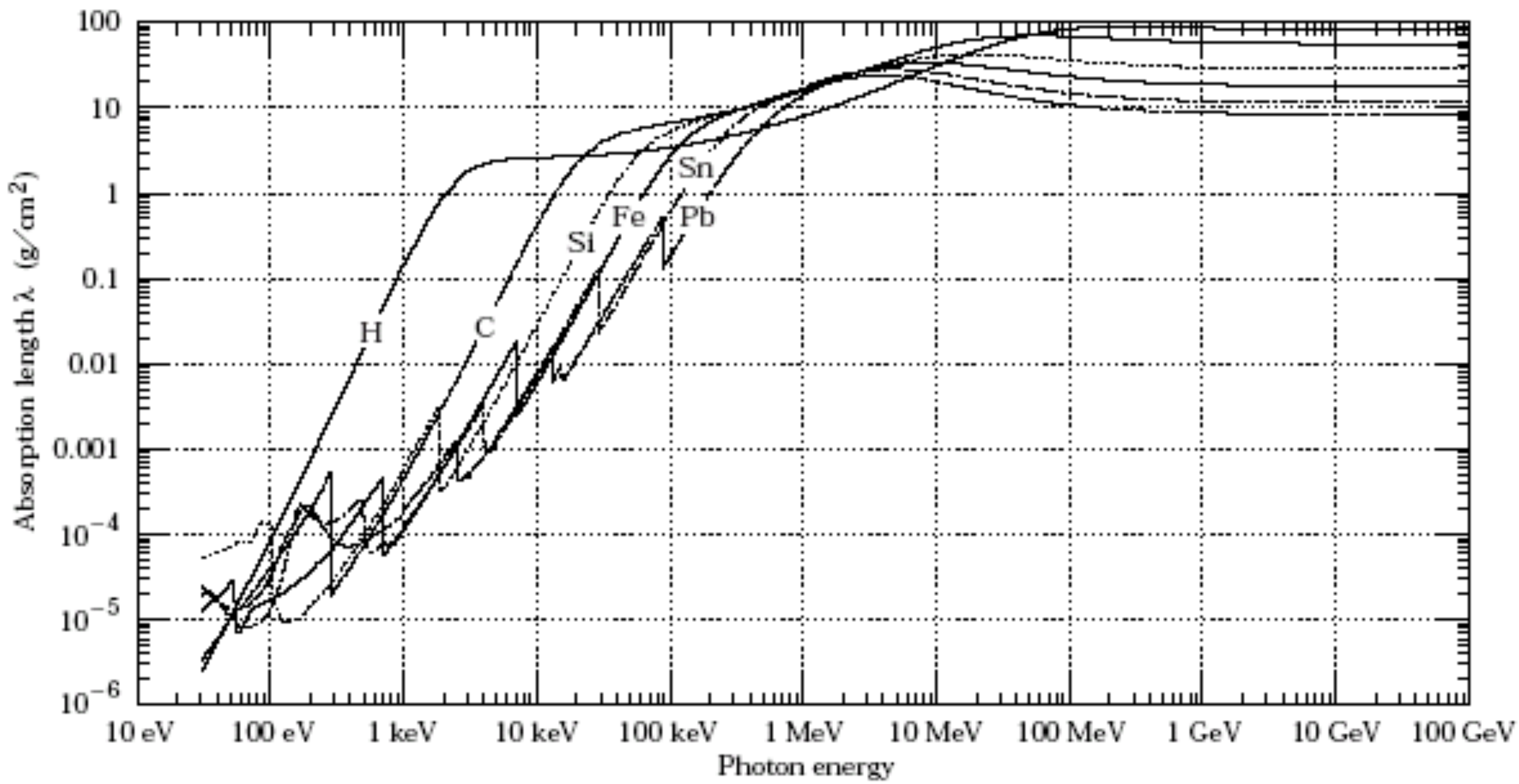

PDG

Absorption of γ-rays in Matter

- Again, since the process of pair production is closely related to electron beamsstrahlung (interactions with the electron field of the nucleus) both are described by the radiation length

$$I = I_0 \exp\left(-\frac{7x}{9X_0}\right)$$

Element	Z	E_c, MeV	X_0, g cm^{-2}
hydrogen	1	340	63.1
helium	2	220	94.3
carbon	6	103	42.7
aluminium	11	47	24.0
iron	26	24	13.8
lead	82	6.9	6.4

- Absorption length:

$9/7\ X_0$

Other important processes

- Interactions
  - charged hadrons
    - p, π, K, etc.
  - neutral hadrons
    - neutrons
    - K^0_L
  - nuclear breakup
- Decays in flight
  - eg. $\pi \rightarrow \mu\ \nu_\mu$

Properties of Materials

Material	Z	A	$\langle Z/A \rangle$	Nuclear [a] collision length λ_T {g/cm^2}	Nuclear [a] interaction length λ_I {g/cm^2}	$dE/dx\vert_{min}$ [b] $\left\{\frac{\text{MeV}}{\text{g/cm}^2}\right\}$	Radiation length [c] X_0 {g/cm^2}	{cm}	Density {g/cm^3} ({g/ℓ} for gas)	Liquid boiling point at 1 atm(K)	Refractive index n (($n-1$)$\times 10^6$ for gas)
H_2 gas	1	1.00794	0.99212	43.3	50.8	(4.103)	61.28 [d]	(731000)	(0.0838)[0.0899]		[139.2]
H_2 liquid	1	1.00794	0.99212	43.3	50.8	4.034	61.28 [d]	866	0.0708	20.39	1.112
D_2	1	2.0140	0.49652	45.7	54.7	(2.052)	122.4	724	0.169[0.179]	23.65	1.128 [138]
He	2	4.002602	0.49968	49.9	65.1	(1.937)	94.32	756	0.1249[0.1786]	4.224	1.024 [34.9]
Li	3	6.941	0.43221	54.6	73.4	1.639	82.76	155	0.534		—
Be	4	9.012182	0.44384	55.8	75.2	1.594	65.19	35.28	1.848		—
C	6	12.011	0.49954	60.2	86.3	1.745	42.70	18.8	2.265 [e]		—
N_2	7	14.00674	0.49976	61.4	87.8	(1.825)	37.99	47.1	0.8073[1.250]	77.36	1.205 [298]
O_2	8	15.9994	0.50002	63.2	91.0	(1.801)	34.24	30.0	1.141[1.428]	90.18	1.22 [296]
F_2	9	18.9984032	0.47372	65.5	95.3	(1.675)	32.93	21.85	1.507[1.696]	85.24	[195]
Ne	10	20.1797	0.49555	66.1	96.6	(1.724)	28.94	24.0	1.204[0.9005]	27.09	1.092 [67.1]
Al	13	26.981539	0.48181	70.6	106.4	1.615	24.01	8.9	2.70		—
Si	14	28.0855	0.49848	70.6	106.0	1.664	21.82	9.36	2.33		3.95
Ar	18	39.948	0.45059	76.4	117.2	(1.519)	19.55	14.0	1.396[1.782]	87.28	1.233 [283]
Ti	22	47.867	0.45948	79.9	124.9	1.476	16.17	3.56	4.54		—
Fe	26	55.845	0.46556	82.8	131.9	1.451	13.84	1.76	7.87		—
Cu	29	63.546	0.45636	85.6	134.9	1.403	12.86	1.43	8.96		—
Ge	32	72.61	0.44071	88.3	140.5	1.371	12.25	2.30	5.323		—
Sn	50	118.710	0.42120	100.2	163	1.264	8.82	1.21	7.31		—
Xe	54	131.29	0.41130	102.8	169	(1.255)	8.48	2.87	2.953[5.858]	165.1	[701]
W	74	183.84	0.40250	110.3	185	1.145	6.76	0.35	19.3		—
Pt	78	195.08	0.39984	113.3	189.7	1.129	6.54	0.305	21.45		—
Pb	82	207.2	0.39575	116.2	194	1.123	6.37	0.56	11.35		—
U	92	238.0289	0.38651	117.0	199	1.082	6.00	≈0.32	≈18.95		—

Properties of Materials

Material	Z	A	$\langle Z/A \rangle$	Nuclear [a] collision length λ_T $\{g/cm^2\}$	Nuclear [a] interaction length λ_I $\{g/cm^2\}$	$dE/dx\|_{min}$ [b] $\left\{\frac{MeV}{g/cm^2}\right\}$	Radiation length [c] X_0 $\{g/cm^2\}$	X_0 $\{cm\}$	Density $\{g/cm^3\}$ ($\{g/\ell\}$ for gas)	Liquid boiling point at 1 atm(K)	Refractive index n ($(n-1)\times 10^6$ for gas)
Air, (20°C, 1 atm.), [STP]			0.49919	62.0	90.0	(1.815)	36.66	[30420]	(1.205)[1.2931]	78.8	(273) [293]
H_2O			0.55509	60.1	83.6	1.991	36.08	36.1	1.00	373.15	1.33
CO_2 gas			0.49989	62.4	89.7	(1.819)	36.2	[18310]	[1.977]		[410]
CO_2 solid (dry ice)			0.49989	62.4	89.7	1.787	36.2	23.2	1.563	sublimes	—
Shielding concrete [f]			0.50274	67.4	99.9	1.711	26.7	10.7	2.5		—
SiO_2 (fused quartz)			0.49926	66.5	97.4	1.699	27.05	12.3	2.20 [g]		1.458
Dimethyl ether, $(CH_3)_2O$			0.54778	59.4	82.9	—	38.89	—	—	248.7	—
Methane, CH_4			0.62333	54.8	73.4	(2.417)	46.22	[64850]	0.4224[0.717]	111.7	[444]
Ethane, C_2H_6			0.59861	55.8	75.7	(2.304)	45.47	[34035]	0.509(1.356) [h]	184.5	(1.038) [h]
Propane, C_3H_8			0.58962	56.2	76.5	(2.262)	45.20	—	(1.879)	231.1	—
Isobutane, $(CH_3)_2CHCH_3$			0.58496	56.4	77.0	(2.239)	45.07	[16930]	[2.67]	261.42	[1900]
Octane, liquid, $CH_3(CH_2)_6CH_3$			0.57778	56.7	77.7	2.123	44.86	63.8	0.703	398.8	1.397
Paraffin wax, $CH_3(CH_2)_{n\approx 23}CH_3$			0.57275	56.9	78.2	2.087	44.71	48.1	0.93		—
Nylon, type 6 [i]			0.54790	58.5	81.5	1.974	41.84	36.7	1.14		—
Polycarbonate (Lexan) [j]			0.52697	59.5	83.9	1.886	41.46	34.6	1.20		—
Polyethylene terephthlate (Mylar) [k]			0.52037	60.2	85.7	1.848	39.95	28.7	1.39		—
Polyethylene [l]			0.57034	57.0	78.4	2.076	44.64	≈47.9	0.92–0.95		—
Polyimide film (Kapton) [m]			0.51264	60.3	85.8	1.820	40.56	28.6	1.42		—
Lucite, Plexiglas [n]			0.53937	59.3	83.0	1.929	40.49	≈34.4	1.16–1.20		≈1.49
Polystyrene, scintillator [o]			0.53768	58.5	81.9	1.936	43.72	42.4	1.032		1.581
Polytetrafluoroethylene (Teflon) [p]			0.47992	64.2	93.0	1.671	34.84	15.8	2.20		—
Polyvinyltolulene, scintillator [q]			0.54155	58.3	81.5	1.956	43.83	42.5	1.032		—
Aluminum oxide (Al_2O_3)			0.49038	67.0	98.9	1.647	19.27	4.85	3.97		1.761
Barium fluoride (BaF_2)			0.42207	92.0	145	1.303	9.91	2.05	4.89		1.56
Bismuth germanate (BGO) [r]			0.42065	98.2	157	1.251	7.97	1.12	7.1		2.15
Cesium iodide (CsI)			0.41569	102	167	1.243	8.39	1.85	4.53		1.80
Lithium fluoride (LiF)			0.46262	62.2	88.2	1.614	39.25	14.91	2.632		1.392
Sodium fluoride (NaF)			0.47632	66.9	98.3	1.69	29.87	11.68	2.558		1.336
Sodium iodide (NaI)			0.42697	94.6	151	1.305	9.49	2.59	3.67		1.775
Silica Aerogel [s]			0.52019	64	92	1.83	29.83	≈150	0.1–0.3		$1.0+0.25\rho$
NEMA G10 plate [t]				62.6	90.2	1.87	33.0	19.4	1.7		—

Detectors of Single Charged Particles

- Detectors of Single Charged Particles
  - Pictorial Detectors: Cloud Chambers, Emulsions, Streamer Chambers, Spark Chambers, Bubble chambers, Time Projection Chambers
  - Proportional counters, Spark and streamer chambers, Drift chambers, Scintillation counters, Cerenkov counters, Solid-state counters
  - Tracking based on gaseous and solid state detectors
    - Time Projection Chamber
    - Silicon Tracking

- References: Donald H. Perkins, Introduction to High Energy Physics, Fourth Edition

Spatial and Temporal Resolutions

Detector Type	Accuracy (rms)	Resolution Time	Dead Time
Bubble chamber	10 to 150 μm	1 ms	50 ms[a]
Streamer chamber	300 μm	2 μs	100 ms
Proportional chamber	$\geq$ 300 μm[b,c]	50 ns	200 ns
Drift chamber	50 to 300 μm	2 ns[d]	100 ns
Scintillator	—	150 ps	10 ns
Emulsion	1 μm	—	—
Silicon strip	$\frac{\text{pitch}}{3 \text{ to } 7}$ [e]	[f]	[f]
Silicon pixel	2 μm[g]	[f]	[f]

[a] Multiple pulsing time.
[b] 300 μm is for 1 mm pitch.
[c] Delay line cathode readout can give $\pm$150 μm parallel to anode wire.
[d] For two chambers.
[e] The highest resolution ("7") is obtained for small-pitch detectors ($\lesssim$25 μm) with pulse-height-weighted center finding.
[f] Limited at present by properties of the readout electronics. (Time resolution of $\leq$ 25 ns is planned for the ATLAS SCT.)
[g] Analog readout of 34 μm pitch, monolithic pixel detectors.

Pictorial Detectors

- Cloud chamber
  - condensation on track
- Emulsions
  - enhanced silver content, reveals (after development) particle tracks with extreme precision
- Streamer chambers
  - ionization of gas generates light through recombination which is photographed
- Spark chambers
  - breakdown through electrodes
- Bubble chambers
  - liquid is expanded to superheated condition

Cloud Chamber

- Invented by C.T.R. Wilson for study of formation of rain in clouds
- Perfected around 1912
- expands moist air in a closed container
  - expansion cools the air
  - it becomes supersaturated
  - moisture condenses on dust particles
  - ………or paths ionized by charged particles
- Example: beta particles

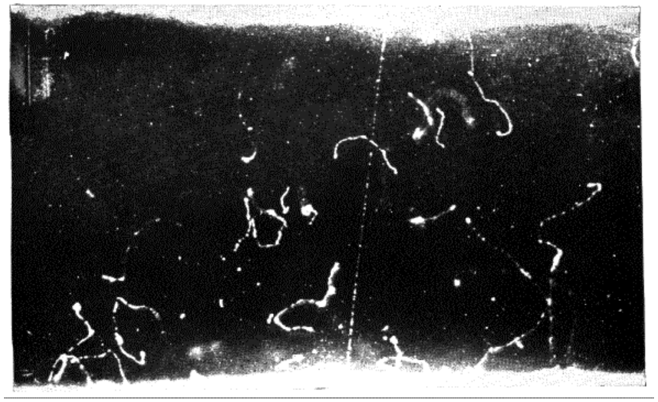

Cloud Chamber

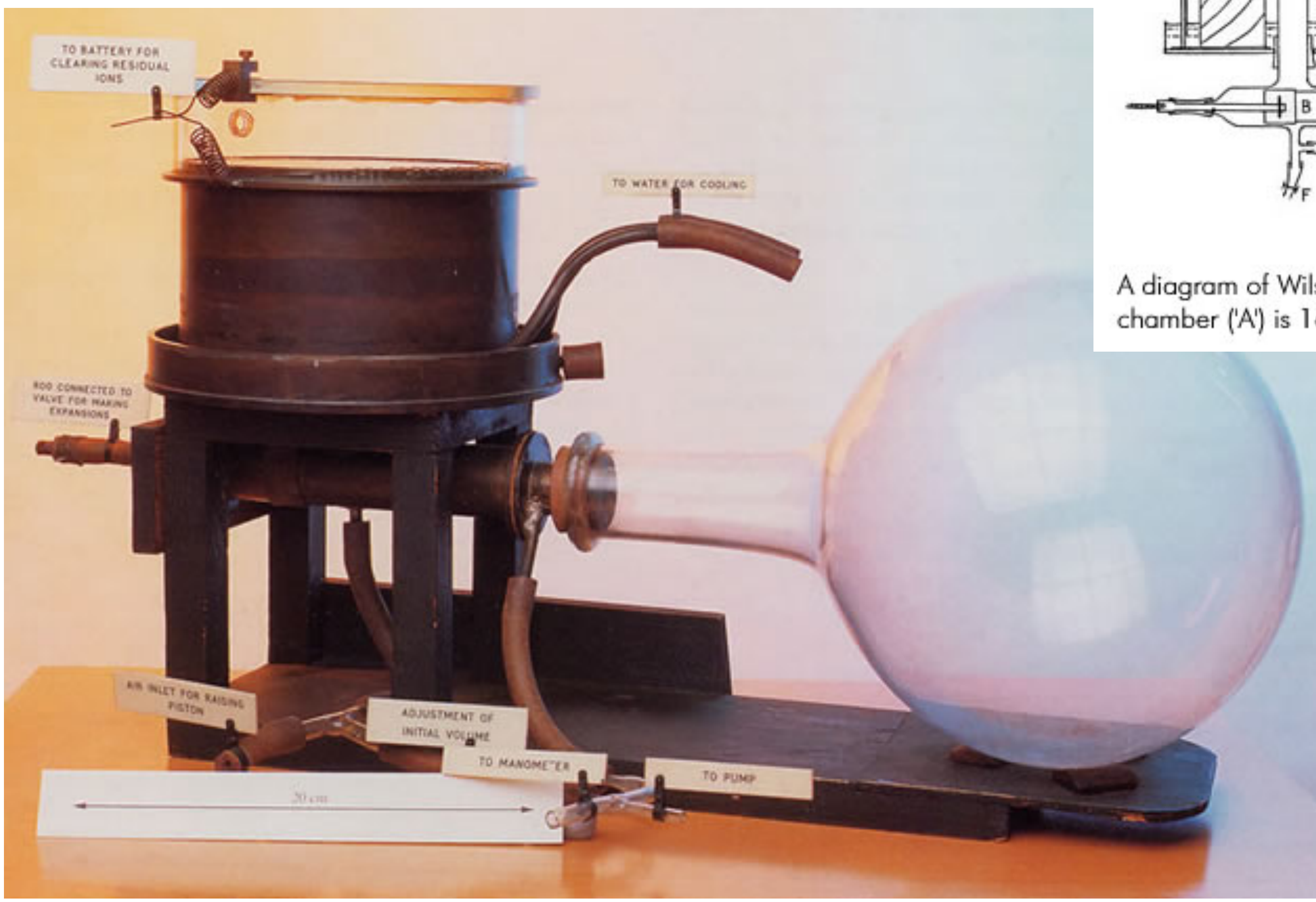

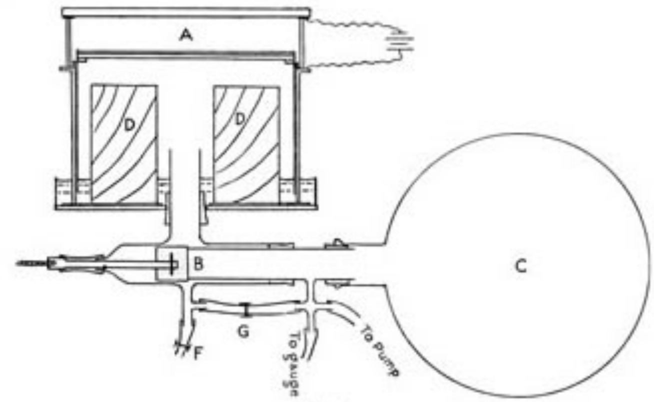

Fig. 1.

A diagram of Wilson's apparatus. The cylindrical cloud chamber ('A') is 16.5cm across by 3.4cm deep.

Emulsions

- Photographic film contains tiny crystals (or "grains") of very slightly soluble silver halide salts such as silver bromide.
- The grains are embedded in gelatine which is melted and applied as a thin coating on a substrate.
- Light or radiation striking a silver halide crystals initiates a series of reactions which produce a small amount of free silver in the grain.
- Free silver produced in the exposed emulsion constitutes the "latent image," which is later amplified by the development process.
- The free silver grains are easily reduced by "developers" to form relatively large amounts of free silver; the deposit of free silver produces a dark area on the film.
- Emulsions have superb spatial precision (~ 1 μm) but poor time precision, being continuously active.

Emulsions

- Historical example:
  - Discovery of the pion, announced in 1947 by Powell et al

Four examples of π–μ-e decays recorded in photographic emulsions

Emulsions

- Example:
  - Chorus experimentat CERN
  - Searched for tau-neutrino interactions

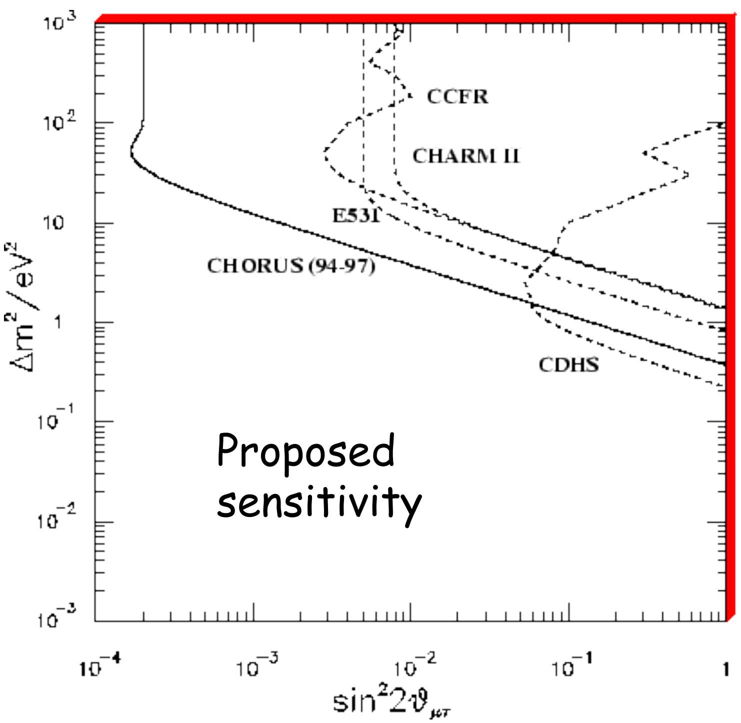

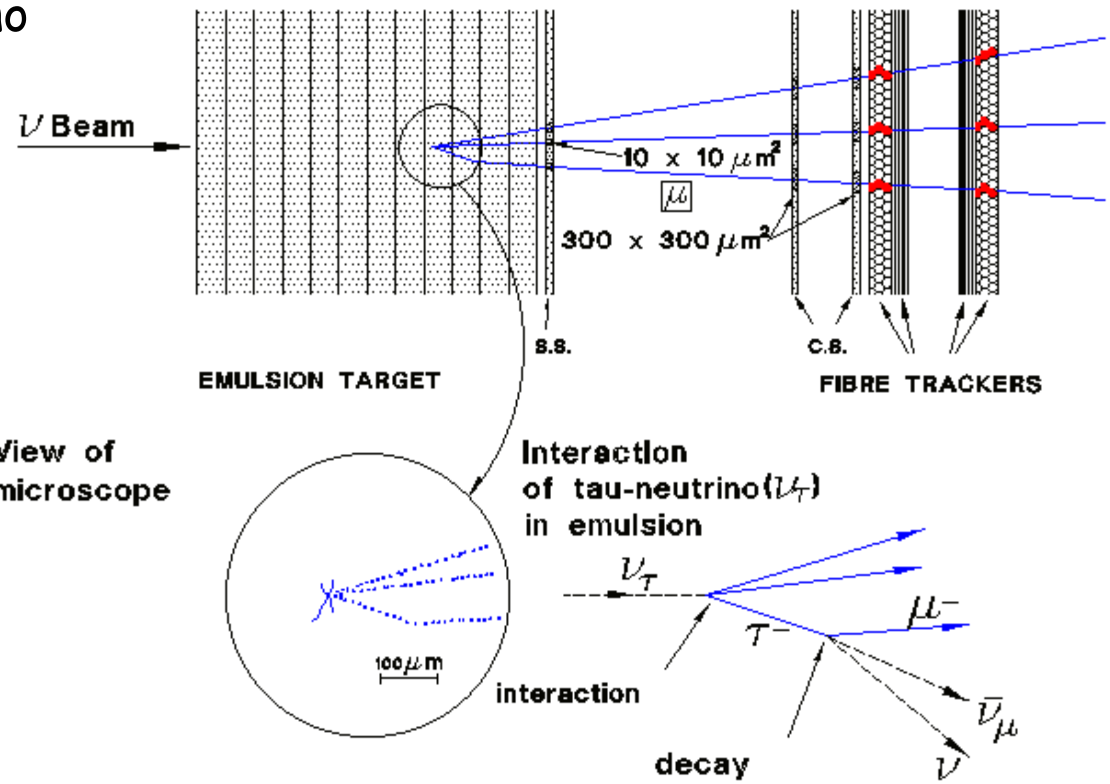

Emulsions

- DONUT (Direct Observation of NU-Tau)
  - Discovered tau neutrino interactions
  - Search for

$$\nu_\tau + \mathrm{N} \to \tau^- + \mathrm{X}$$

$$\tau^- \to (\mu^- \text{ or } e^-)\, \nu_\mu \nu_\tau \text{ or } \tau^- \to \mathrm{h}^- \nu_\tau$$

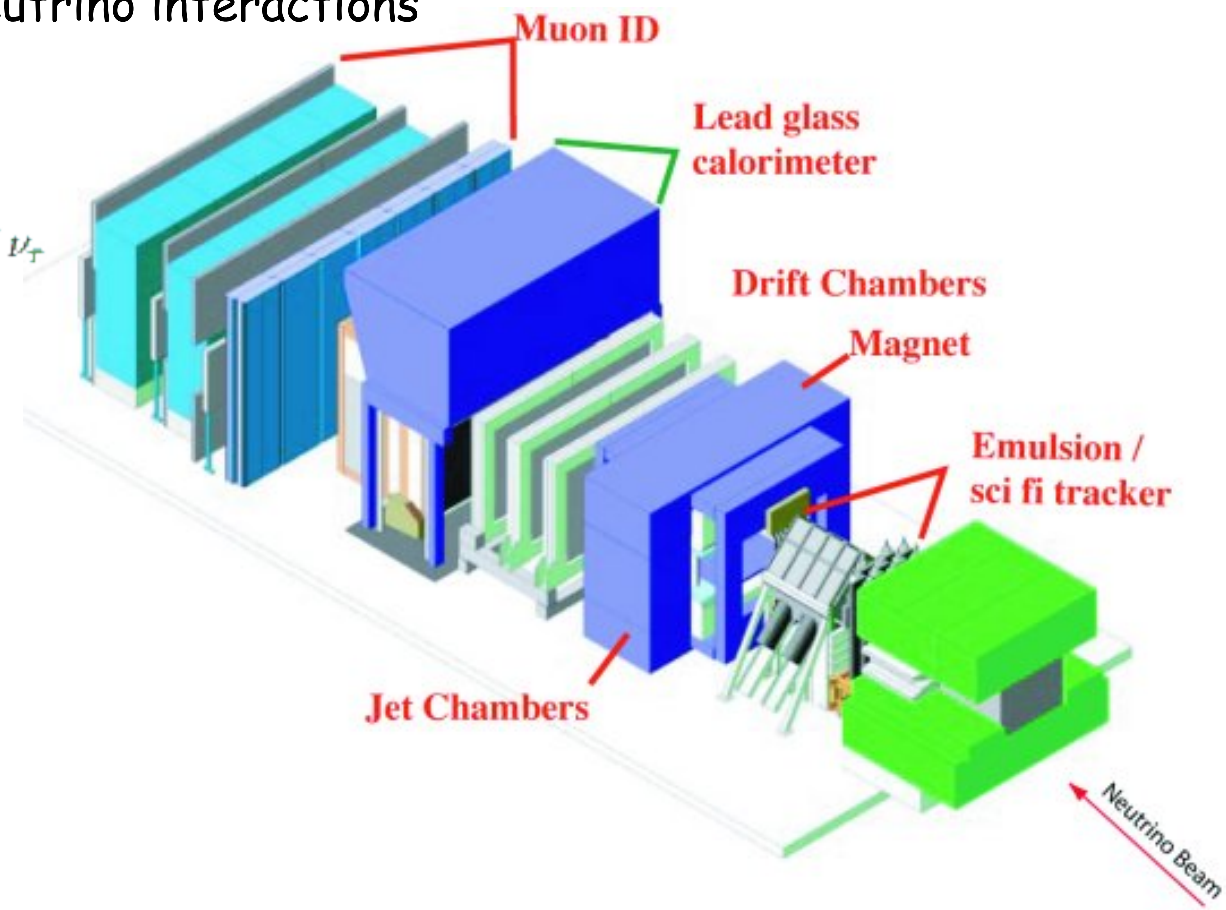

Emulsions

- DONUT

Tau neutrino interaction

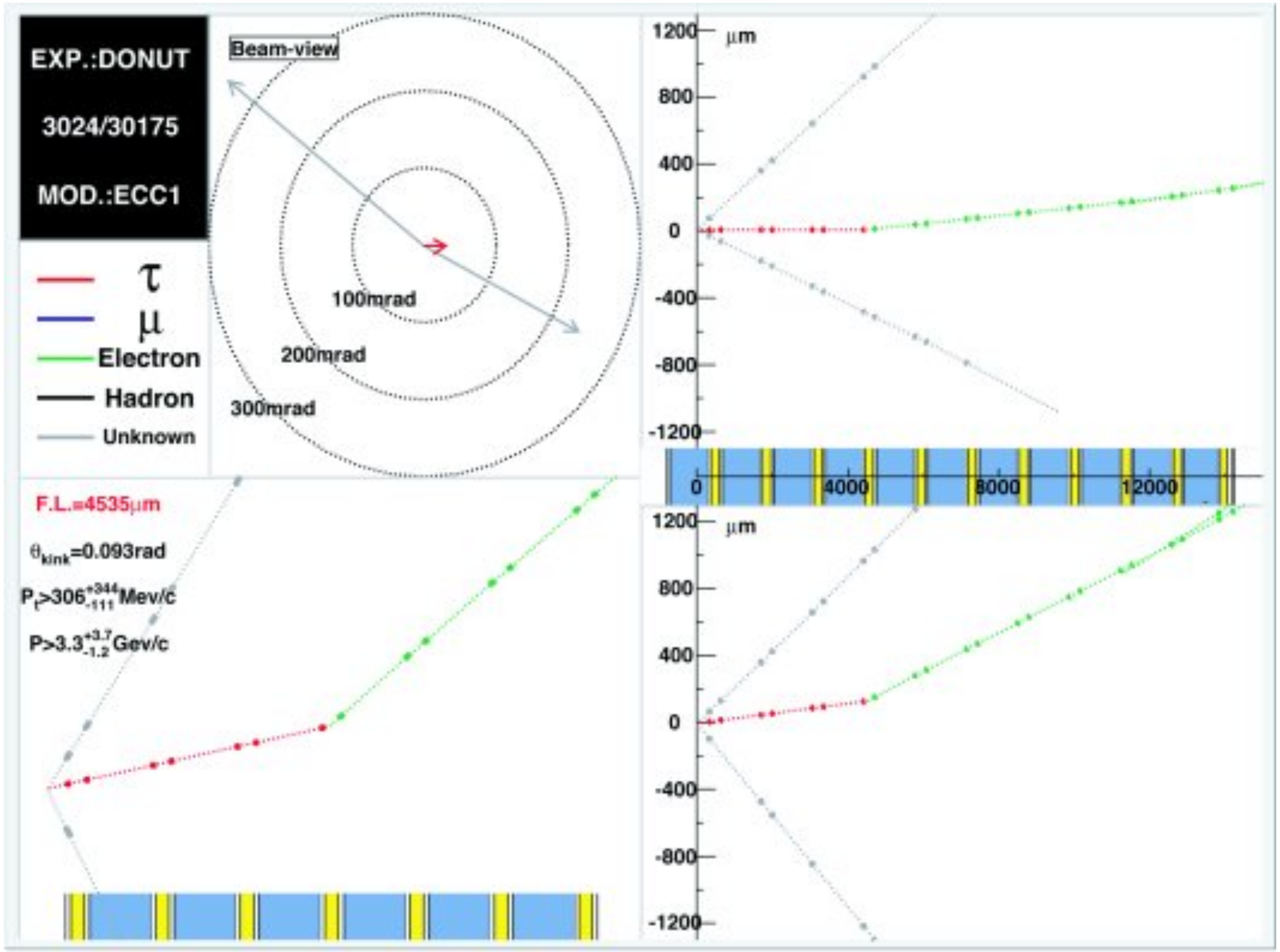

Spark Chambers

- Extremely high voltages across gaps lead to breakdown, and emission of light
- Space charge within an avalanche is strong enough to shield external field
  - recombination occurs, and emission of light
- Often multiple gaps were employed

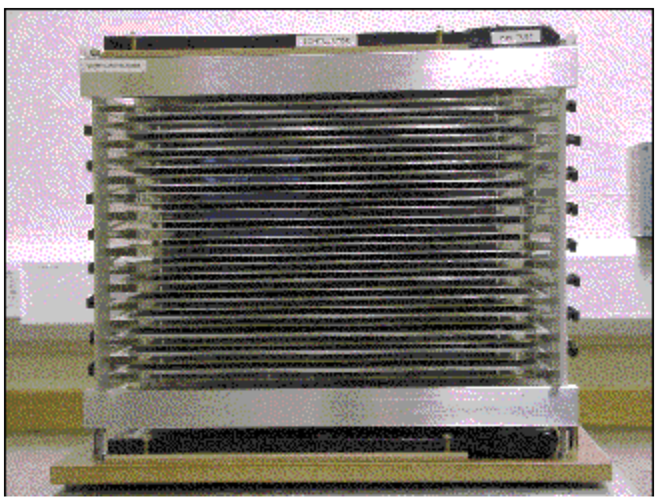

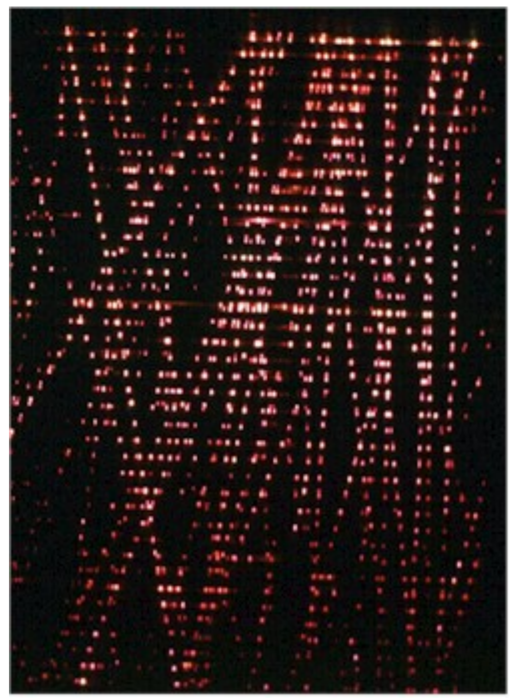

Spark Chambers

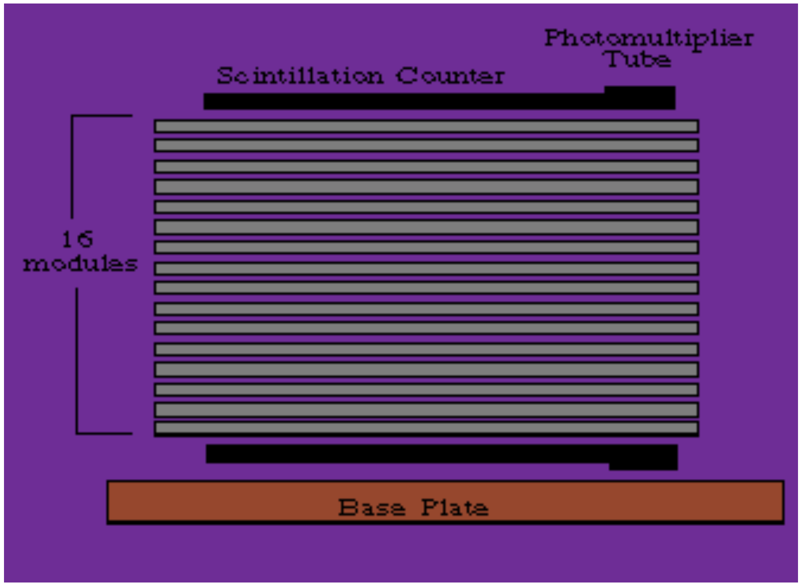

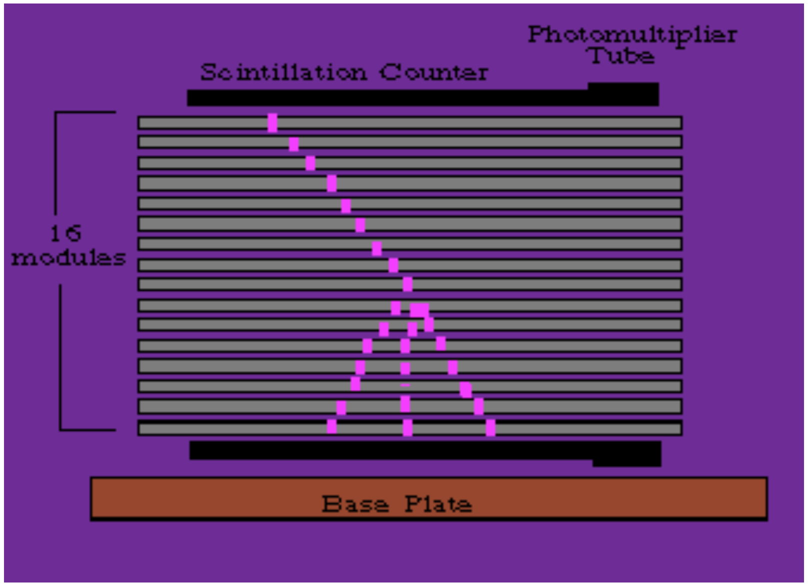

Streamer Chambers

- If a short (10 ns) high-voltage pulse (10-50kV/cm) is applied between parallel plate electrodes, a short (2-3 mm) streamer discharge develops

- Good multi-track efficiency and spatial resolution
- triggerable
- long recovery time
- processing of optical images required

- Fermilab experiment, triggered on muons, scanned for V^0s (search for charm)

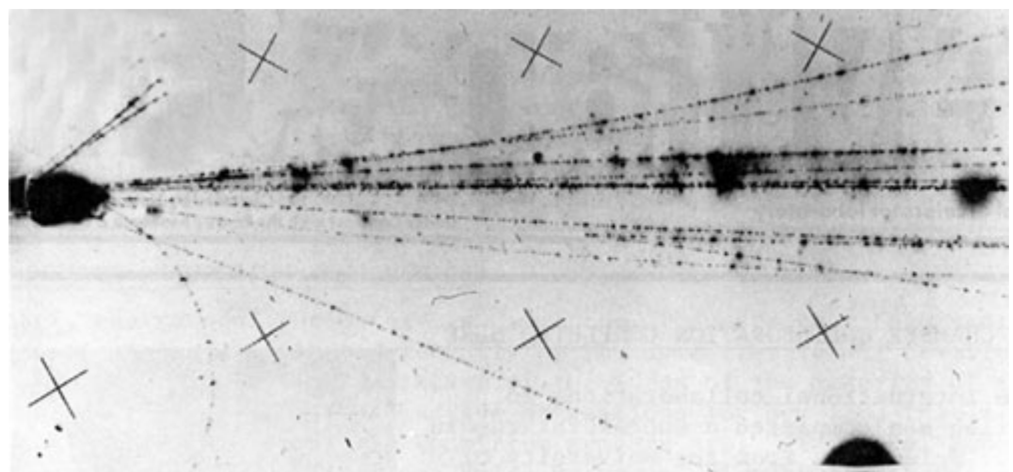

Bubble Chamber

- Invented in early 1950's by Glaser
- Dominant detector for decades
- Superheated liquid begins to boil along path of charged particle
- Superheating achieved by maintaining liquid at high pressure (5-20 atmospheres), and sudden expansion.
- Bubble grow for a period of time (ms typically)
- Photograph and recompress

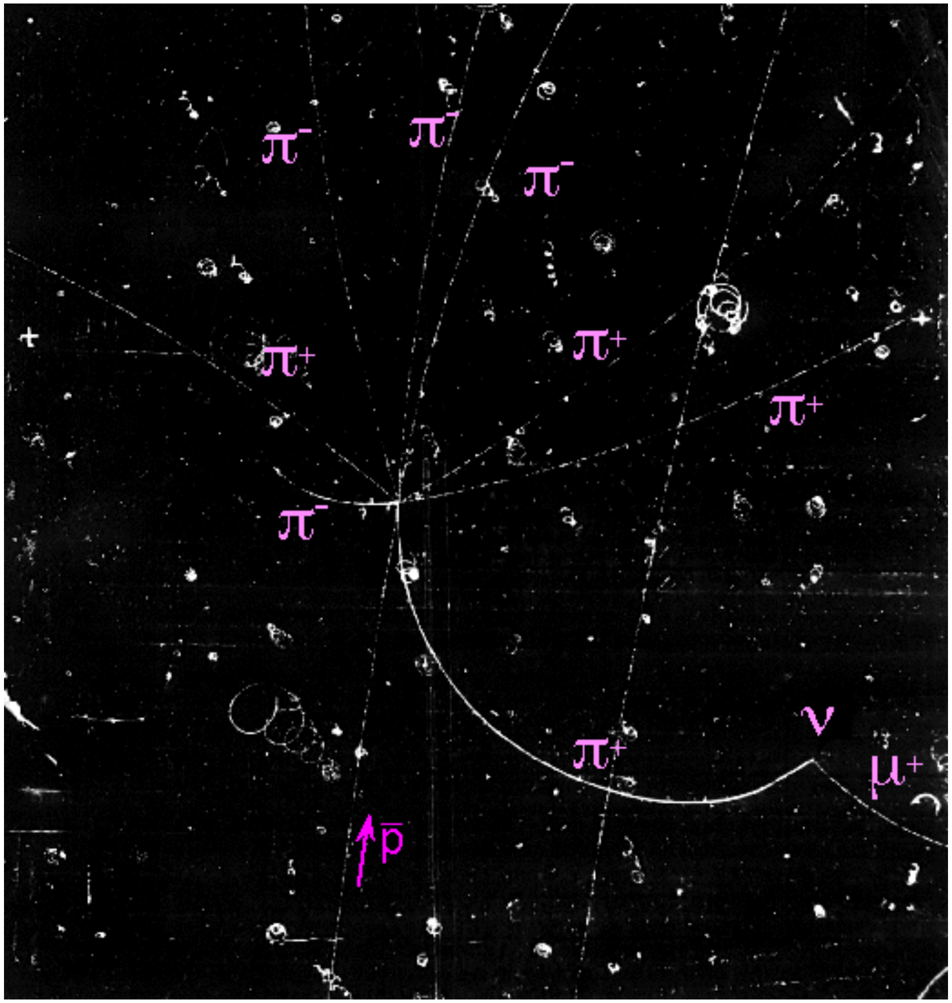

Bubble Chamber

- Several cameras provide stereo image
  - very detailed measurements following reconstruction
- Disadvantages
  - low repetition rate (1-20 Hz)
  - analysis of film complicated
  - very low duty cycle (~ 10^{-2})
  - not matched to colliding beam geometry

Bubble Chamber

- Liquids used
  - hydrogen - most elementary target material (proton)
  - deuterium - most elementary form of neutron targets
  - heavy liquids - short radiation length, or higher interaction rate

Table 2. Properties of bubble chamber liquid.

Liquid	Temperature [K]	Density [g/cm^3]	Radiation length [cm]
H2	25	0.0645	968
D2	30	0.14	900
Ne	35	1.02	27
He	3.2	0.14	1027
Xe	252	2.3	3.9
C_3H_8	333	0.43	110
CF_3Br	303	1.5	11
Ar	135	1.0	20
N_2	115	0.6	65

Gert G. Harigel, CERN

SLAC 1-meter Bubble Chamber

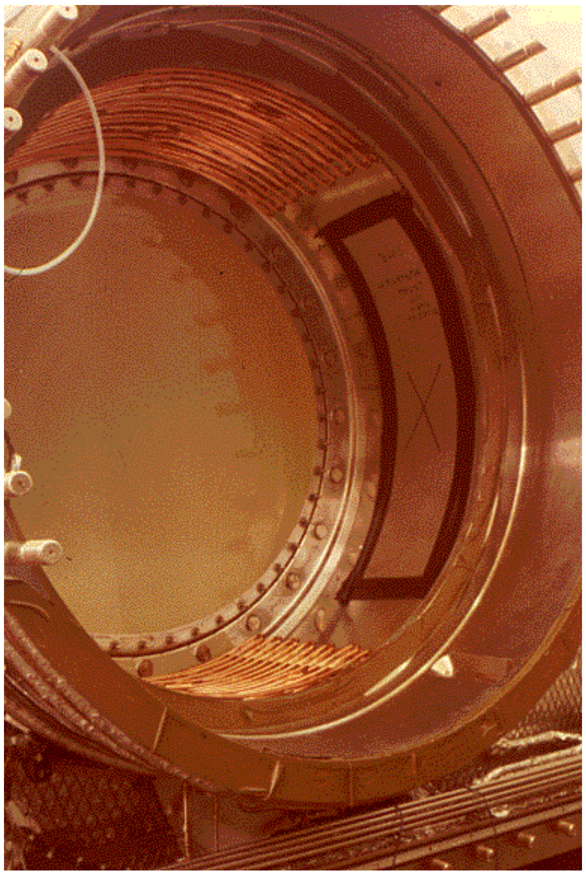

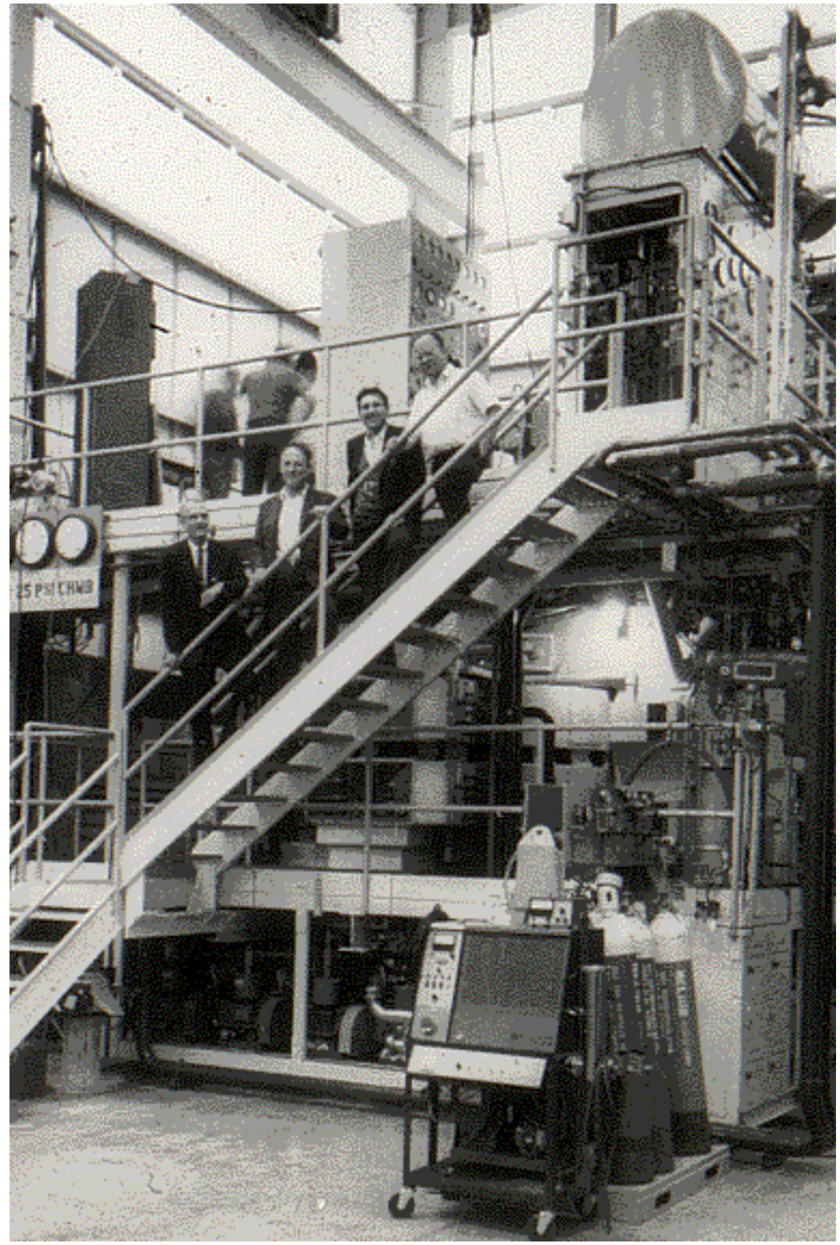

Bubble Chamber

- BEBC at CERN, 3.7 m diameter,
  - with EMI (MWPCs)
  - B = 2-3.5 Tesla

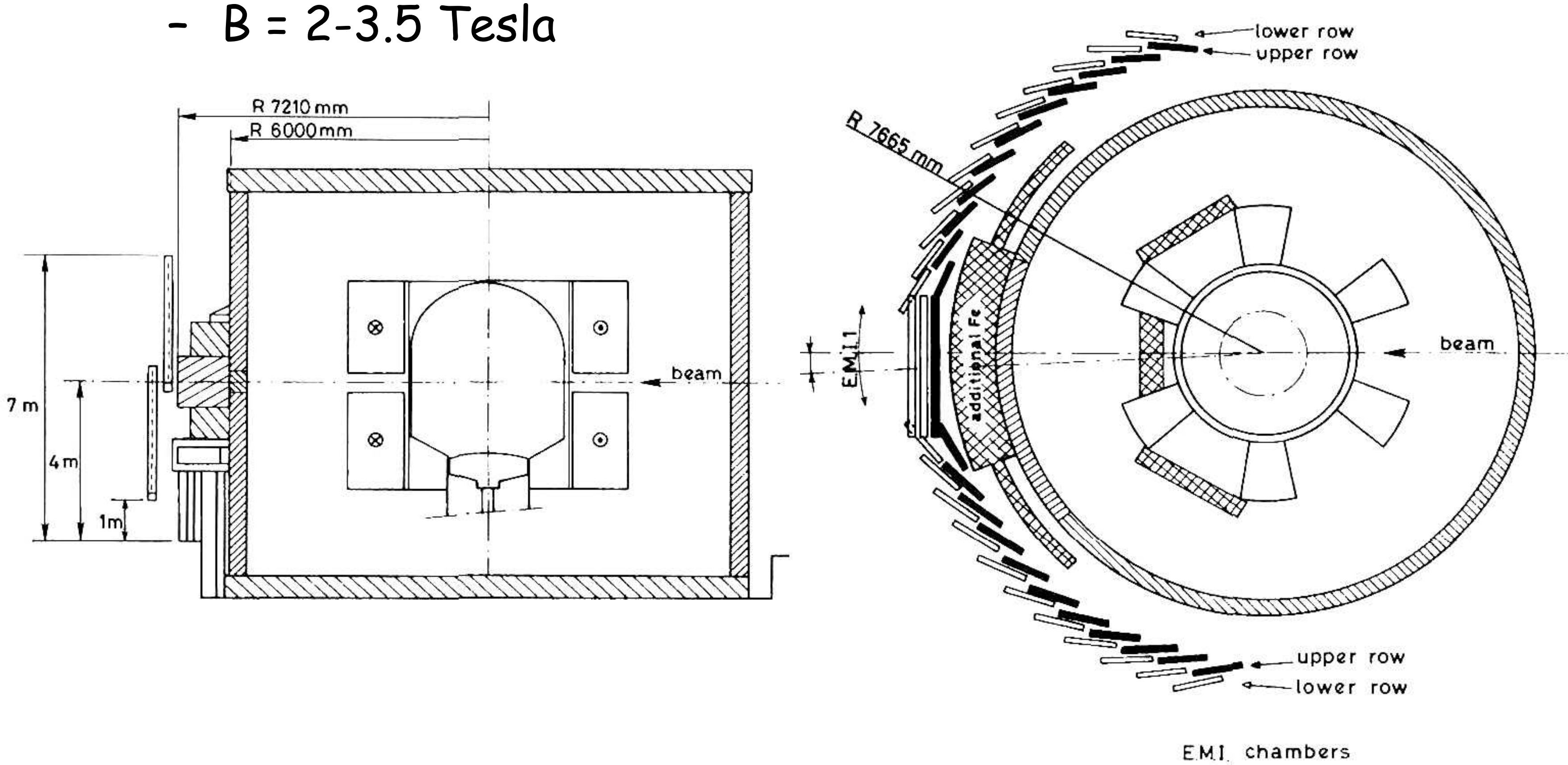

Bubble Chamber

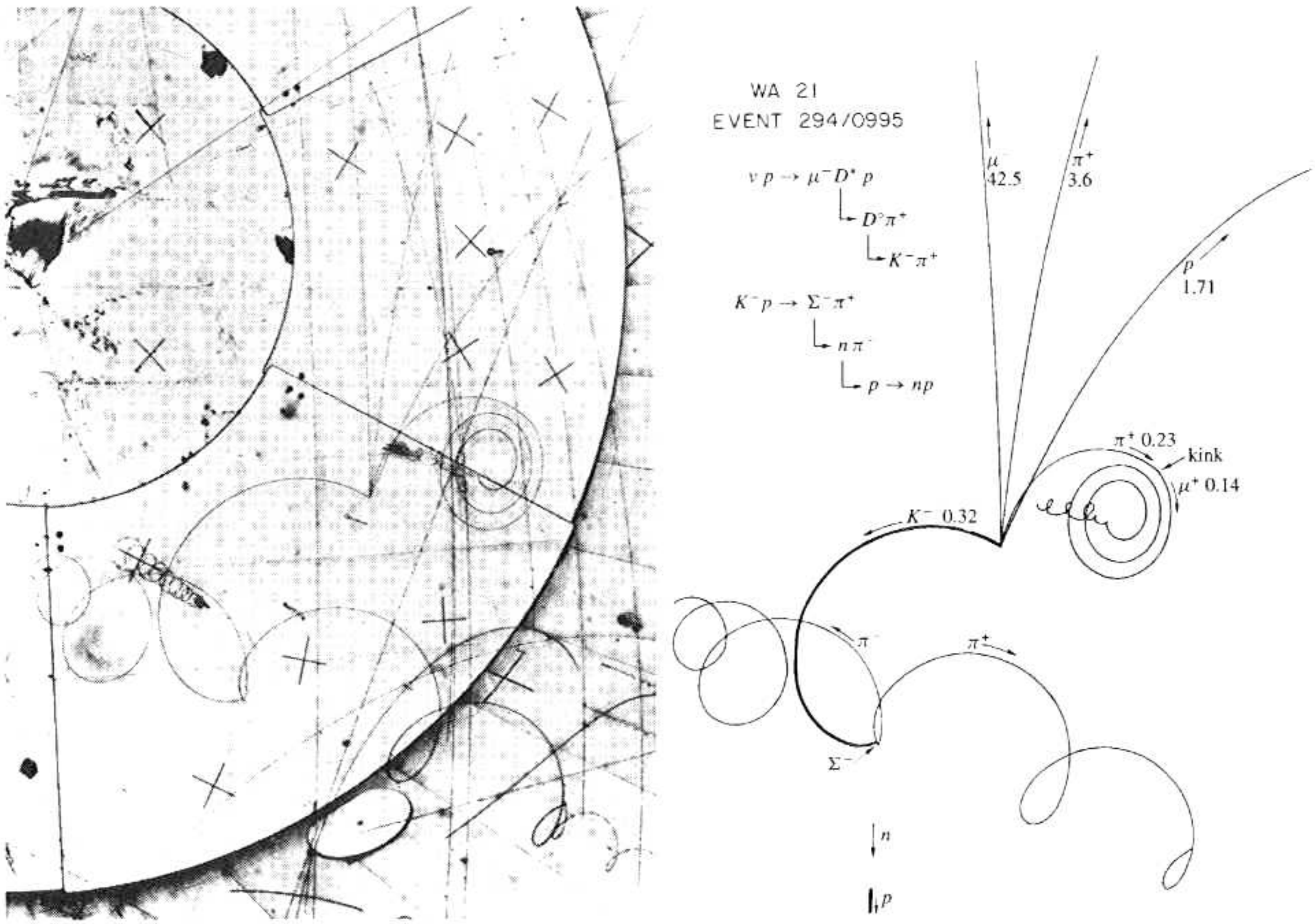

Hybrid Bubble Chamber

- Combine bubble chamber with a downstream system
- Example was the Fermilab 30-inch hybrid bubble chamber system
- Upstream measurements to tag beam particle
- Downstream measurement needed to achieve good momentum resolution on high energy tracks (beam momentum ~ 150 GeV/c)

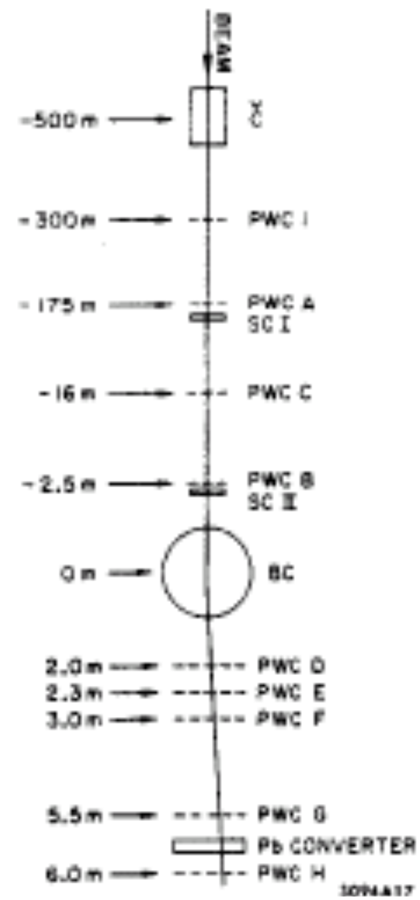

Triggered Bubble Chamber

- Use downstream system to trigger bubble chamber flash
- Only take picture when event, or selected event, occurs in BC
- Example was the SLAC Hybrid Facility (1 meter BC)

- π^+p -> K^+X
- Flash in 2.5 msec
- 40% of photos had event
- ~15/1 reduction in photos

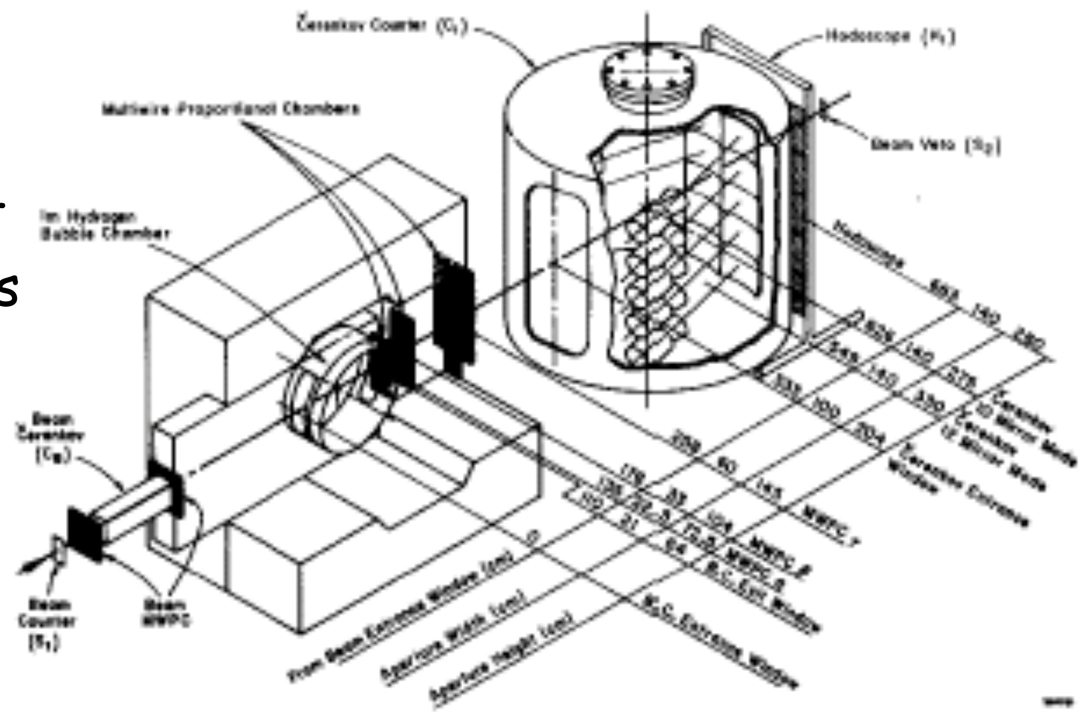

Triggered Bubble Chamber

- Event detected at SLAC 1 meter bubble chamber.
- Careful analysis shows this event is

$$\bar{p}\,p \rightarrow p\,\pi^{+}\,K^{-}\,\pi^{-}\,\pi^{0}\,K^{0}\,\bar{n}$$

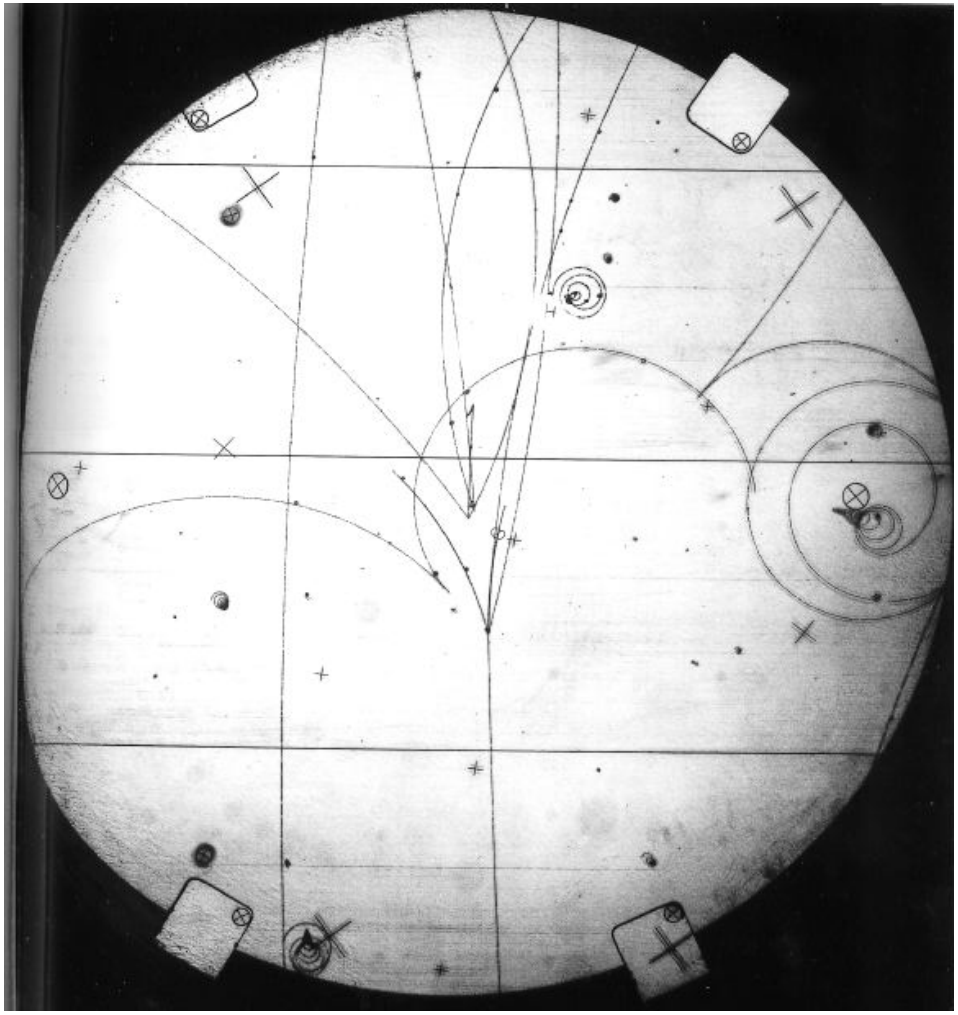

High Resolution Bubble Chamber

- Special optics were developed to improve resolution
  - Run bubble chamber "hot" (29K) to slow bubble growth and increase bubble density
  - Achieved bubble size of <50 μm (compared to standard ~300 μm)
  - Example, charm lifetime measurements in SLAC Hybrid Facility

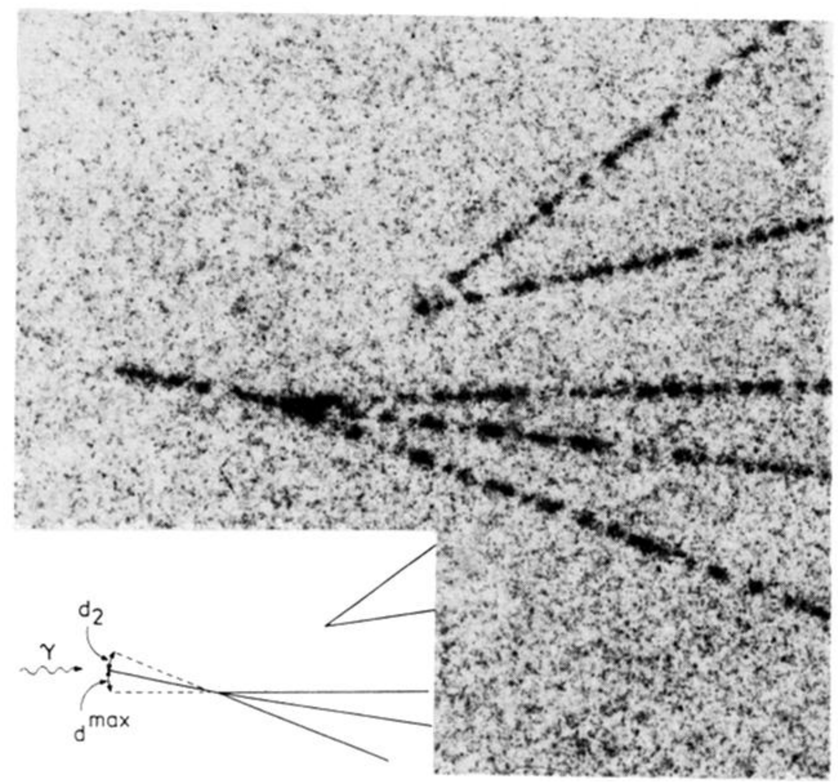

Decay lengths of 0.86 mm and 1.8 mm

Holographic Bubble Chamber

- In a conventional optics system the depth of field is coupled with the resolution:
  - DOF ~ λ / D^2
  - Resolution ~ λ / D
- Therefore, high resolution implies limited depth of field, reducing useful volume of bubble chamber
- A holographic system uncouples DOF and resolution
  - DOF ~ laser coherence length
  - Resolution ~ λ / D where D is the size of the recording medium
- Applied in two experiments at Fermilab in search of tau neutrino interactions in 1980s
  - Sensitive to large volumes – critical for neutrino experiments

Spatial and Temporal Resolutions

Detector Type	Accuracy (rms)	Resolution Time	Dead Time
Bubble chamber	10 to 150 μm	1 ms	50 ms[a]
Streamer chamber	300 μm	2 μs	100 ms
Proportional chamber	$\geq$ 300 μm[b,c]	50 ns	200 ns
Drift chamber	50 to 300 μm	2 ns[d]	100 ns
Scintillator	—	150 ps	10 ns
Emulsion	1 μm	—	—
Silicon strip	$\frac{\text{pitch}}{3 \text{ to } 7}$ [e]	[f]	[f]
Silicon pixel	2 μm[g]	[f]	[f]

[a] Multiple pulsing time.
[b] 300 μm is for 1 mm pitch.
[c] Delay line cathode readout can give ± 150 μm parallel to anode wire.
[d] For two chambers.
[e] The highest resolution ("7") is obtained for small-pitch detectors ($\lesssim 25$ μm) with pulse-height-weighted center finding.
[f] Limited at present by properties of the readout electronics. (Time resolution of ≤ 25 ns is planned for the ATLAS SCT.)
[g] Analog readout of 34 μm pitch, monolithic pixel detectors.

Electronic Detectors

- Scintillators
- Proportional counters
- Multi-wire proportional counters
- Wire drift chambers
- Time projection chamber

Scintillators

- Certain materials scintillate when excited by ionizing particles
- Rutherford had his grad students counting the scintillations from zinc-sulfide
- Plastic or polystyrene are in common use today, but other material scintillate as well
- Organic
  - crystalline
  - liquid
  - plastic
- Inorganic

Scintillator Mechanism

- Scintillation:
  - Molecules are excited by a passing charged particle.
  - Certain molecules will release a small fraction (~3%) of this energy as optical photons, in a process known as scintillation.
  - Scintillation is particularly important in organic substances which contain aromatic rings, such as polystyrene, polyvinyltoluene, and napthalene.
  - Liquids which scintillate include toluene and xylene.

PDG

Scintillator Mechanism

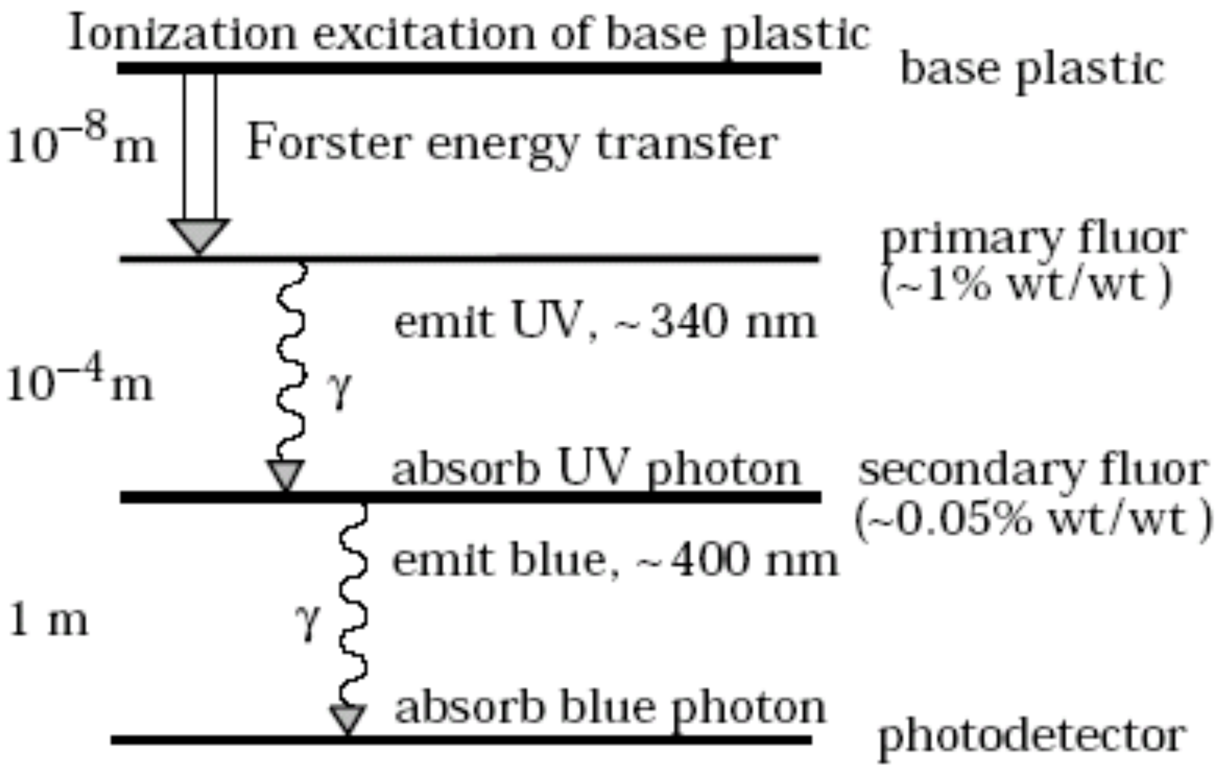

- Fluors
  (a) increase wavelength,
  (b) extend range of photons, and
  (c) speed up decay time

PDG

Fluorescence

- Fluorescence:
  - In fluorescence, the initial excitation takes place via the absorption of a photon, and de-excitation by emission of a longer wavelength photon.
  - Fluors are used as “waveshifters" to shift scintillation light to a more convenient wavelength.
  - Occurring in complex molecules, the absorption and emission are spread out over a wide band of photon energies, and have some overlap, that is, there is some fraction of the emitted light which can be re-absorbed.
  - This “self-absorption" is undesirable for detector applications because it causes a shortened attenuation length.

PDG

Scintillators

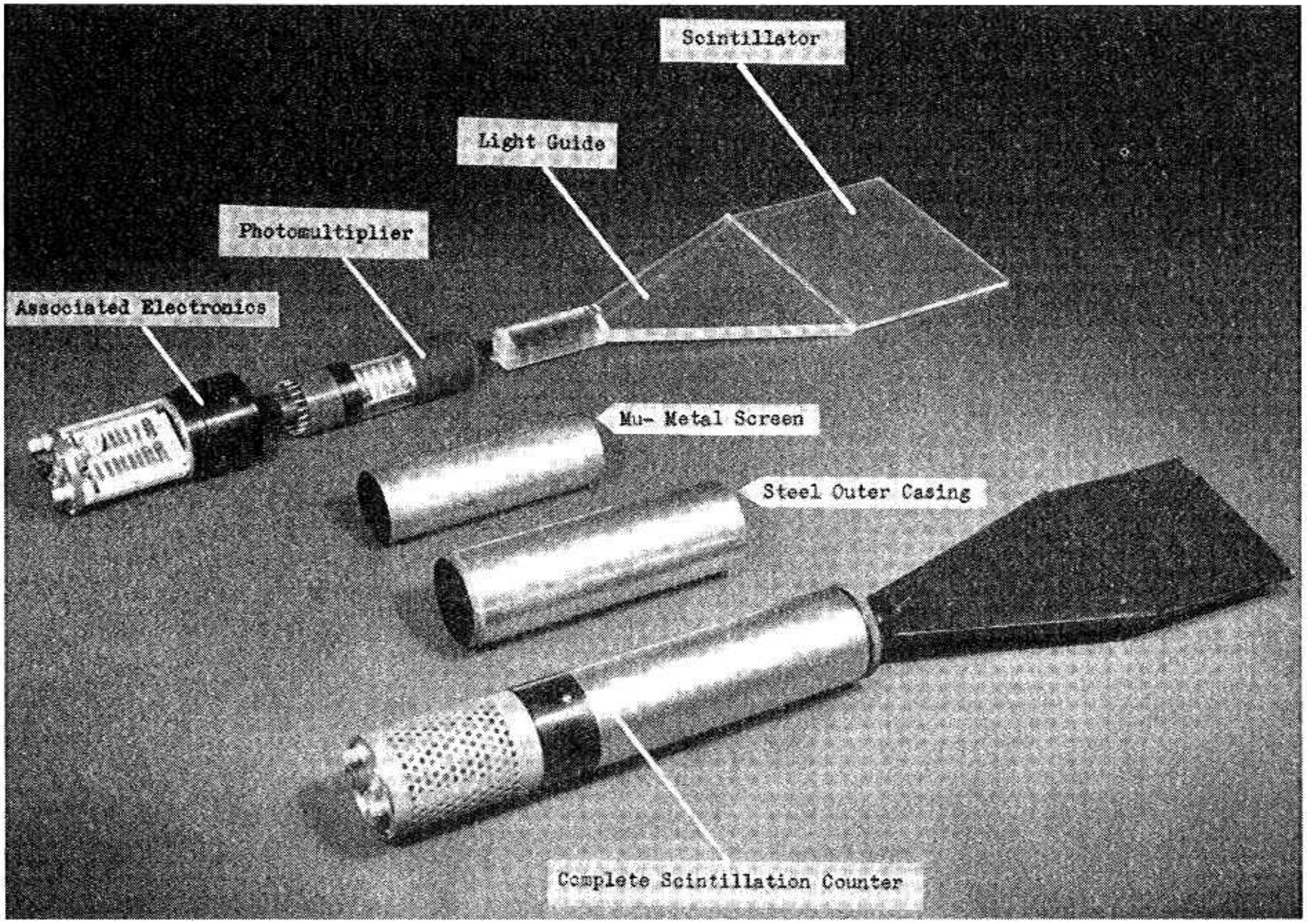

Organic Scintillators

- Most applications in HEP are plastic or liquid
- wide range of applications, extremely versatile

	Pulse height (relative to anthracene)	Decay time, ns	λ_{max}, Å	Density, g cm^{-3}
polystyrene + *p*-terphenyl	0.28	3	3550	0.9
polystyrene + tetraphenylbutadiene	0.38	4.6	4800	0.9
sodium iodide (+ thallium)	2.1	250	4100	3.7
anthracene	1.0	32	4100	3.7
toluene	0.7	<3	4300	0.9

Plastic Scintillators

- Plastic scintillators are reliable, robust, and convenient, but there are issue that must be dealt with
  - aging and handling
    - exposure can reduce light yield, and surface crazing destroys light transmission
  - attenuation length
    - care must be taken to ensure good transmission
  - afterglow
    - long-lived luminescence
  - atmospheric quenching
    - decrease light yield
  - magnetic field
    - small effects on light yield
  - radiation damage
    - reduced light yield, and attenuation length

Non-linear Response

- Plastic scintillators do not respond linearly to the ionization density.
  - Very dense ionization columns emit less light than expected on the basis of *dE/dx* for minimum ionizing particles.
  - A widely used semi-empirical model by Birks' posits that recombination and quenching effects between the excited molecules reduce the light yield.
  - These effects are more pronounced the greater the density of the excited molecules.
  - Birks' formula is

$$\frac{d\mathscr{L}}{dx} = \mathscr{L}_0 \frac{dE/dx}{1 + k_B\, dE/dx}$$

  - where $\mathcal{L}$ is the luminescence, $\mathcal{L}_0$ is the luminescence at low specic ionization density, and k_B is Birks' constant, which must be determined for each scintillator by measurement.

PDG

Inorganic Scintillators

Crystal	ρ (g/cm^3)	X_0 (cm)	$r_{\text{Molière}}$ (cm)	dE/dx (MeV/cm)	λ_I (cm)	τ_{decay} (ns)	λ_{max}	n_D	Rel. output*	Hygro?
NaI(Tl)	3.67	2.59	4.5	4.8	41.4	250	410	1.85	1.00	very
BGO	7.13	1.12	2.4	9.2	22.0	300	410	2.20	0.15	no
BaF_2	4.89	2.05	3.4	6.6	29.9	0.7^f	220^f	1.56	0.05^f	slightly
						620^s	310^s		0.20^s	
CsI(Tl)	4.53	1.85	3.8	5.6	36.5	1000	565	1.80	0.40	some
CsI(pure)	4.53	1.85	3.8	5.6	36.5	$10, 36^f$	305^f	1.80	0.10^f	some
						$36^f, 620^s$	$\sim 480^s$		0.20^s	
$PbWO_4$	8.28	0.89	2.2	13.0	22.4	5–15	420–440†	2.3	0.01	no
CeF_3	6.16	1.68	2.6	7.9	25.9	10–30	310–340	1.68	0.10	no

* For standard photomultiplier tube with a bialkali photocathode. See Ref. 27 for photo-diode results.

† Emission $\sim$ 500 nm also possible due to crystal defects.

f = fast component, s = slow component

Photomultiplier Tubes

- Light from scintillator was, in the past, typically recorded by photomultiplier tubes
  - Silicon-based photodiodes have now become quite common, replacing the role of phototubes
- photcathode coated by alkali metals
- amplification through dynode chain
  - 10^8 for 14 dynodes
- transit time ~ 50 nsec
- jitter ~ nsec
- quantum efficiency ~25%

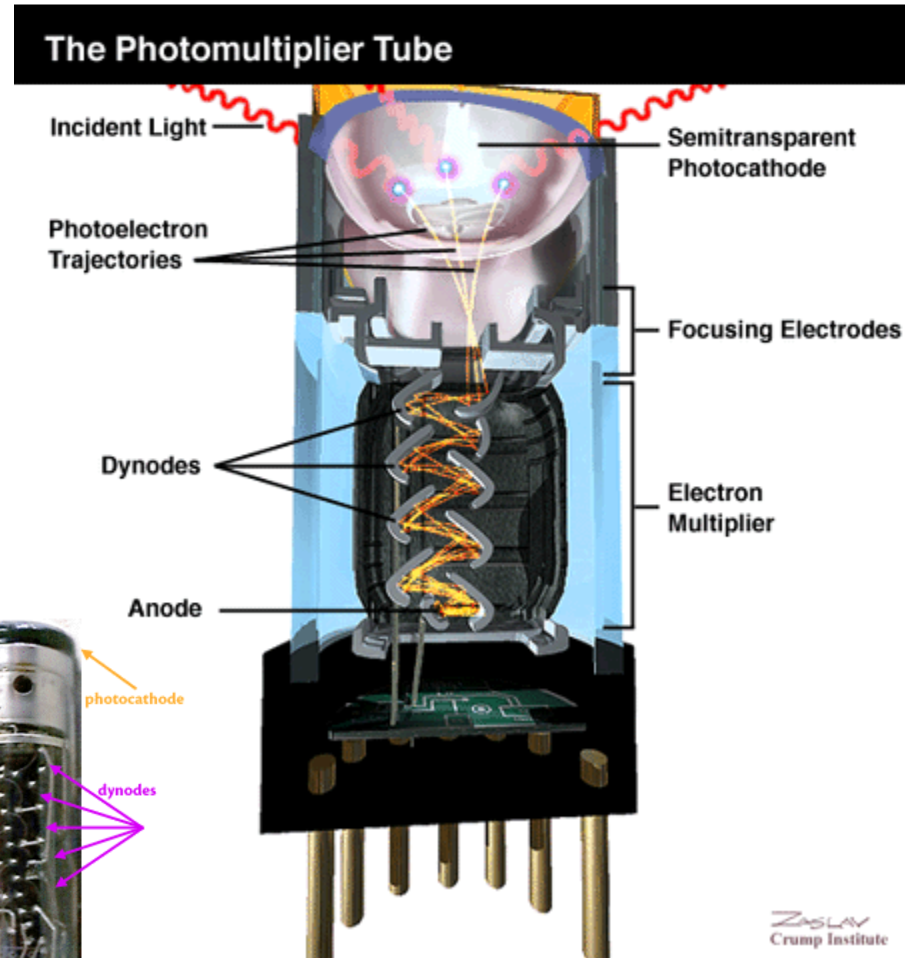

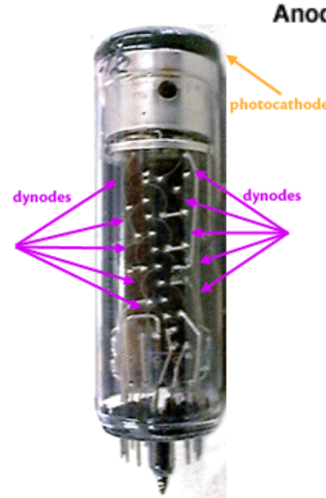

Typical Phototube - 931A

931A, 931B

Photomultiplier

28-mm (1-1/8 inch) Diameter 9-Stage, Side Window PMTs

- Anti-Hysteresis Design
- Narrow Range of Anode Sensitivities
  931A: 30 A/lm - 600 A/lm
  931B: 100 A/lm - 1000 A/lm
- Low Dark Current

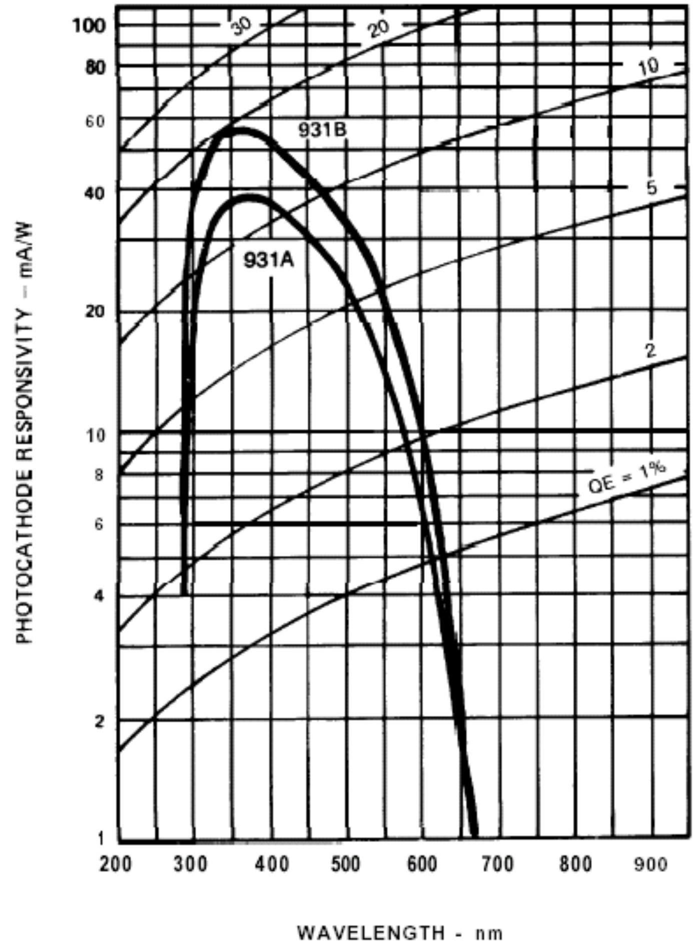

Figure 1 - Typical Photocathode Spectral Response Characteristics

Super K Phototubes

- Super Kamiokande
  - 11,146 tubes (20-inch diameter)

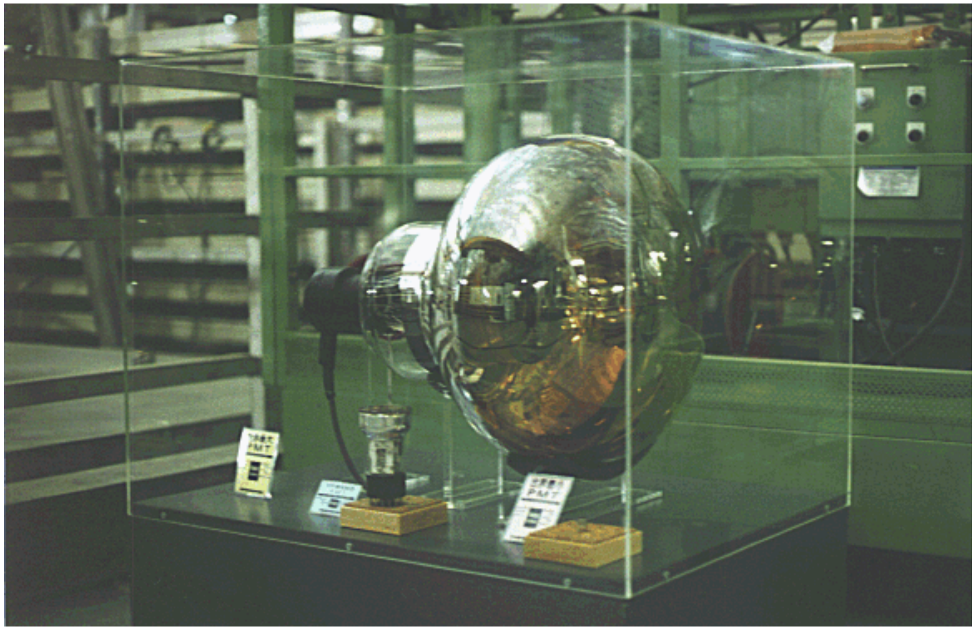

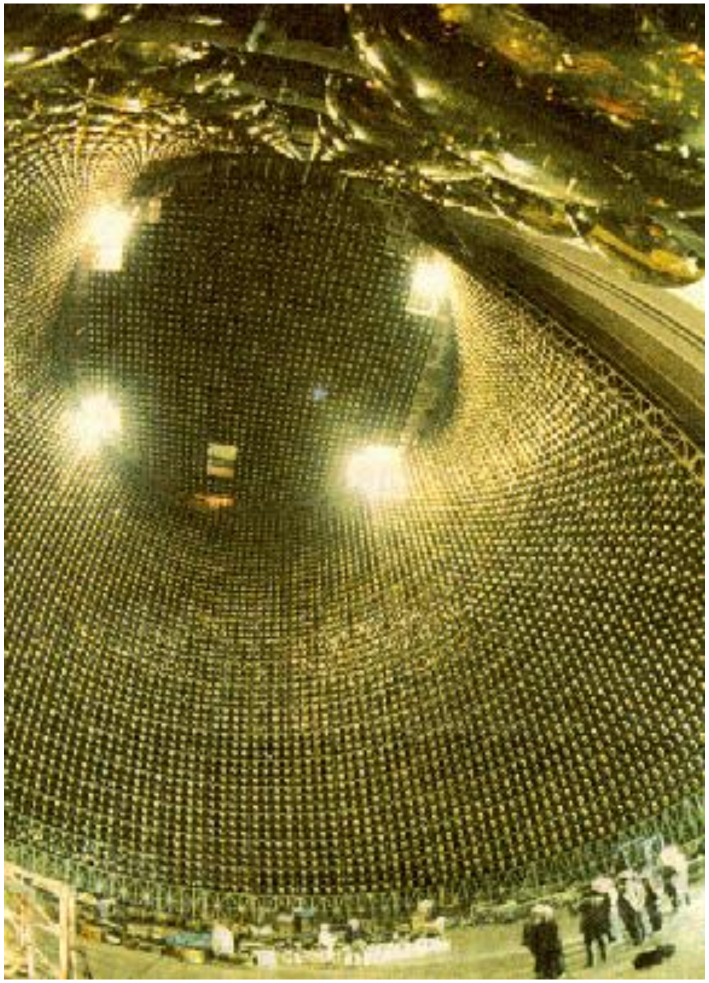

Photodiodes

- Higher quantum efficiency
- Lower power consumption
- More compact
- Improved ruggedness
- Immune to magnetic fields
- Good time response

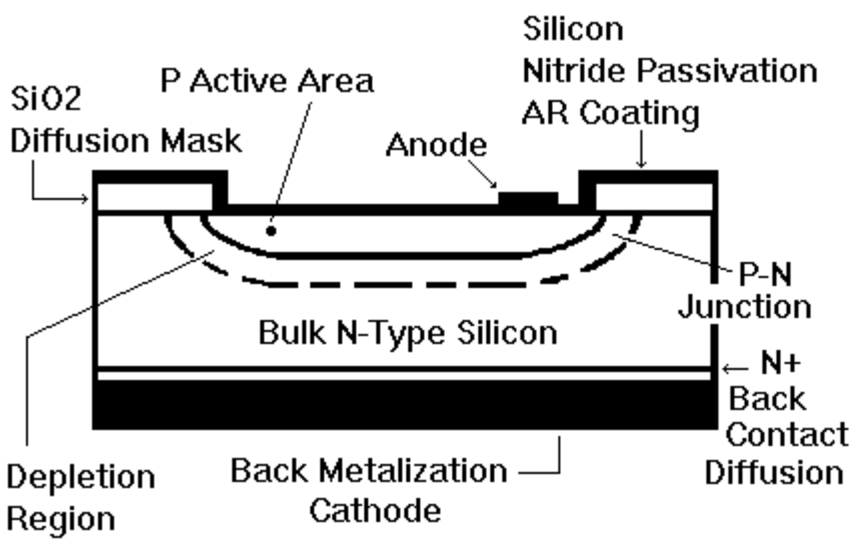

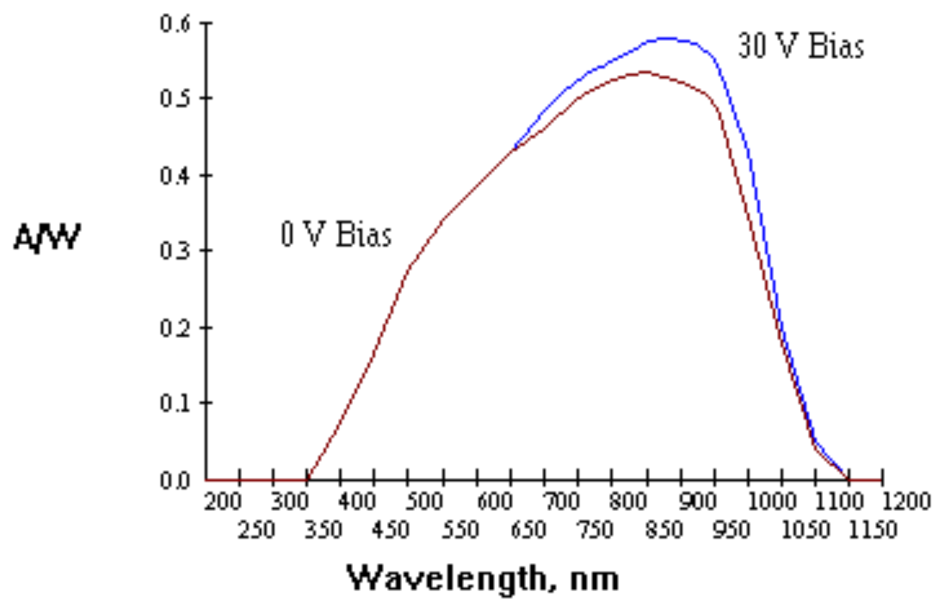

Light Path in Scintillator

- Light may be extracted from scintillator to phototube or photodiode by internal reflection (multiple reflection down light guide)
- Alternative approach - wavelength shifter bars along edge of scintillator
  - blue light from scintillator re-emitted as green

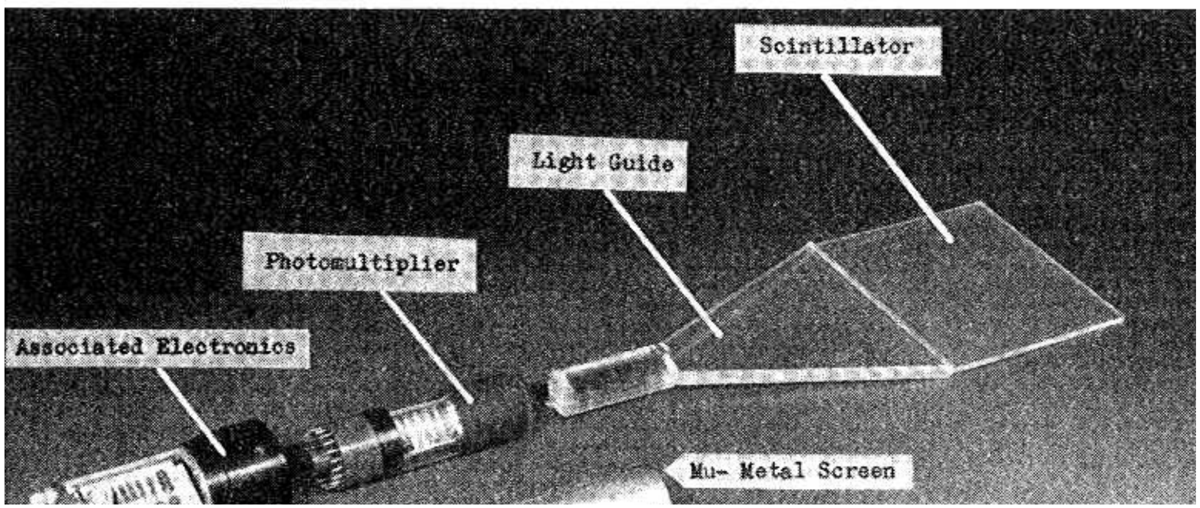

Proportional Counter

- Developed over a century ago
- Gas-filled cylindrical tube of radius r_2 at negative potential, with central anode wire of radius r_1 at positive potential

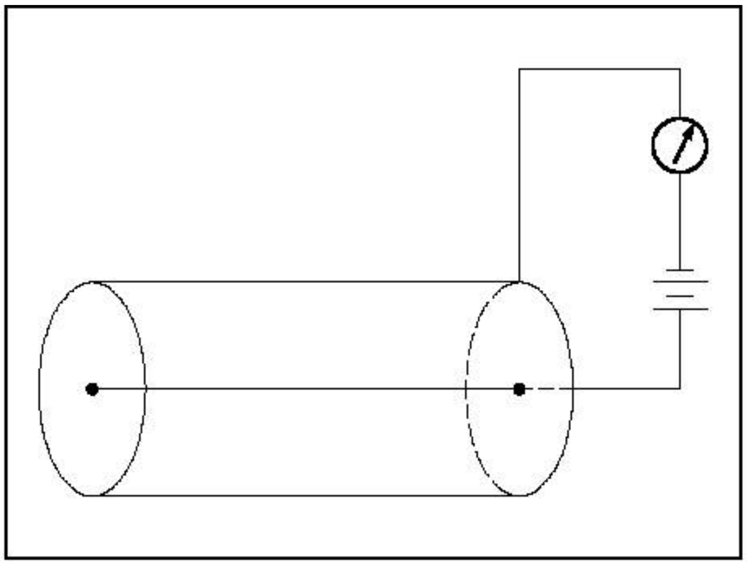

Proportional Counter

- For potential difference V_0, the electric field is

$$E(r) = \frac{V_0}{r \ln(r_2/r_1)}$$

- Liberated electrons drift toward anode, gaining energy.
- An avalanche is initiated if energy gain exceeds ionization energy
- Gas amplification of ~10^5 is typical, but independent of the number of primary ions "proportional counter"

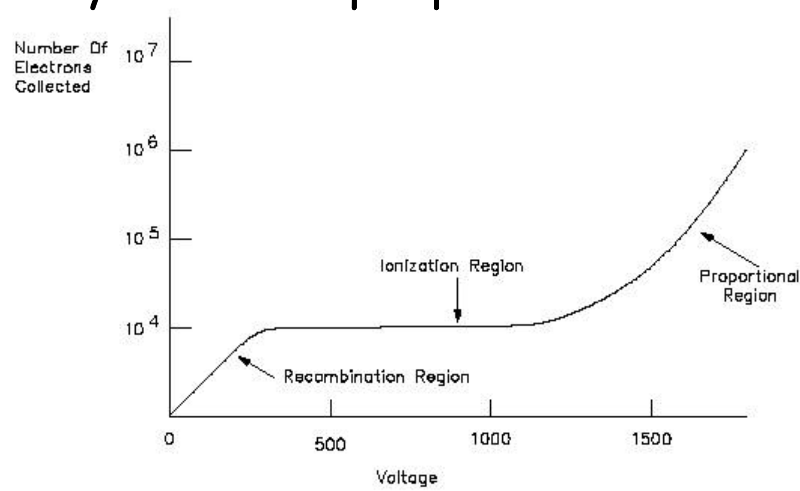

Multiwire Proportional Counter (MWPC)

- Around 1968, Charpak developed the MWPC
- Many parallel anode wires in a plane between two cathode planes
- Each wire is an independent detector
- Typical: 20 μm diameter wires, 5/cm, 12mm between cathodes, 5kV, argon-isobutane gas

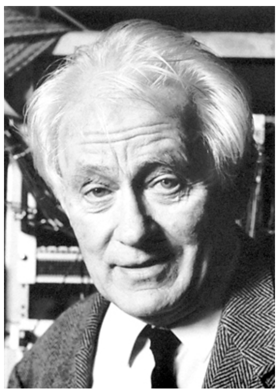

G. Charpak
1992 Nobel Prize

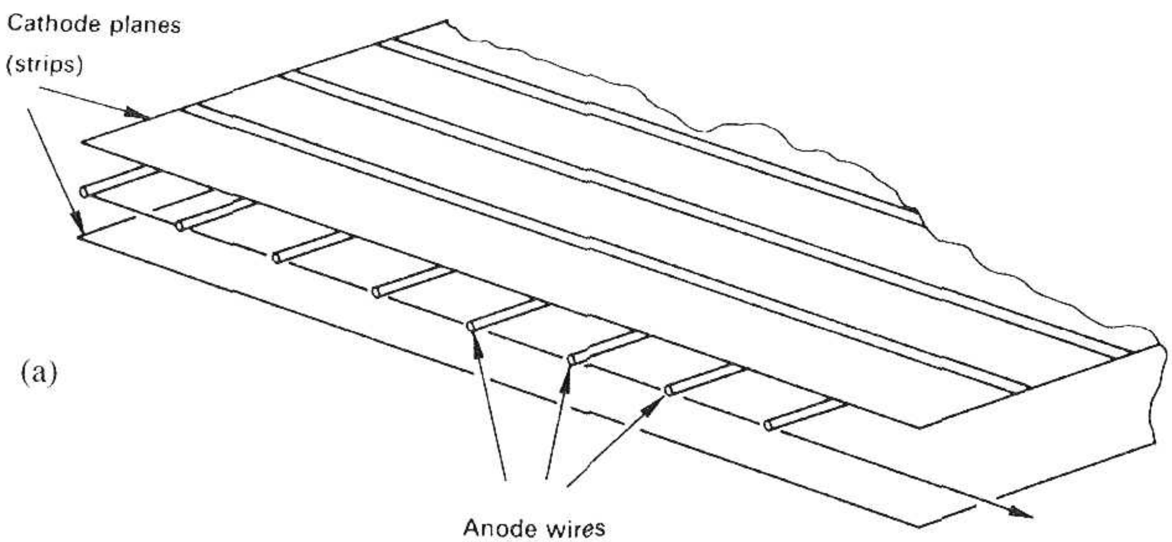

Multiwire Proportional Counter (MWPC)

- Electric Field Lines

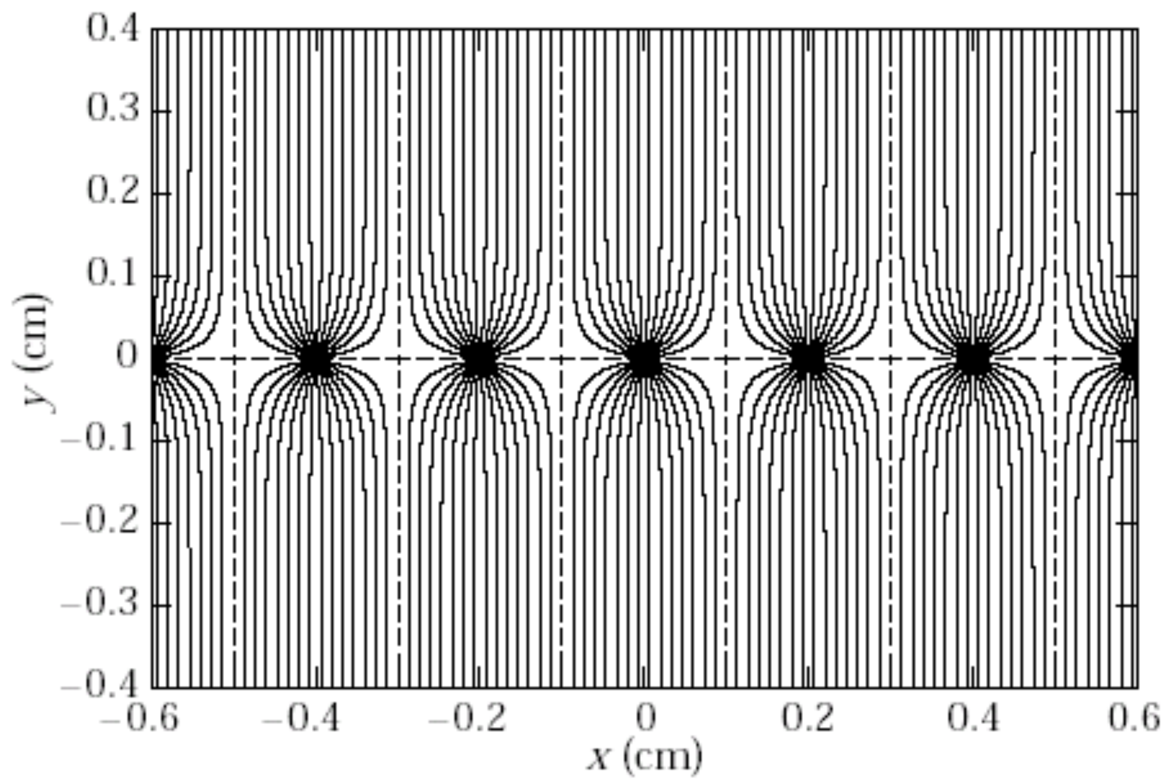

Multiwire Proportional Counter (MWPC)

- Fast rise time (0.1 nsec) arising from first arriving electrons
- Positive ions are slower, resulting in pulses of ~30 nsec duration
- Spatial resolution ~ 0.7 mm from anode pulses
- Cathode strips can be used to measure spatial coordinate of the avalanche (with about 0.05 mm precision)

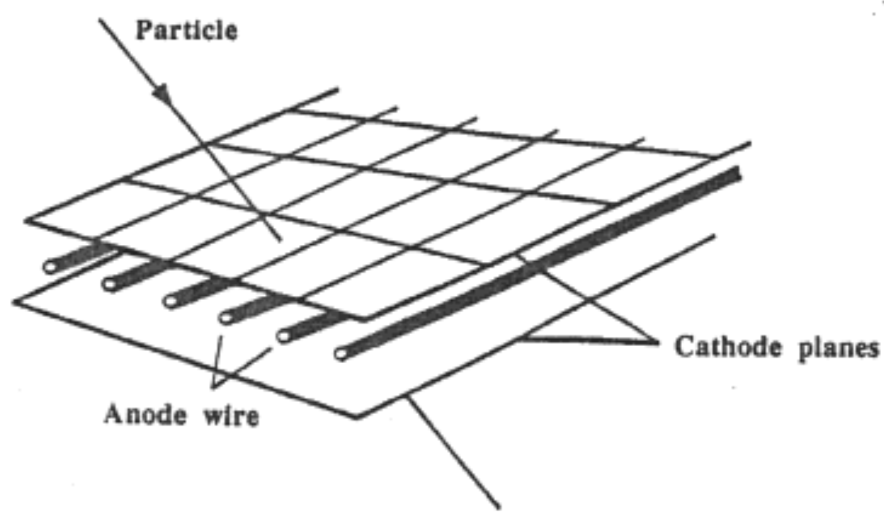

Wire Drift Chambers

- MWPCs require large number of wires and are limited to resolutions of about 1 mm and time resolutions of about 30 ns
- By drifting the charge, the number of wires can be significantly reduced, and the resolutions improved.
- Drift in field of ~ 1 kV/cm over 10 cm, amplify at anode
  - arrival time give measure of position

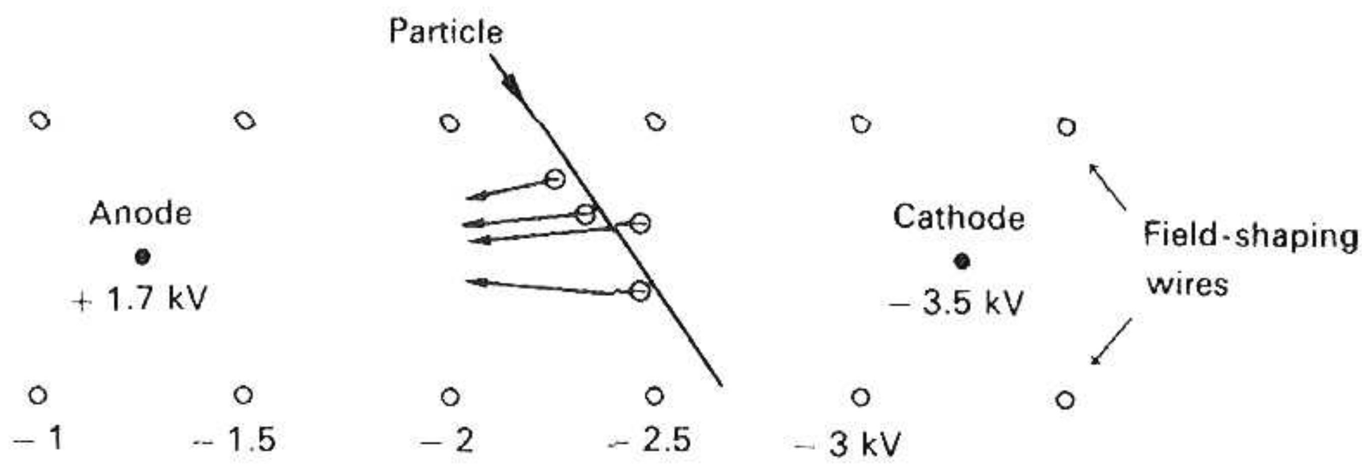

Wire Drift Chambers

- SLD Drift Chamber

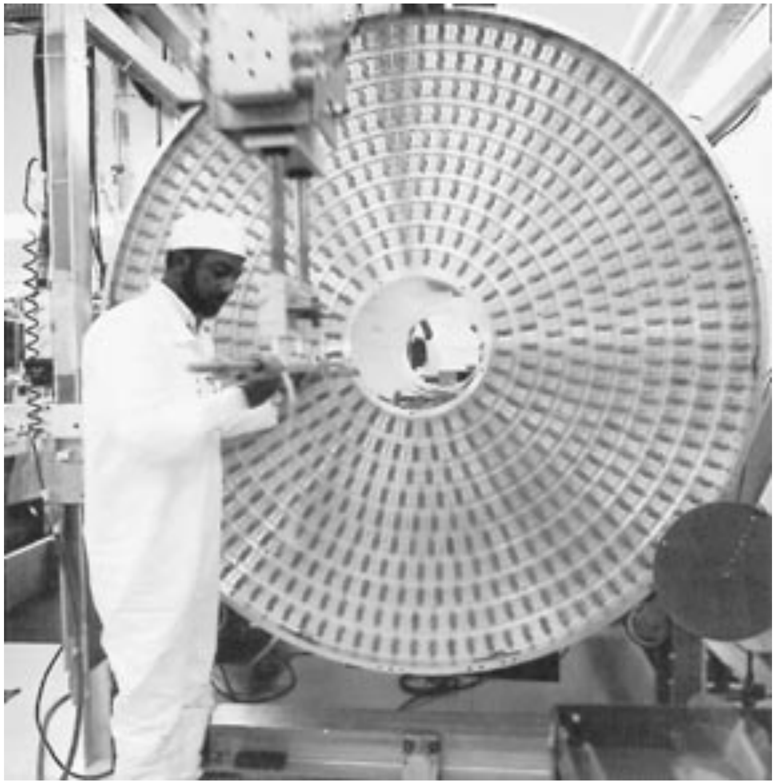

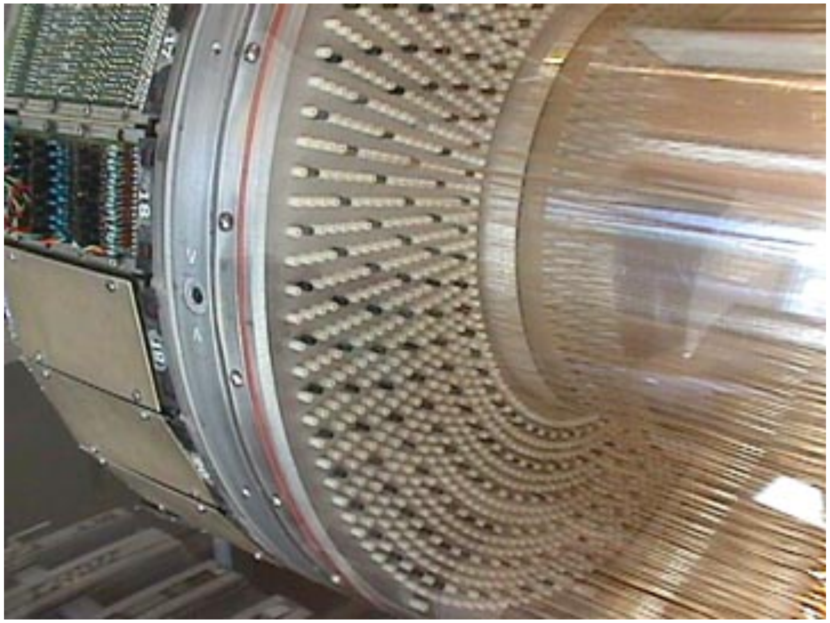

Wire Drift Chambers

- SLD Drift Chamber

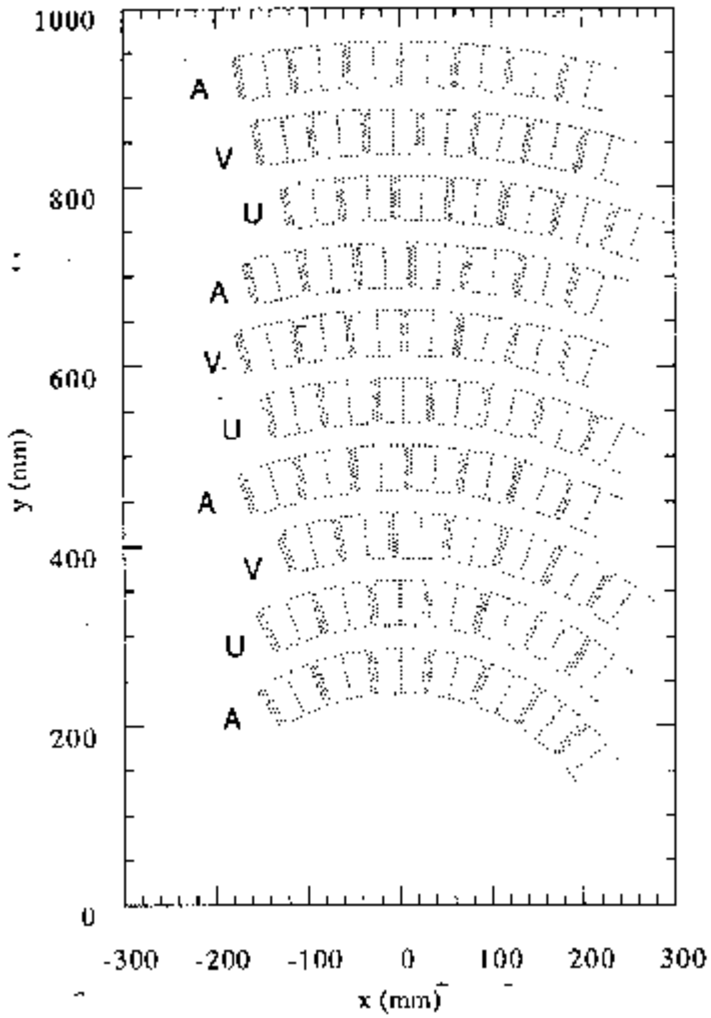

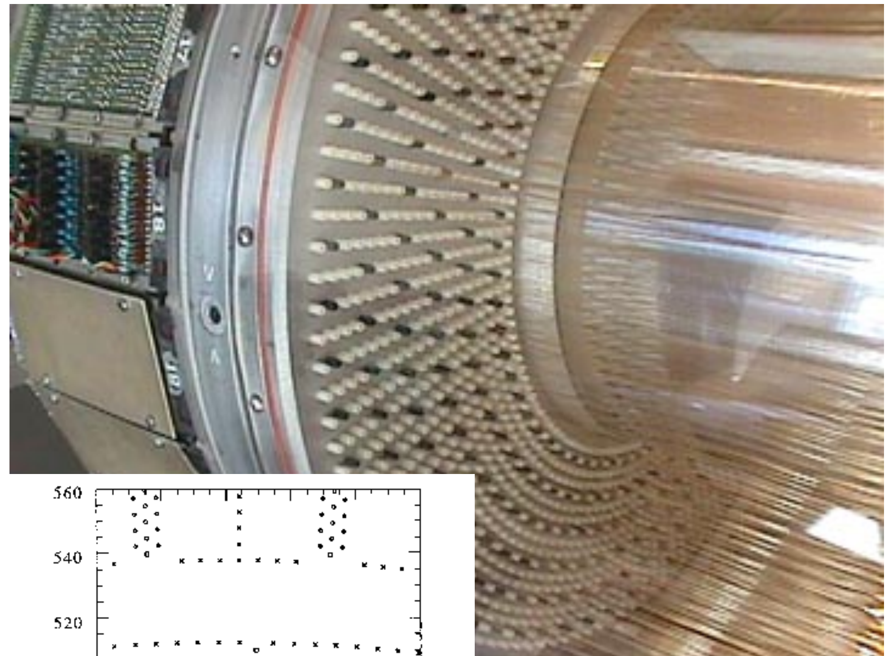

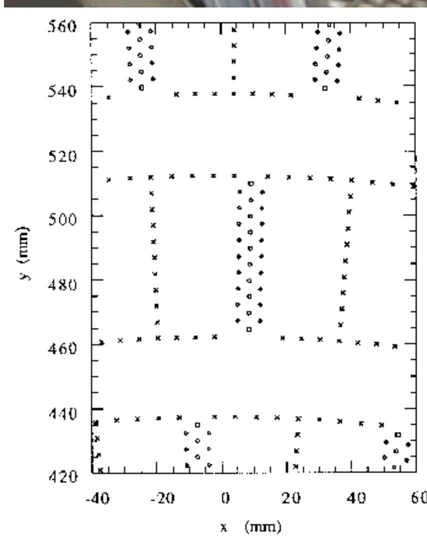

~100 μm resolution

Wire Drift Chambers

- SLD Drift Chamber

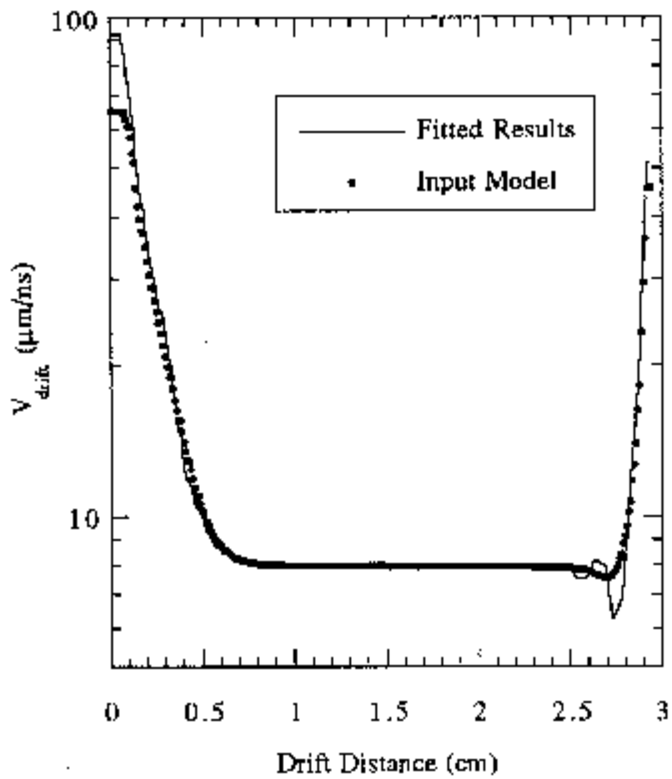

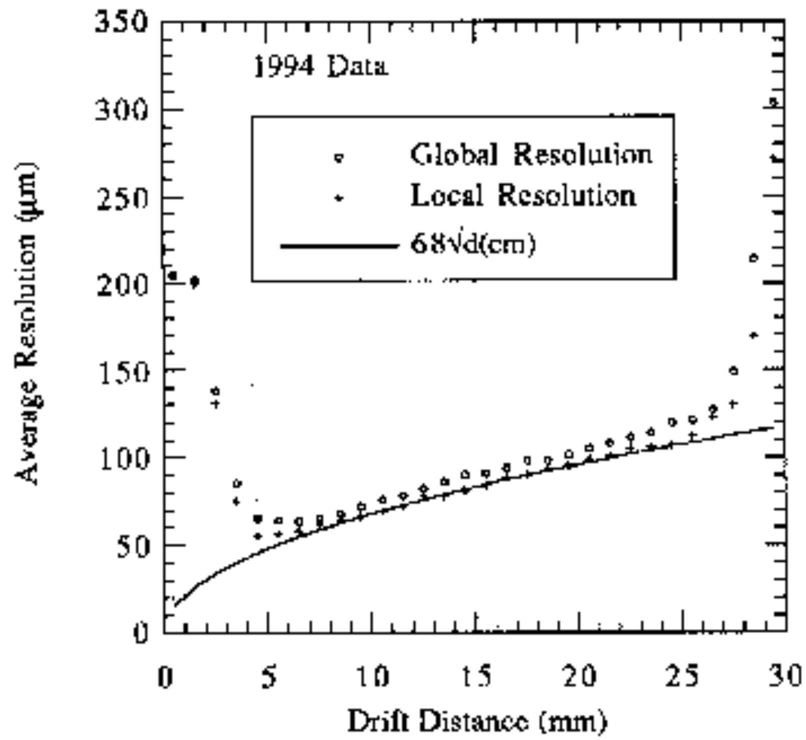

Time Projection Chamber

- Uniform electric field drifts ionization electrons to a 2D array of detectors at the end.
  - drift along the magnetic field direction to eliminate v x B force

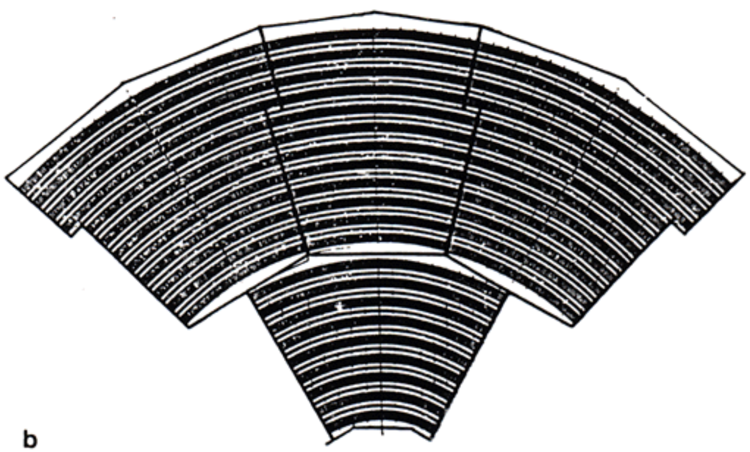

ALEPH TPC

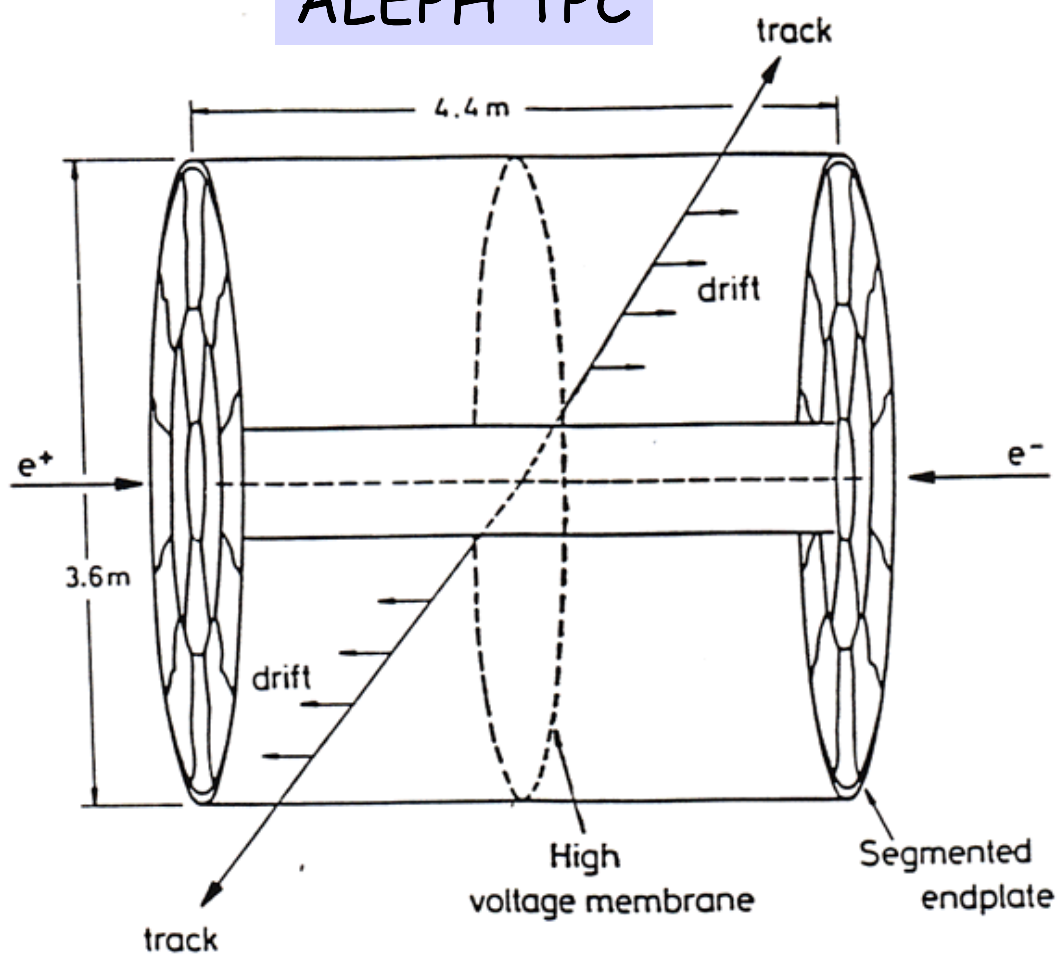

ALICE TPC @ LHC

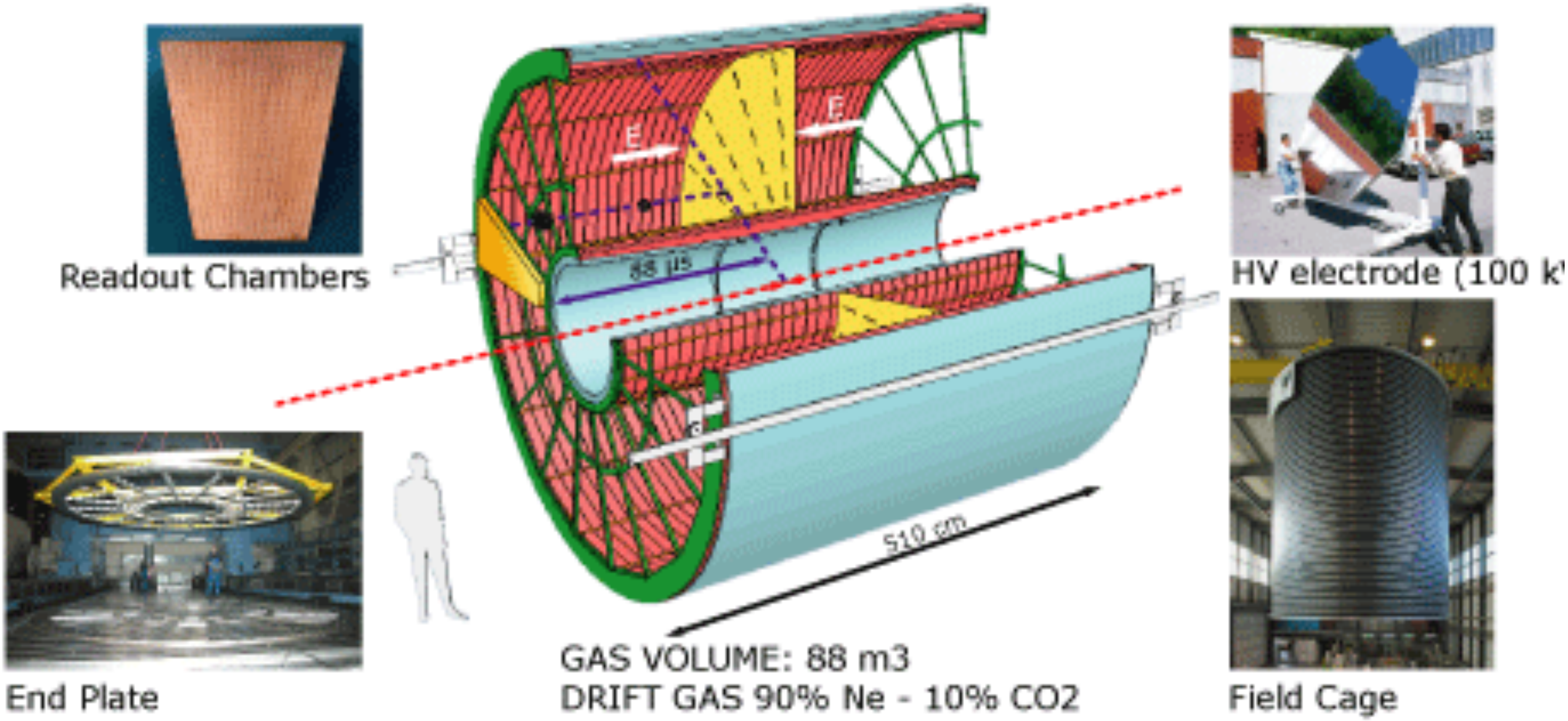

Cerenkov Counters

- Threshold detectors
- Differential detectors
- Ring Imaging detectors

Cerenkov Counters

- Part of the light emitted as a particle passes through a dielectric medium at a velocity exceeding the speed of light in the medium appears as a coherent wavefront

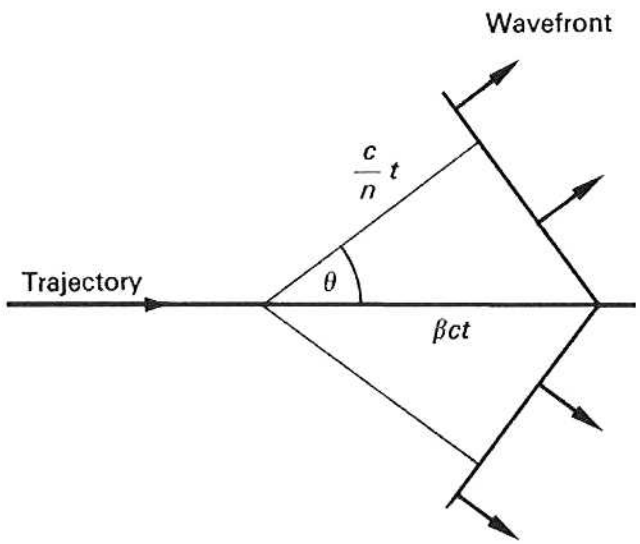

$$\cos\theta = \frac{ct/n}{\beta ct} = \frac{1}{\beta n}, \qquad \beta > \frac{1}{n}$$

Cerenkov Counters

- Cerenkov radiation

$$\frac{d^2 N_\gamma}{dx\,dE} = \frac{\alpha z^2}{\hbar c}\left(1 - \frac{1}{\beta^2 n^2}\right)$$

- blue light predominates
  - well known blue glow from reactor
- Total rate of energy loss:

$$\frac{dW}{dx} = \frac{\alpha z^2}{\hbar c}\int\left(1 - \frac{1}{\beta^2 n^2}\right) E\,dE$$

$$= \frac{\alpha z^2}{2\hbar c}\left[(h\nu_1)^2 - (h\nu_2)^2\right]\left(1 - \frac{1}{\beta^2 n^2}\right)_{\text{av}}$$

  - a small fraction of the energy loss

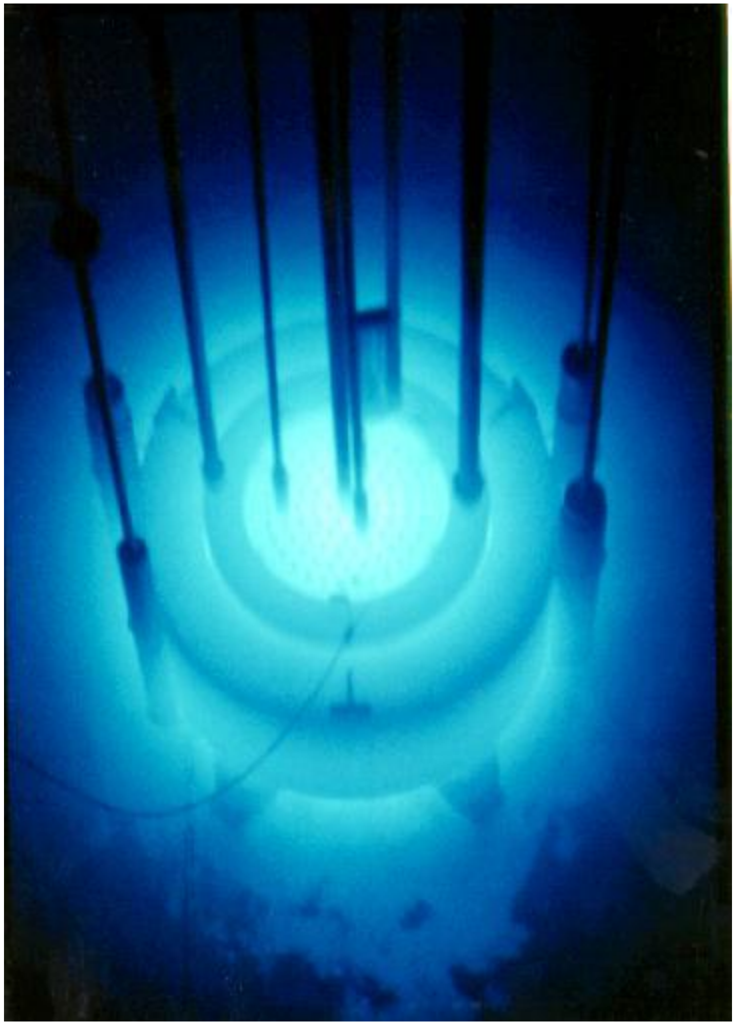

Cerenkov Counters

- The angle of emission of radiation is a measure of the velocity of the particle

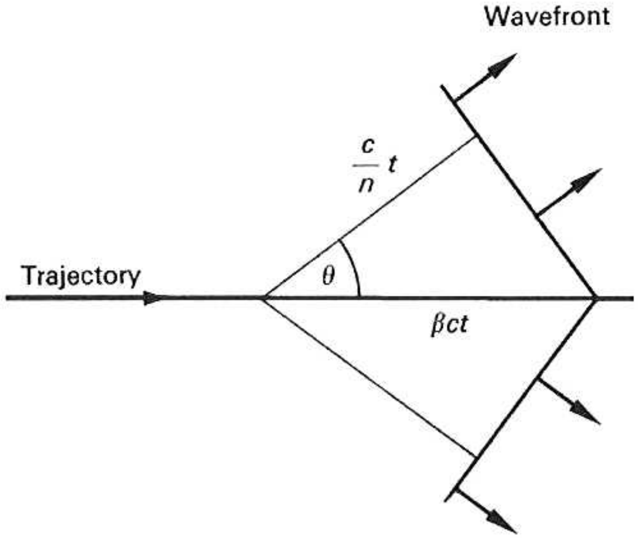

$$\cos\theta = \frac{ct/n}{\beta ct} = \frac{1}{\beta n}, \qquad \beta > \frac{1}{n}$$

Medium	$n-1$	γ (threshold)
helium (NTP)	3.3×10^{-5}	123
CO_2 (NTP)	4.3×10^{-4}	34
pentane (NTP)	1.7×10^{-3}	17.2
aerogel	$0.075 \to 0.025$	$2.7 \to 4.5$
H_2O	0.33	1.52
glass	$0.75 \to 0.46$	$1.22 \to 1.37$

Threshold Cerenkov Counters

- If two particles of different mass carry the same momentum, the lighter particle may emit Cerenkov radiation, while the heavier does not

•For example, in helium at NTP, the threshold for radiation is γ = 123

• A 100 GeV/c pion has a $\gamma \approx$ 700, above the threshold while a 100 GeV/c proton has a $\gamma \approx$ 106, below threshold

Medium	$n - 1$	γ (threshold)
helium (NTP)	3.3×10^{-5}	123
CO_2 (NTP)	4.3×10^{-4}	34
pentane (NTP)	1.7×10^{-3}	17.2
aerogel	$0.075 \rightarrow 0.025$	$2.7 \rightarrow 4.5$
H_2O	0.33	1.52
glass	$0.75 \rightarrow 0.46$	$1.22 \rightarrow 1.37$

Differential Cerenkov Counters

- Since the angle of emission of radiation is a measure of the velocity of the particle, by measuring the angle, one can determine velocity

$$\cos\theta = \frac{ct/n}{\beta ct} = \frac{1}{\beta n}, \qquad \beta > \frac{1}{n}$$

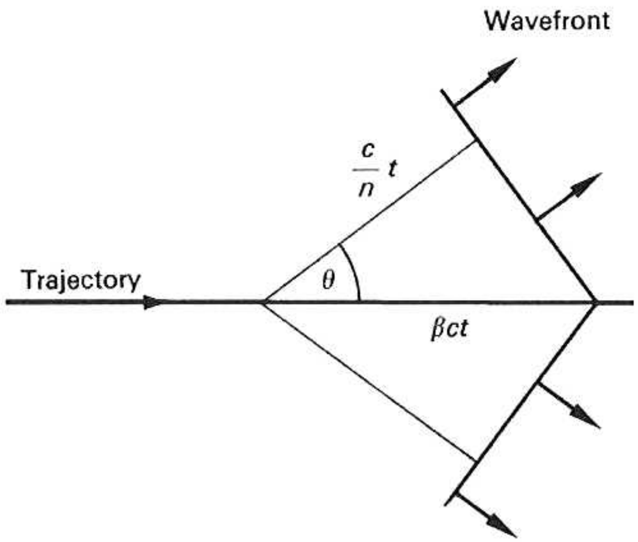

Medium	$n - 1$	γ (threshold)
helium (NTP)	3.3×10^{-5}	123
CO_2 (NTP)	4.3×10^{-4}	34
pentane (NTP)	1.7×10^{-3}	17.2
aerogel	$0.075 \rightarrow 0.025$	$2.7 \rightarrow 4.5$
H_2O	0.33	1.52
glass	$0.75 \rightarrow 0.46$	$1.22 \rightarrow 1.37$

Ring Imaging Cerenkov Counters

- eg. SLD and DELPHI

  light at angle θ_c is focussed by mirror of radius R on ring CD

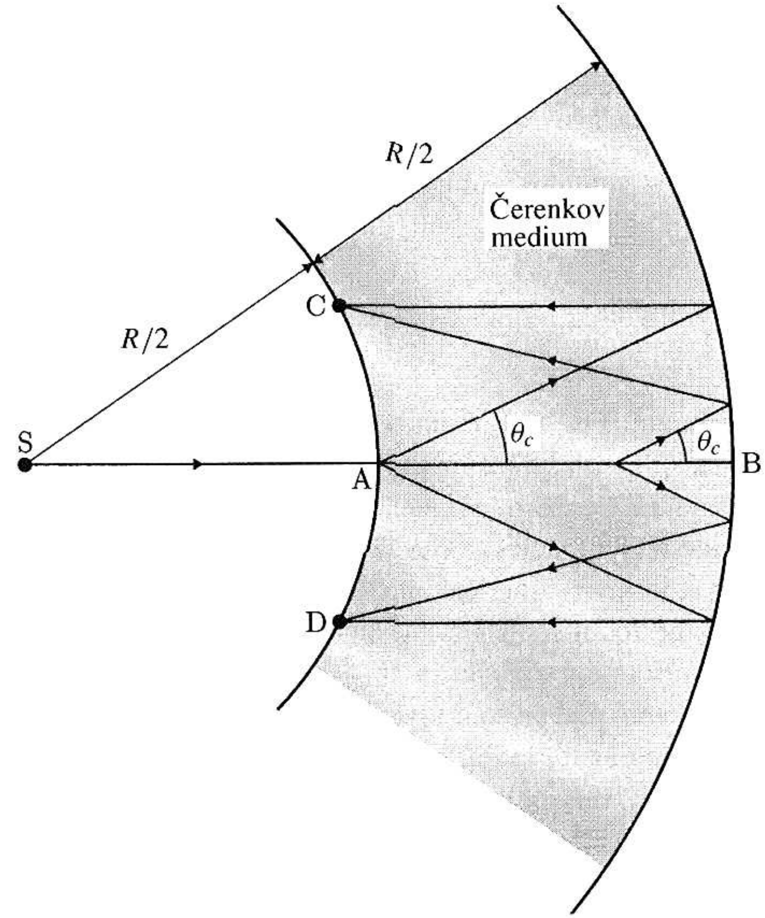

Ring Imaging Cerenkov Counters

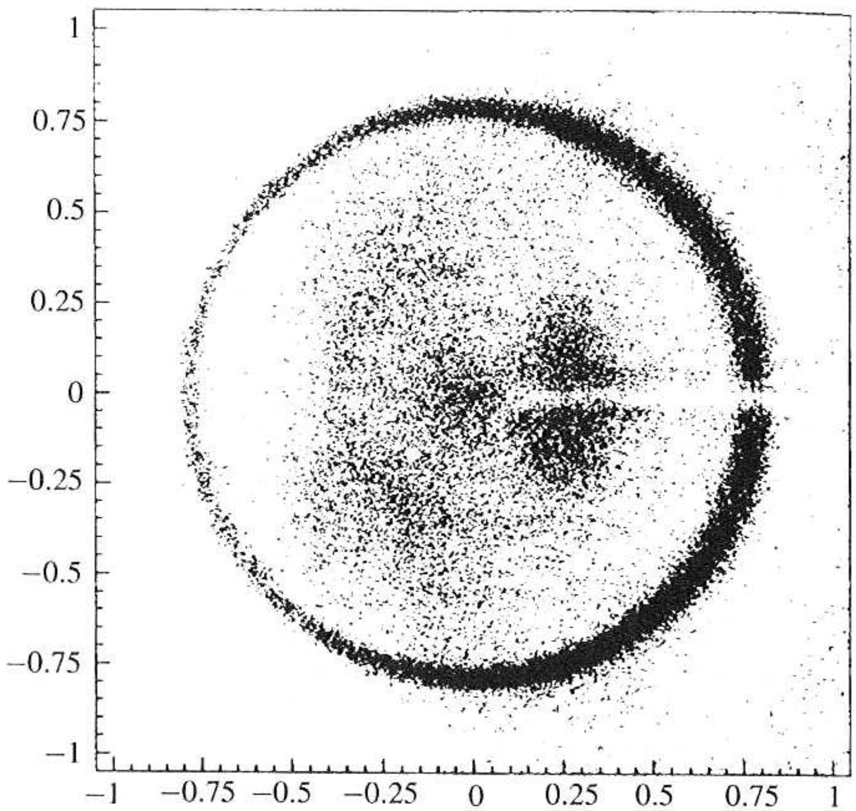

Muon in liquid (C_6F_{14})

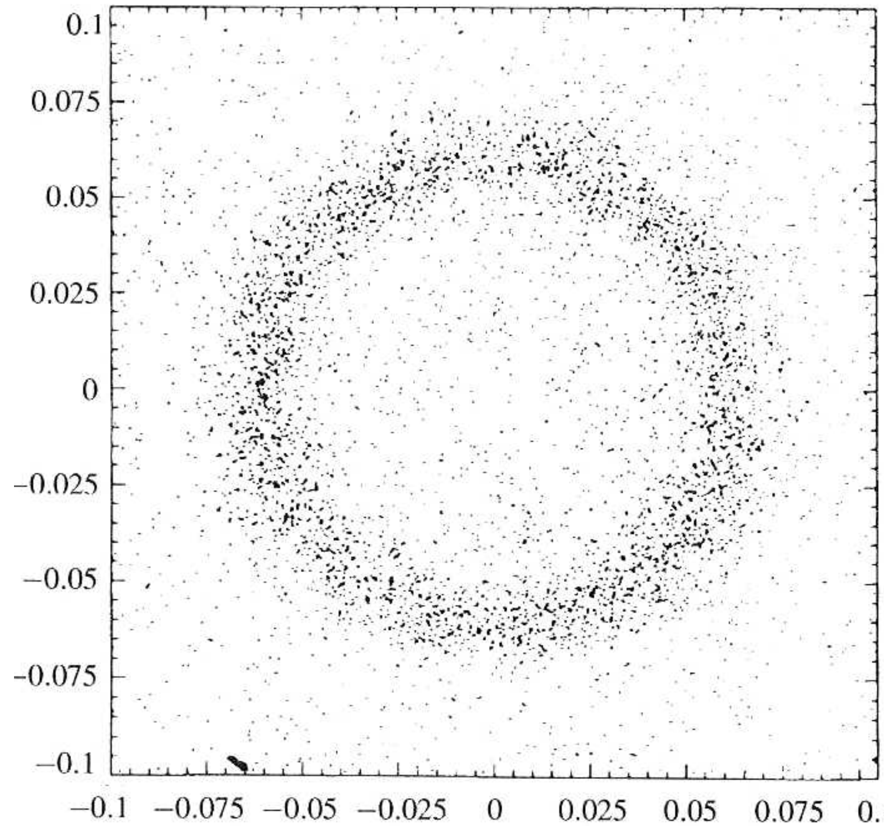

Muon in gas (87% C_5F_{12} 13% N_2)

Ring Imaging Cerenkov Counters

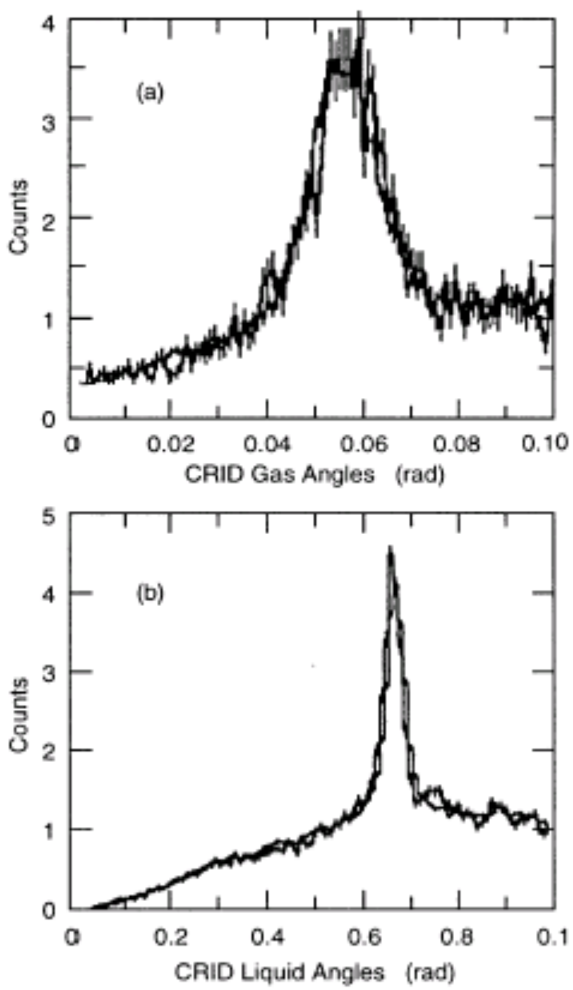

CRID final performance for gas and liquid rings for simple events such as di-muons [11]

Parameter	Gas rings	Liquid rings
Total fraction of photoelectrons contributing to the "final efficiency" compared to the "starting efficiency"	0.70	0.53
Mean photon energy (eV)	6.70	6.50
Mean refractive index	1.001646	1.27202
Mean Cherenkov angle (mrad) ($\beta = 1$ particle)	57.33	666.24
Calculated for radiator length (cm)	45	1
N_o [cm^{-1}]	80	42
Expected average number of photoelectrons per full ring ($\beta = 1$ particle) [11]	11–12	16
Measured average number of photoelectrons per full ring (di-muons) [34]	10	16–17

Transition Radiation

- When a relativistic charged particle crosses the interface of two media of different dielectric constants optical transition radiation is emitted.
- This radiation can be used to discriminate between electrons and photons, due to the the fact that the total energy loss of particle depends on the Lorentz factor
  - for a given energy, the lighter particles have a higher Lorentz factor, and therefore radiate more than heavier particles

ATLAS Transition Radiation Tracker

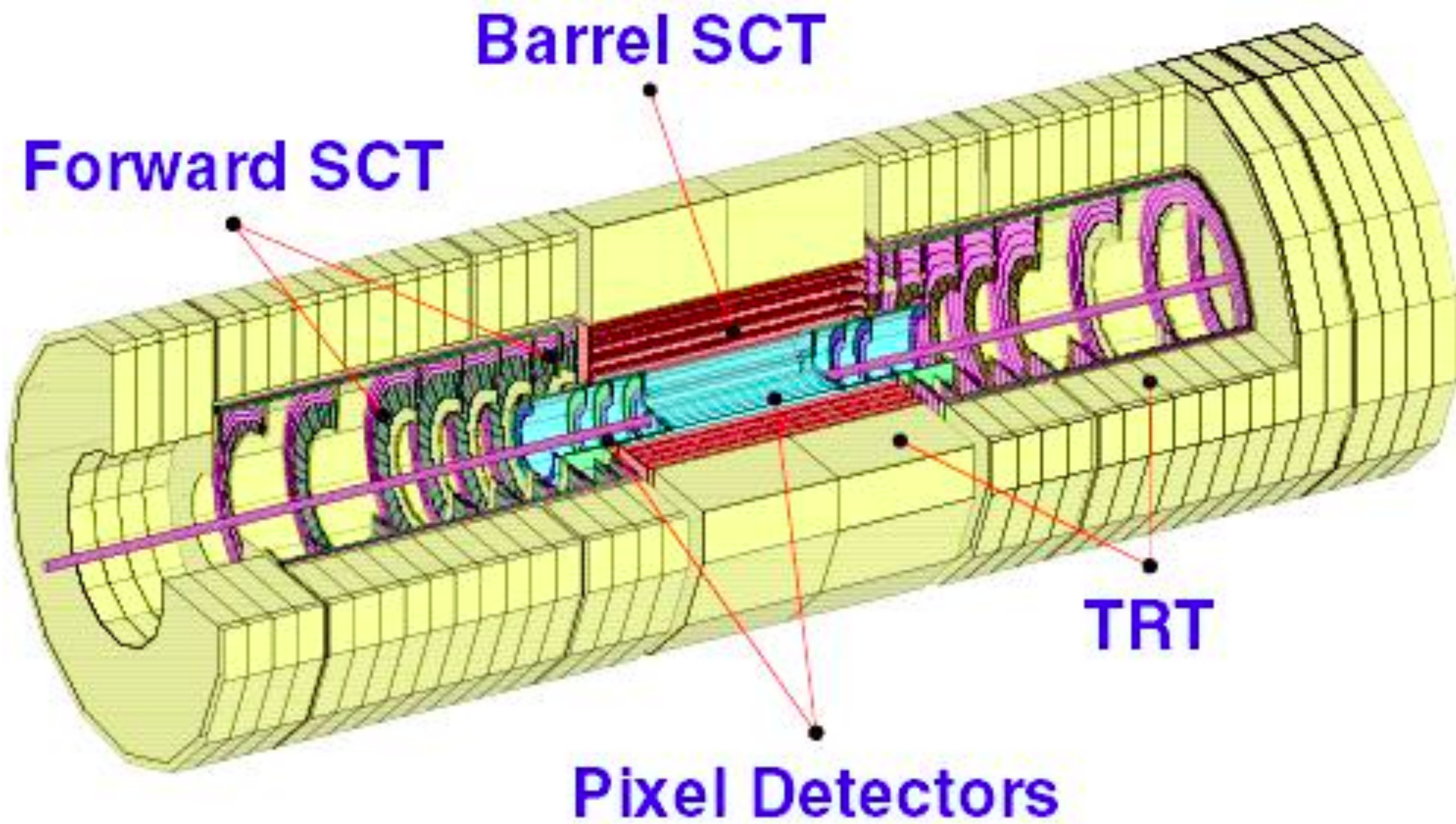

Solid State Detectors

- Silicon detectors in nuclear physics
- Microstrip detectors
- Hybrid pixels detectors
- Silicon drift detectors
- CCDs
- CMOS detectors
- Diamond detectors

Silicon Detectors

- Silicon detectors have several advantages over gas detectors
  - one major advantage is the small energy required to produce pair
    - 3.6 eV / electon-hole pair
    - 1.1 eV band-gap
  - excellent response time
    - few nanoseconds
  - many years of use in nuclear physics
    - position localization accuracy of 5 μm in one coordinate
    - two-track separation down to 10 μm
    - geometrical accuracy in the region of 1 μm
    - bias voltages less than 100 V for microstrip detectors
    - time response less than 5 ns
    - relatively simple installation.

Silicon Detectors

- Theory of silicon junction
  - depleted region is the region where the free carriers have been removed
  - electron-hole pairs created in the depletion region will be swept out by the bias voltage

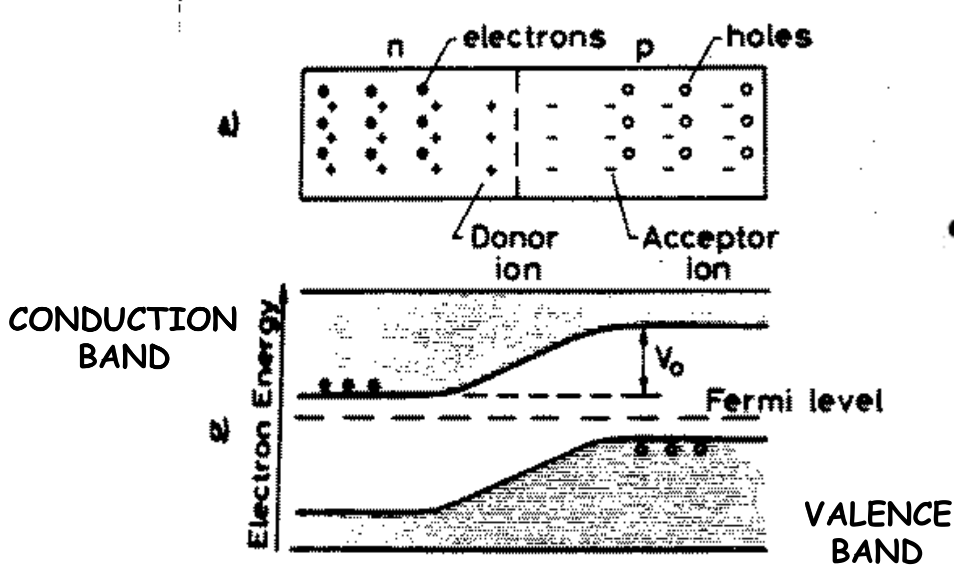

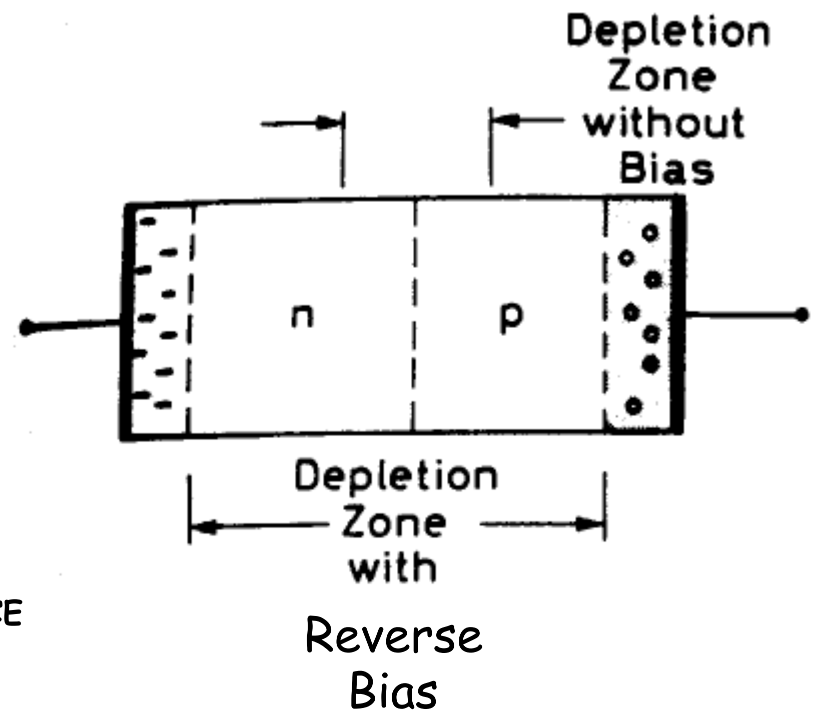

Silicon Detectors

- Theory of silicon junction
  - The thickness of the depletion depth is

$$d = 0.5\ \mu m\ \sqrt{\rho(\Omega cm)\ V(volts)}$$

  - Therefore, for large depletion depth with moderate voltage, need high resistivity, ~ 2-5 k Ωcm

$$d = 0.5\ \mu m\ \sqrt{\rho(\Omega cm)\ V(volts)}$$

$$d = 0.5\ \mu m\ \sqrt{4 \times 10^3\ 100}$$

$$d \approx 300\ \mu m$$

Silicon Detectors

- Blankenship Nomogram
  - IEEE Trans NS7, 190 (1960)

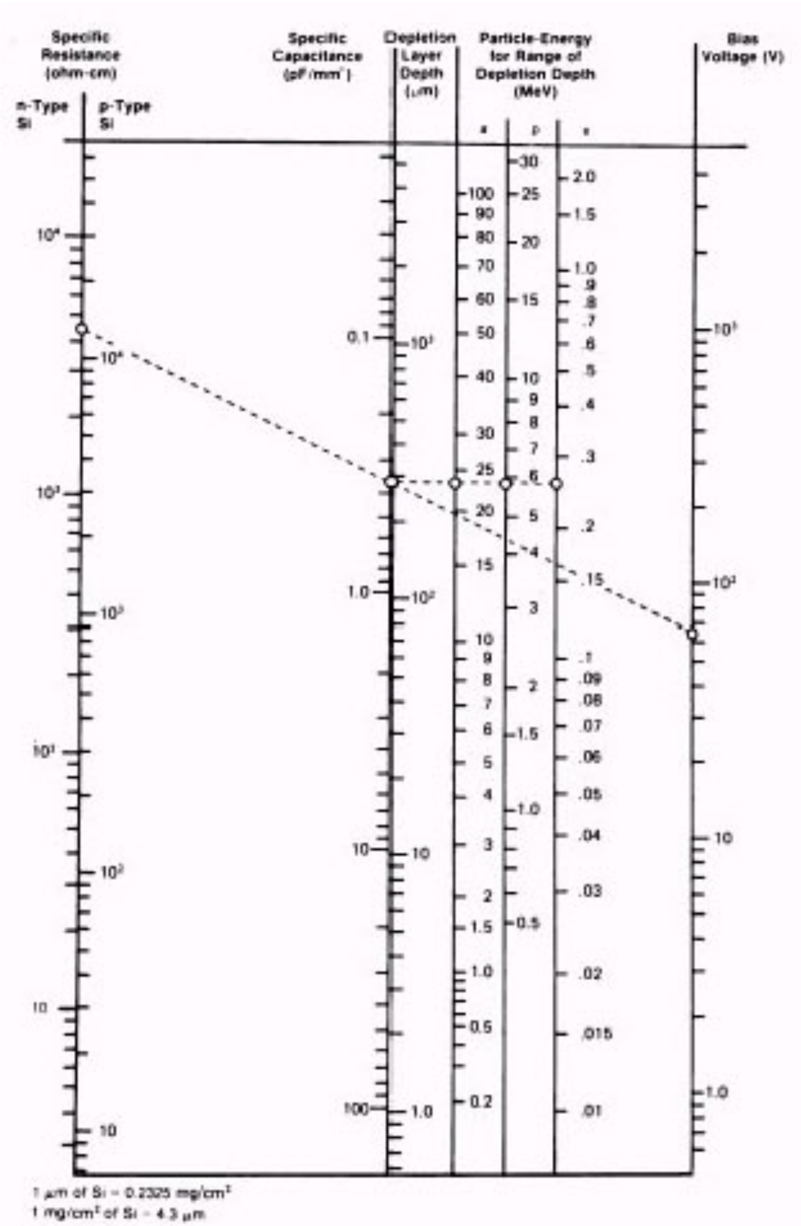

A straight edge intersecting the center vertical line at the required depletion depth will give combinations of resistivity and detector bias that may be used to achieve that depth. (Shown, for example, is the voltage that must be applied to a 13,000 Ω-cm p-type or 4500 Ω-cm n-type silicon detector to stop a 23-MeV alpha, a 6-MeV proton, or a 250-keV electron within the depletion depth.)

Silicon Microstrip Detectors

- 1980 - Kemmer introduced planar technology
- Outstanding performance has since been achieved with microstrip detectors

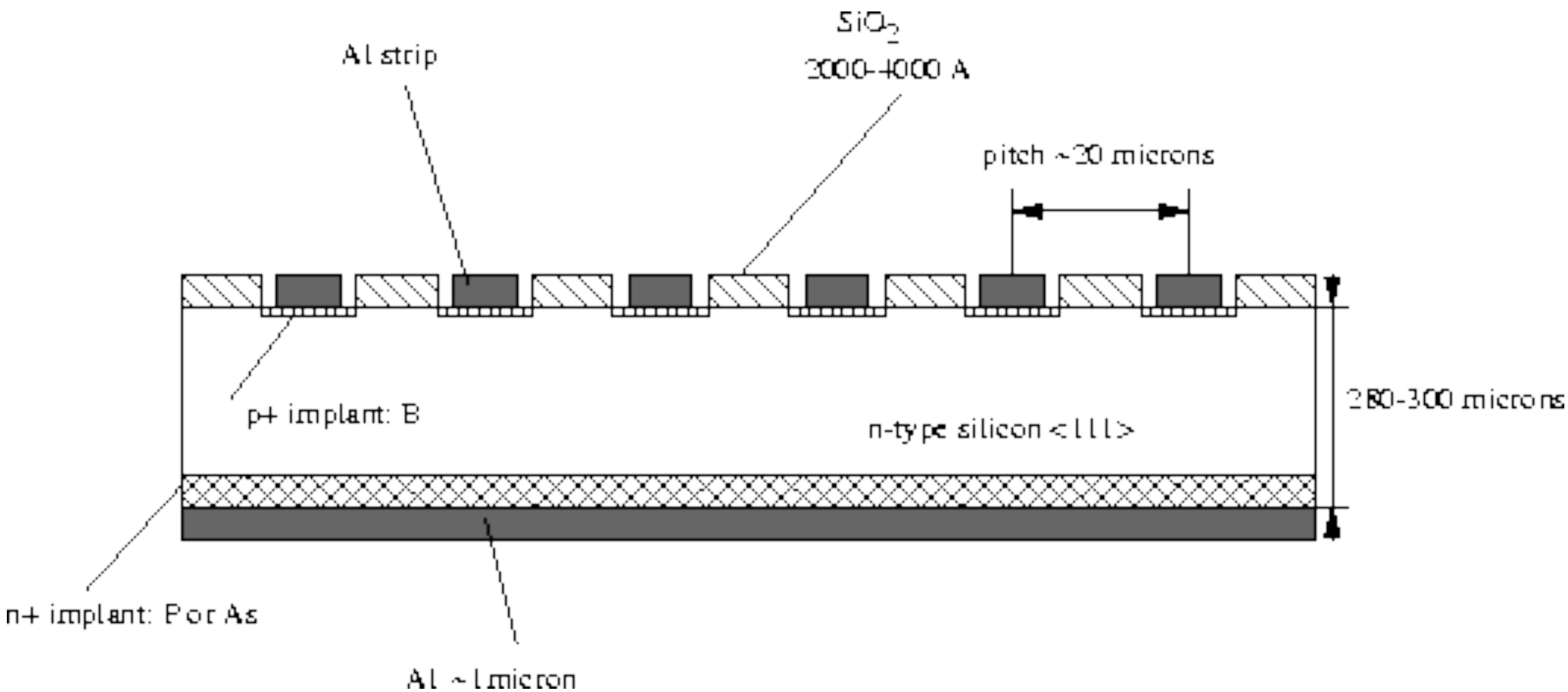

Silicon Microstrip Detectors

- Star ladder construction

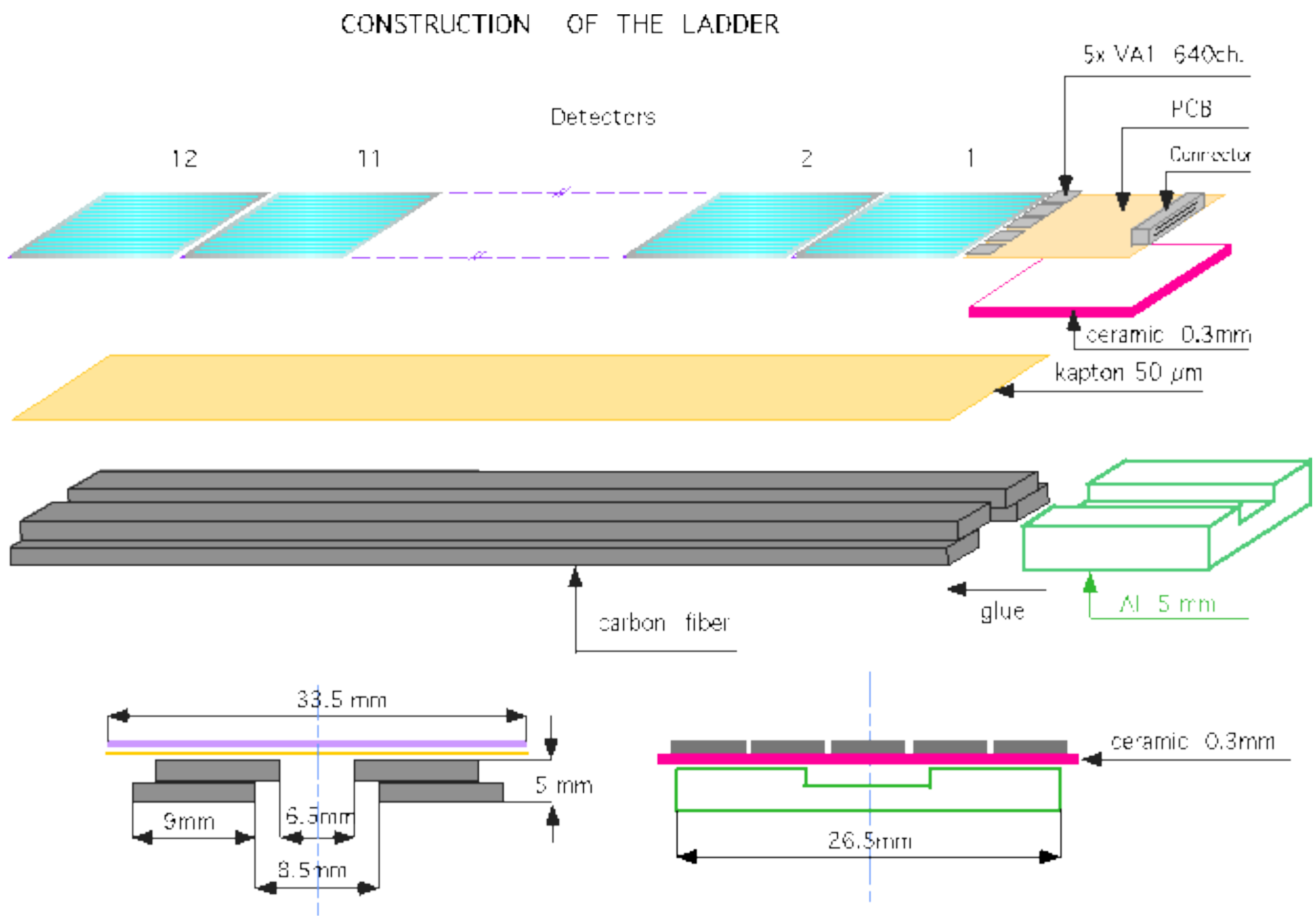

Hybrid Pixel Detectors

- Pixel detectors are 2D detectors

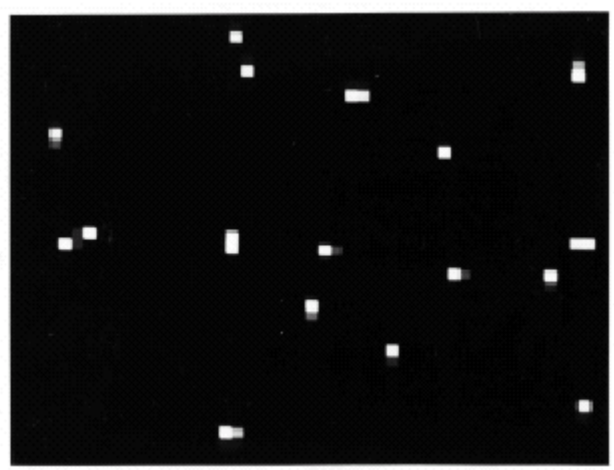

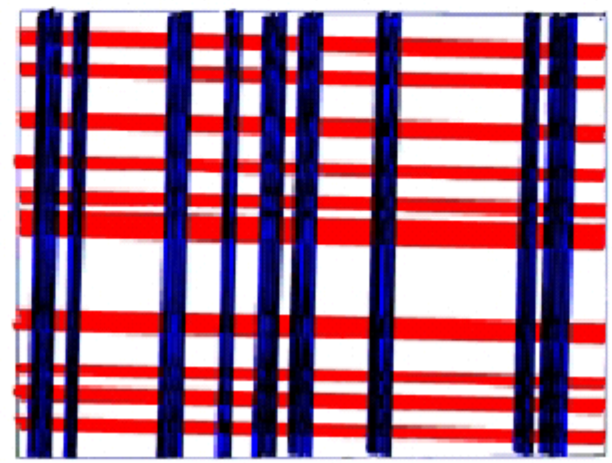

- Great reduction in ambiguities

Hybrid Pixel Detectors

- Hybrid pixel detectors have been developed for LHC
  - rad hard
  - fast
  - high background rate near IP rules out microstrips

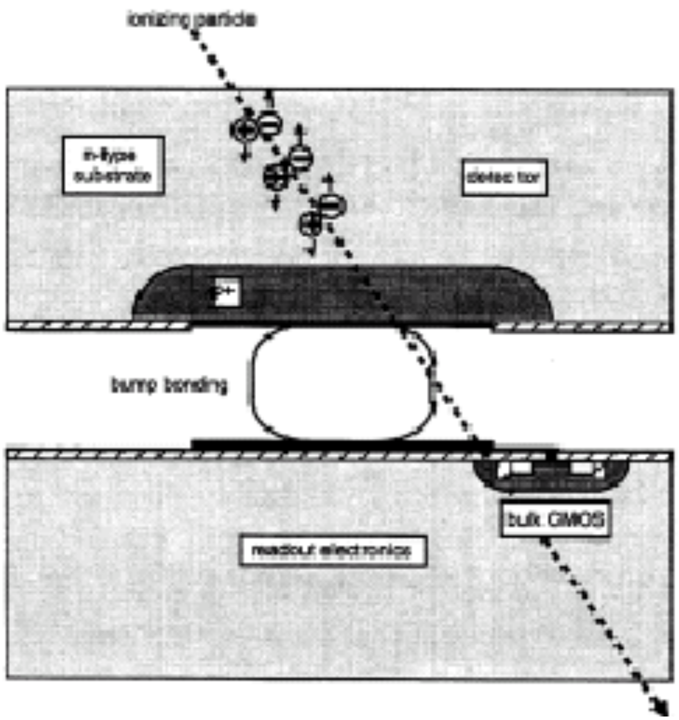

<u>Disadvantages</u>
- large power consumption
- large pixel sizes
- thick devices (multiple scatt)
  (compared to CCDs)

Silicon Drift Detectors

- The passage of an ionizing particle through the detector generates about 25,000 electron-hole pairs in 300 μm of silicon.
- A silicon drift detector is a fully depleted device with rectifying junctions on both sides of the wafer.
- Applying a negative voltage on both sides of the wafer, a potential minimum for electrons is formed near the center of wafer.
- Holes are collected at the nearest rectifying junction.
- The potential in the center of the wafer is linearly decreasing towards the anodes at the edge of the detector, and electrons drift in this direction at speed v=uE.
- From the position of the signal in the anode coordinate, and from the drift time it is possible to reconstruct the original hit position.

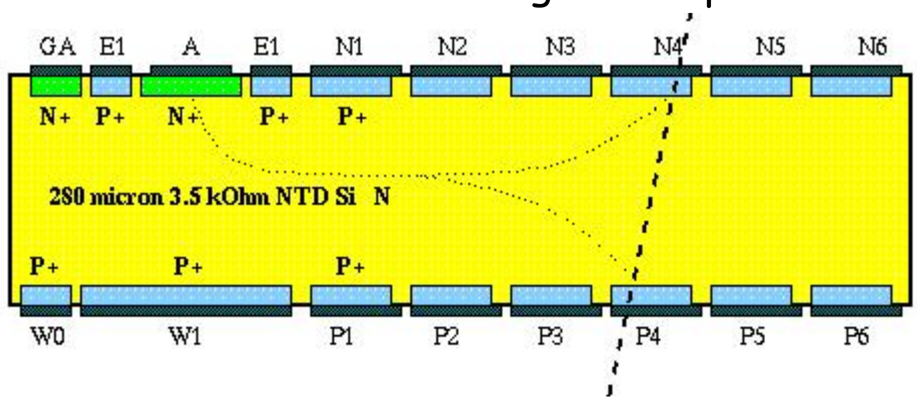

CCD Principles

CCDs were invented more than 40 years ago:

W.S. Boyle, G.E. Smith, Bell Syst. Tech. J. 49, 587 (1970)

Their use a particle detectors was first proposed more than 30 years ago:

C.J.S. Damerell et al., Nucl. Inst. and Meth. 185, 33 (1981)

The most advantageous feature of the CCD for particle detection is the highly segmented pixel structure (20 μm x 20 μm x 20 μm)

when charge sharing between pixels is used to optimize position resolution, better than 4 μm resolution has been achieved in a <u>large</u> <u>system</u> (307,000,000 pixels) <u>operating for years</u>

The most limiting feature is the relatively slow readout speed:

eg. about 100 msec is required to read out a large detector (<u>Linear Collider</u> well matched to this speed. Note: > 1000x faster readout is under development)

CCD Charge Collection

Charge collection principles

- n+ on p-type substrate (usually)

- lightly doped epitaxial p layer
- heavily doped p^+ substrate
- top ~ 1 μm of p layer doped by
  - ion implantation (n^+)

- depletion region (~ 5 μm)
  - charge drifts directly
- charge in undepleted p region
  - diffuses, and reflects from
  - p/p+ edge, eventually collected

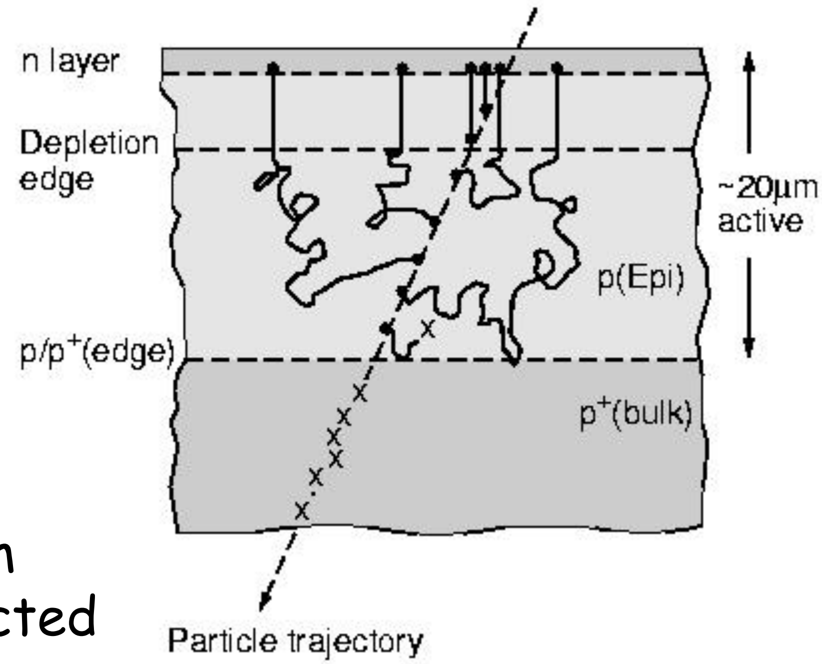

CCD Charge Storage/Redout

Charge storage and readout principles

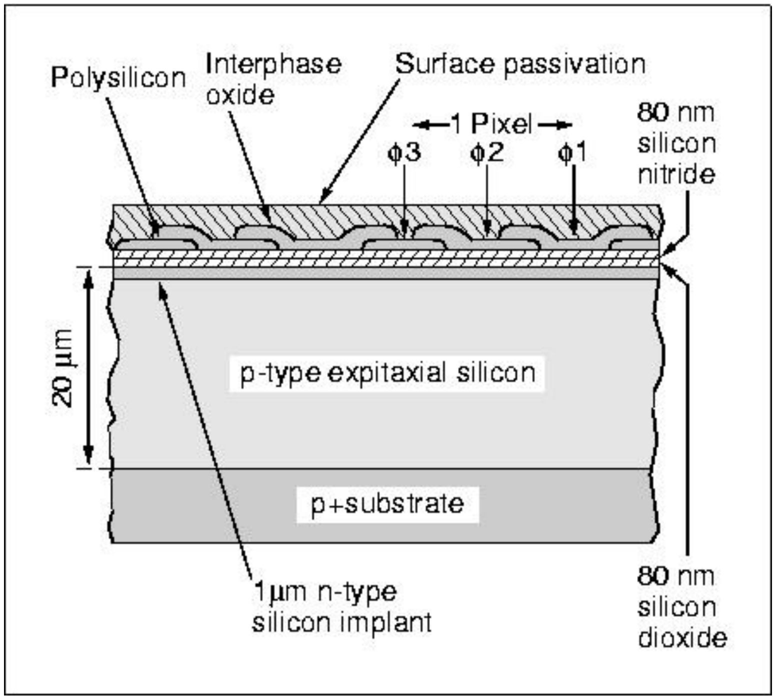

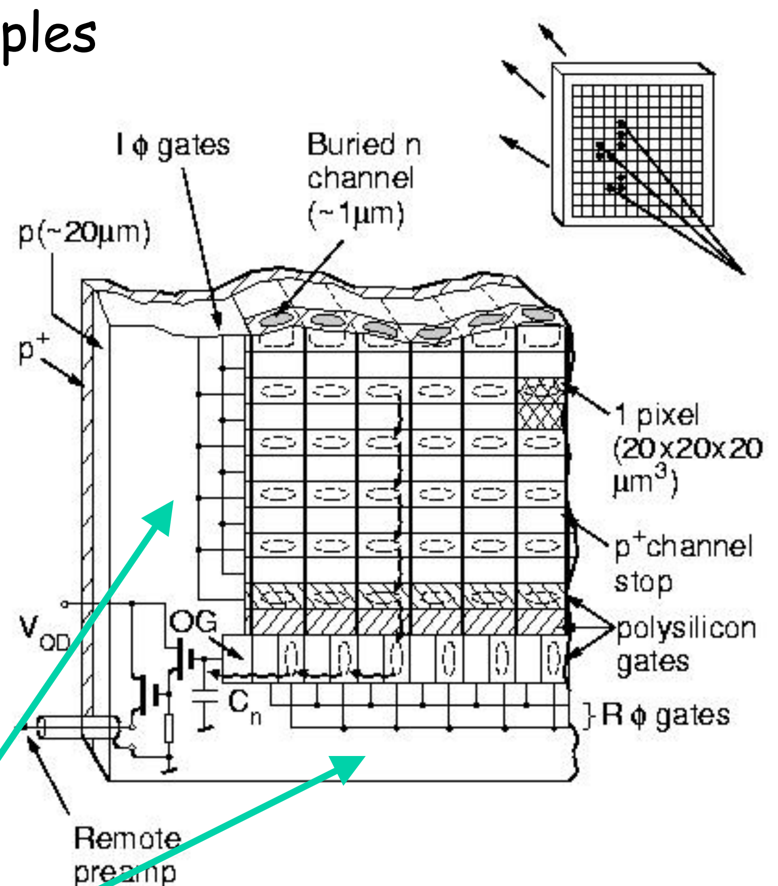

I gates transfer charge from imaging area
R gates transfer charge across the readout register

CCD Noise

< 100 e⁻ ENC for ≤ 10-30 MHz and higher

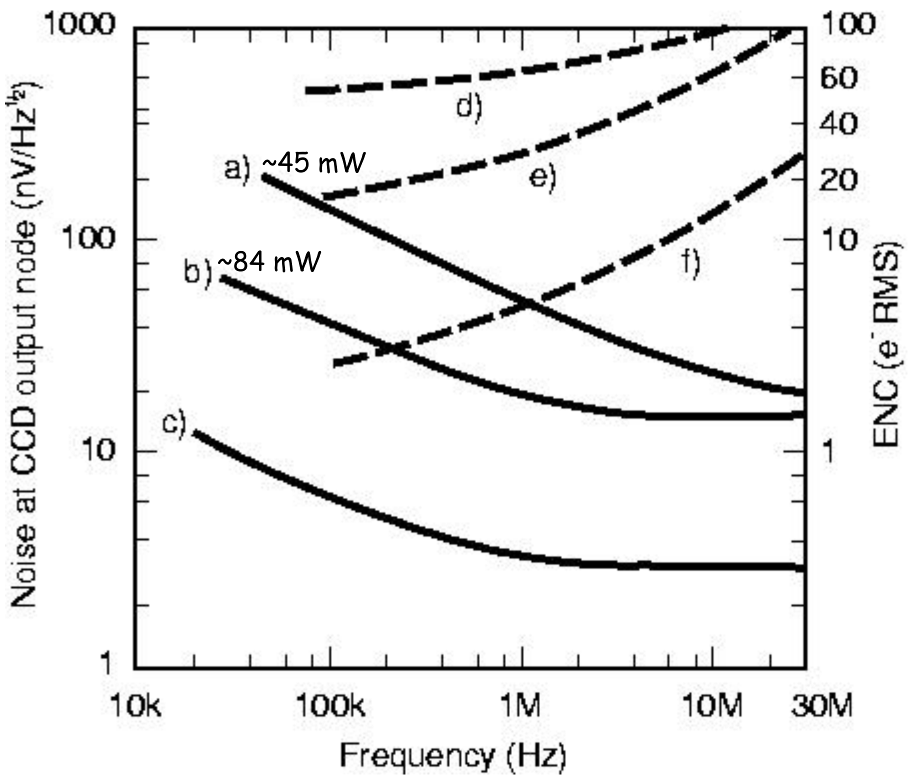

Noise spectra (a-c)
and CDS Noise equiv. (d-f)

- a., d.) surface channel
- b., e.) buried channel
- c., f.) available state-of-the-art output circuits

CCD VXD System History

Physics of future Linear Collider demands the best possible vertex detector performance

event rates will be limited
physics signals will be rich in secondary vertices

A decade of experience with CCDs in the linear collider environment of SLD has proven its exceptional performance

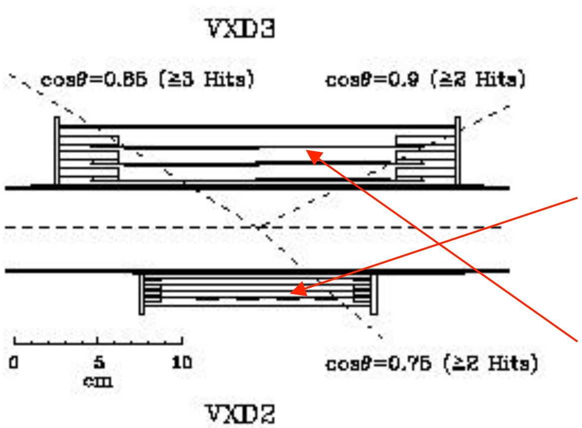

VXD1 (1991)	**prototype** **few ladders**
VXD2 (1992-1995)	**complete detector** **120,000,000 pixels** **2 barrel (effective)**
VXD3 (1996-1998)	**upgrade** **307,000,000 pixels** **3 barrels**

SLD VXD3

- SLD has demonstrated the power of a PIXEL detector in the LC environment

- 307,000,000 pixels

- 3.8 μm point resolution

- Excellent impact parameter resolution
  - $\sigma_{r\varphi}$ (μm)= $7.8 \oplus 33/p \sin^{3/2}\theta$
  - σ_{rz} (μm)= $9.7 \oplus 33/p \sin^{3/2}\theta$

- pure and efficient flavor tagging at the Z-pole
  - ~ 60% b eff with 98% purity
  - > 20% c eff with ~ 60% purity

- decay vertex charge measurement (Q = -1, 0, 1)

VXD3 at SLD

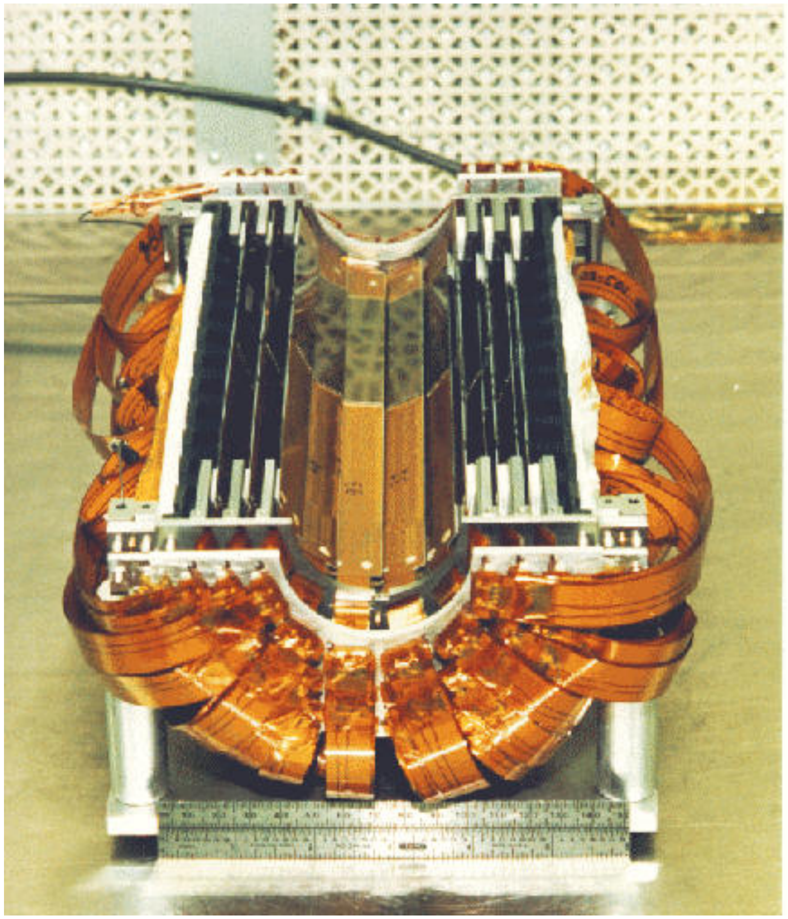

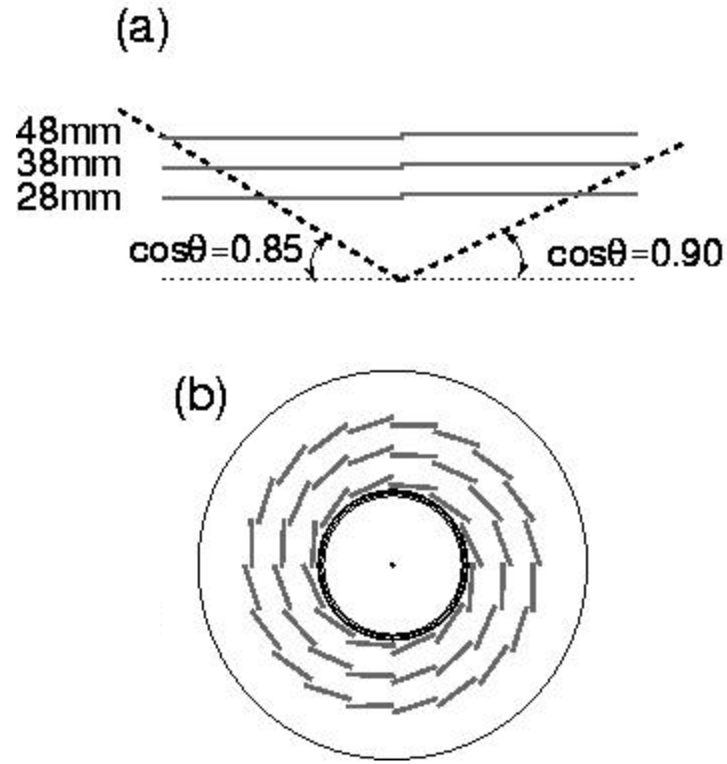

SLD Collab., NIM A400, 287-343 (1997)

307,000,000 pixels
3.8 mm point resolution
Excellent b/c tagging

VXD3 Hit Experience

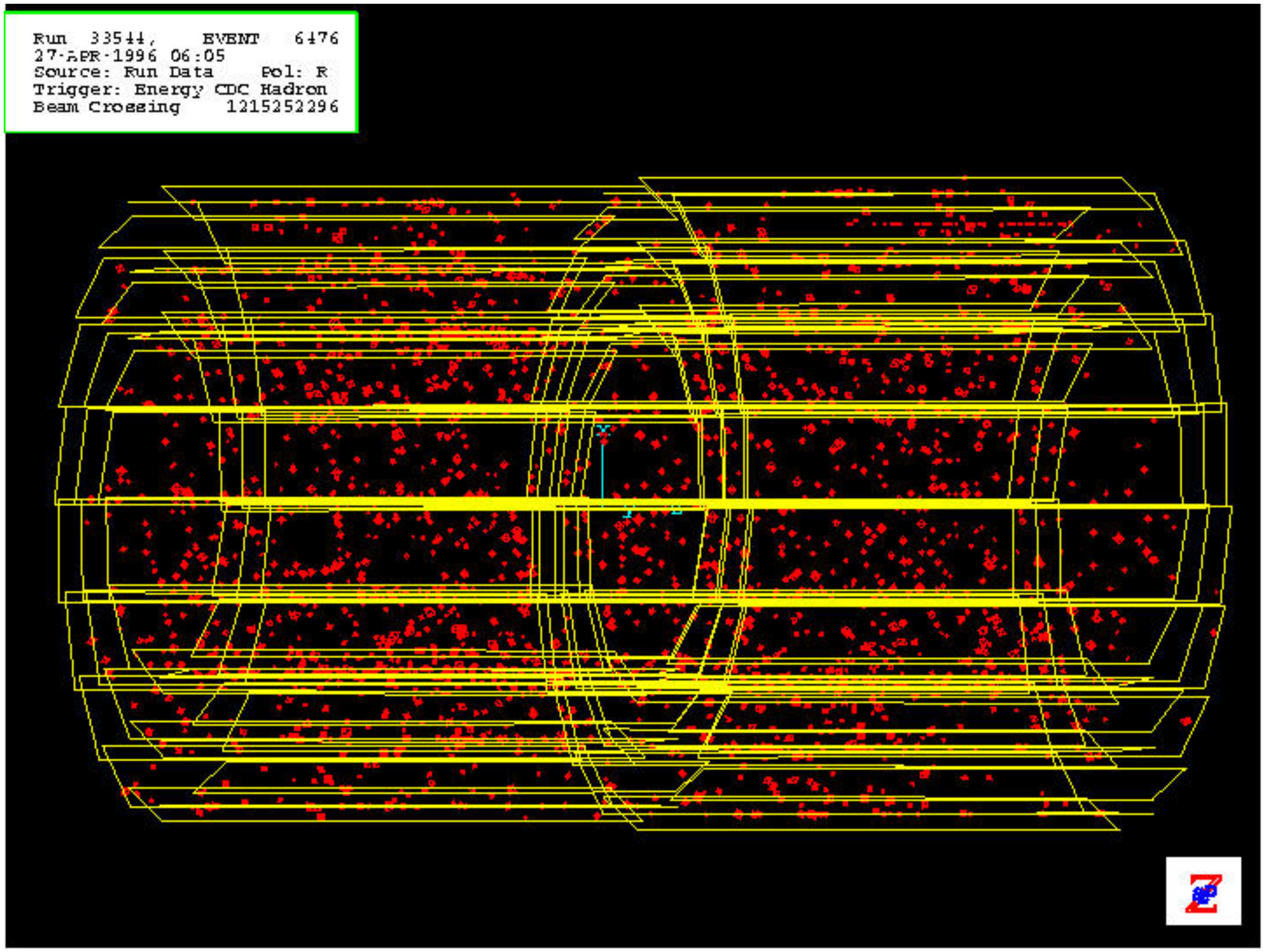

~ few x 10^{-5} hits per pixel at SLC

~ few% are signal

VXD3 CCDs

96 CCDs, n-buried channel
thinned to 180 μm
80x16 mm^2 active area
307,000,000 pixels (20 microns)^3
5 MHz full-frame readout
2 phase R clocking & 3 phase I clocking
4 readout nodes/CCD

<u>Each CCD:</u>
800 (H) x 4000 (V) = 3,200,000
20 μm square elements

800,000 pixels read from each
of four output nodes

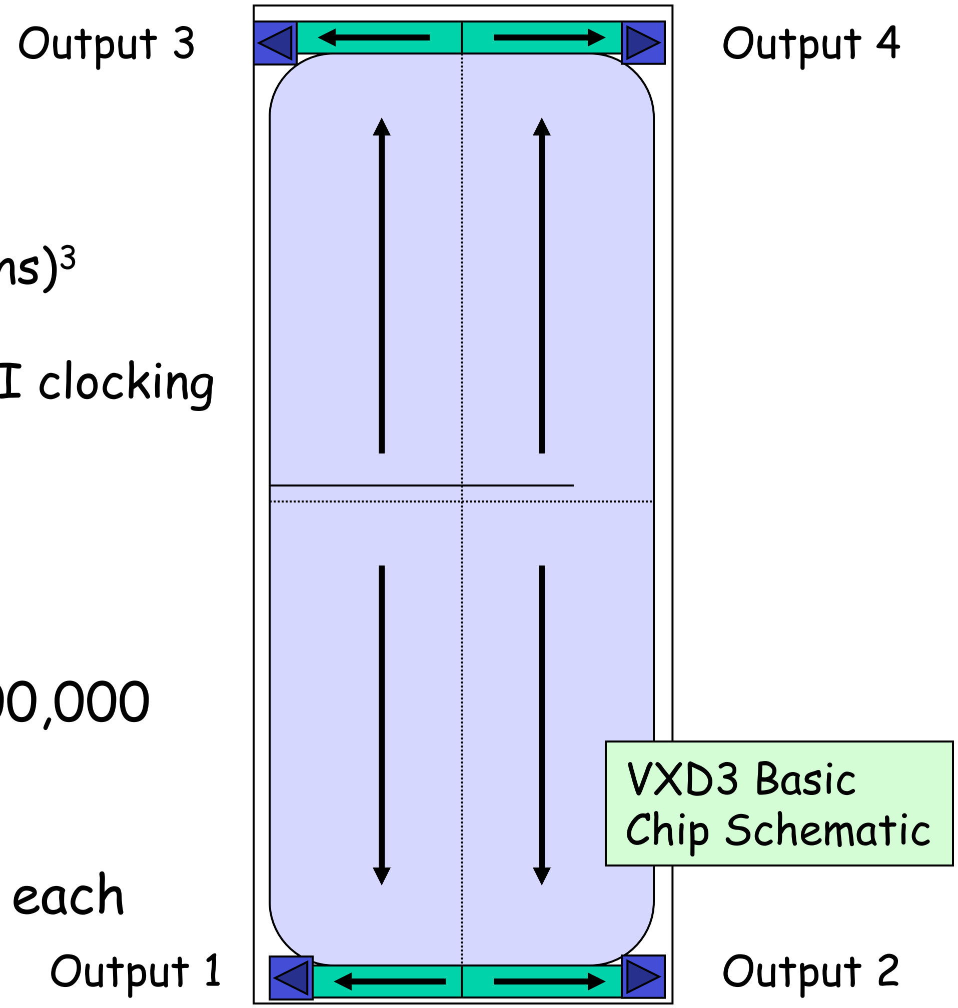

CCD Parameters

Basic design features	
Substrate resistivity	< 20 mΩ cm
Epitaxial layer reistivity	20 Ω cm
Format	4 quadrant full frame
No. pixels	800 Hor x 4000 Vert
Pixel size	20 x 20 μm^2
Sensitive Area	16 mm x 80 mm
Overall chip size	≤ 16.6 mm x 82.8 mm
Inactive edge spacing	< 300 μm
Thickness	180 ± 20 μm
Passivation	2 μm polyimide
Image area clock type	3-phase
Readout register clock type	2-phase
No. of pre-scan elements	6
No. of amplifiers	4
Gate protection	on all gates

Performance parameters	
Clock capacitances	
Image section to substrate	16 nF
Image section interphase	6 nF
Readout register to substrate	85 pF
Readout register interphase	30 pF
Charge storage capacity	
Pixel (supplmentary channel)	100×10^3 e^-
Pixel (total)	350×10^3 e^-
Readout register	400×10^3 e^-
Vertical transfer rate	> 200 kHz
Horizontal transfer rate	> 10 MHz
Output circuit responsivity	3 μV/ e^-
Output impedence	260 Ω
Power dissipation (on-chip)	
Image section (10 V clocks at 200 kHz)	1.3 W
Readout register (10 V clocks at 10 MHz	25 mW
Each output amplifier	45 mW

VXD3 Ladder Assembly

CCDs mounted on kapton flex circuits, stiffened by beryllium

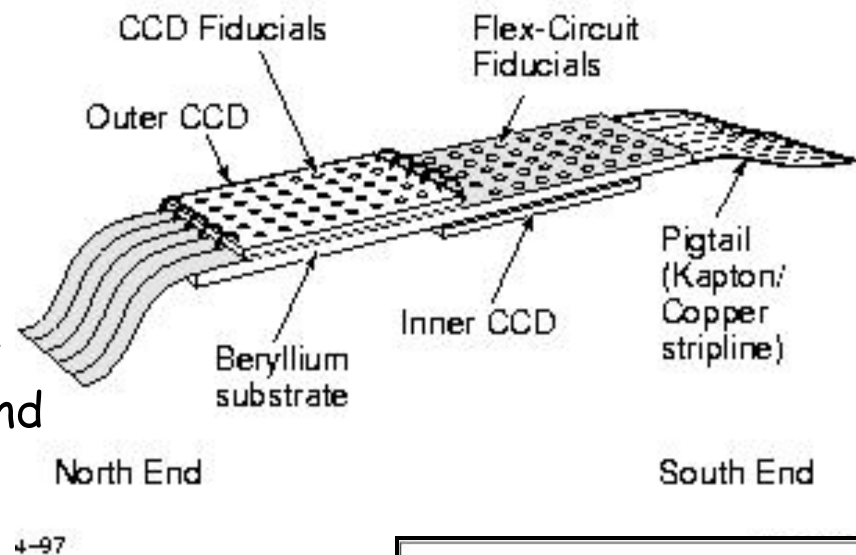

1/2 oz. copper traces
1/2 mil polyimide coverlayer
8 mil diameter round fiducials (48) on south end of outer flex circuit
soft bondable gold deposited on bond pads and fiducials
Beryllium connected to CCD ground

Total thickness: 0.4% X_0 at normal incidence

0.11% Be, 0.16% CCD, 0.05% kapton, 0.09% metal traces

CCDs attached to the ladder with adhesive pads and wire-bonded from each end to gold-plated pads

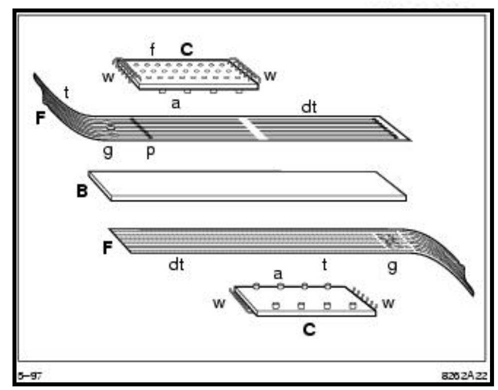

VXD3 Electronics

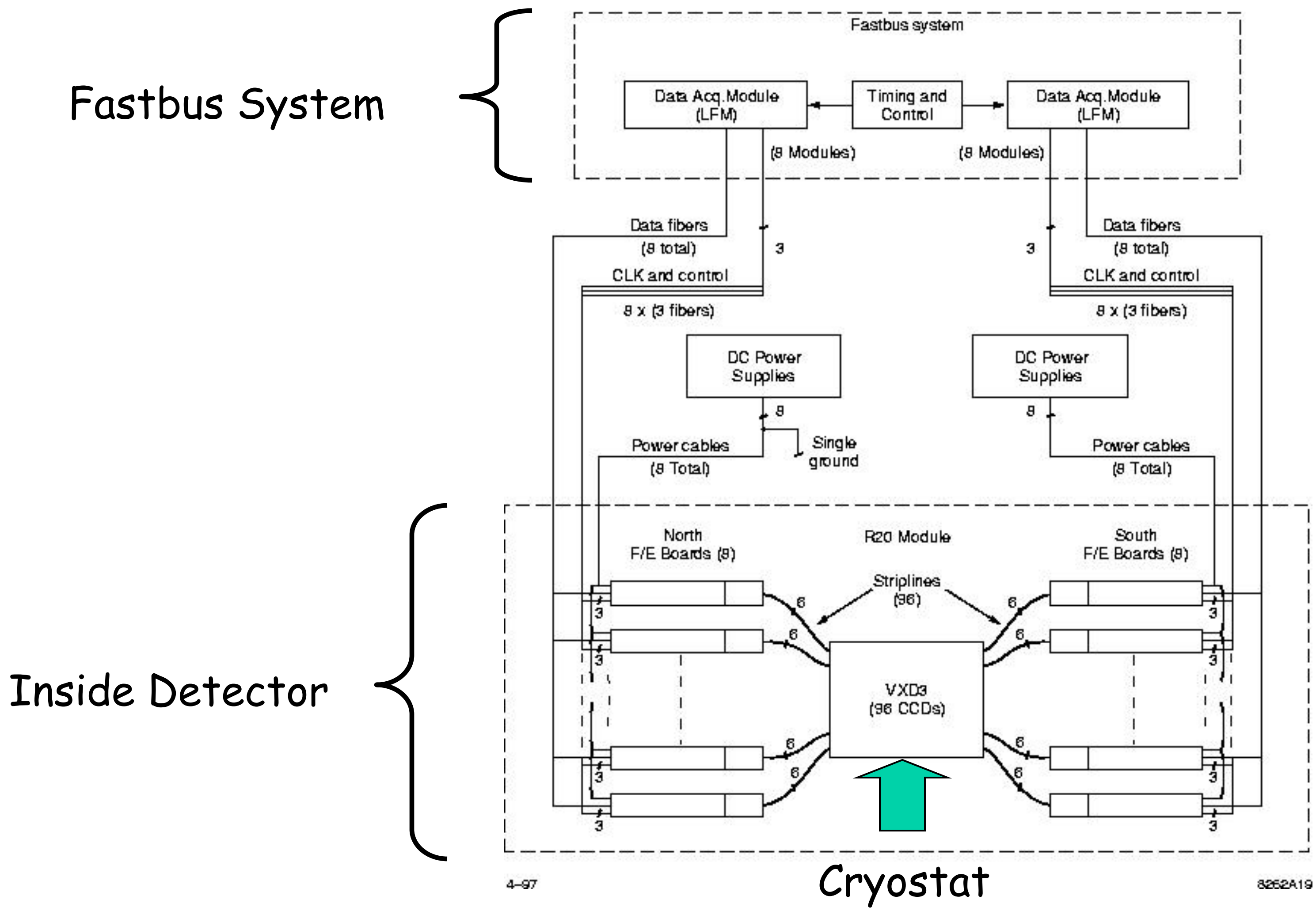

VXD3 Electronics

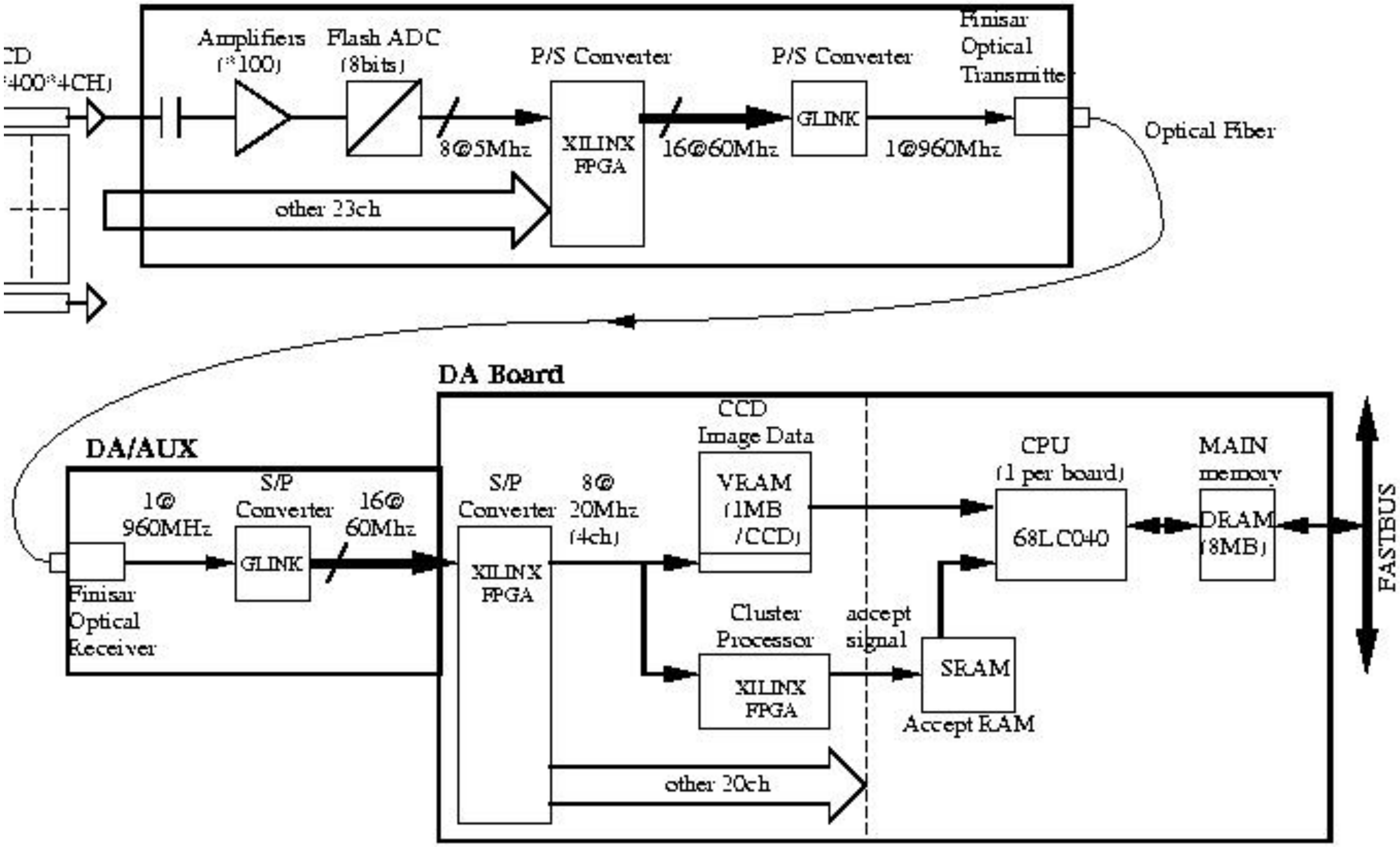

Fig. 3. The VXD3 readout electronics.

Cluster Processing

307 Mpix x 5 bytes/pixel (1 pulse height + 4 address)
= 1.5 Gbytes
System readout capacity ~ 100 kbytes

Clusters
single pixel threshold = 4 ADC counts ⇒ 108 e^-
(min-I ⇒ 1200 e^-)
cluster edge finder (after 2 x 2 kernel)
cluster threshold ~ 270 e^-
cluster: 8 pixels (R) x 6 pixels (I)
99.9% of charge

VXD3 Cooling

<u>Cooling</u>

190K operating temperature (suppresses dark current and CTE losses)
Liquid nitrogen boil-off through fine holes in beryllium beampipe jacket
Foam cryostat
< 20 Watts overall within cryostat

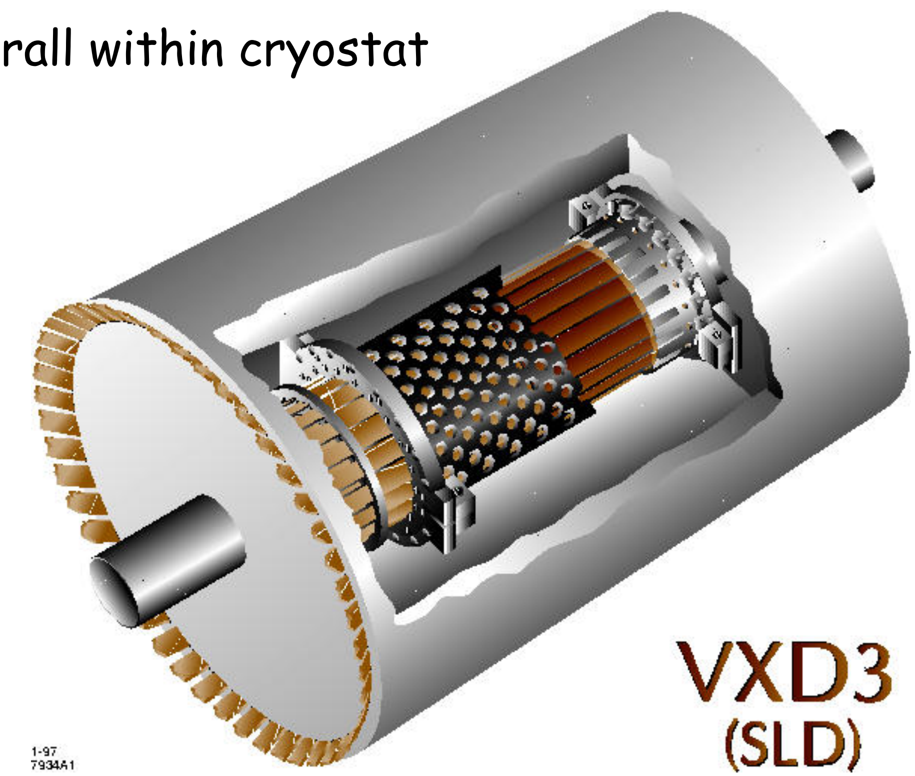

VXD3 Mechanics

Mechanics

VXD3 supported by instrument grade beryllium structure
Components match pinned and doweled for stability
Mating surfaces lapped (1 micron precision)
All joints allow for differential thermal contraction
Two modules clamped together & stablely mounted on beampipe via
3 point kinematic mount

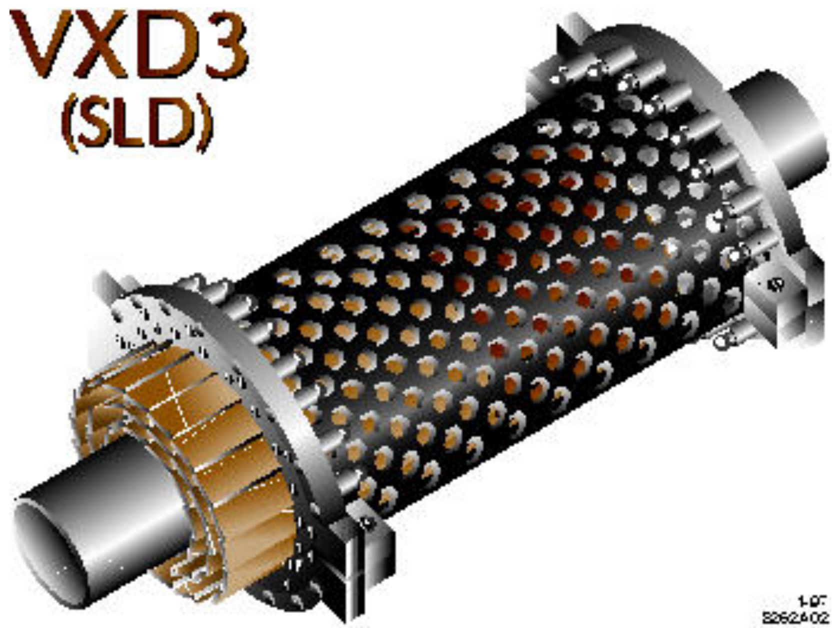

VXD3 Mechanics

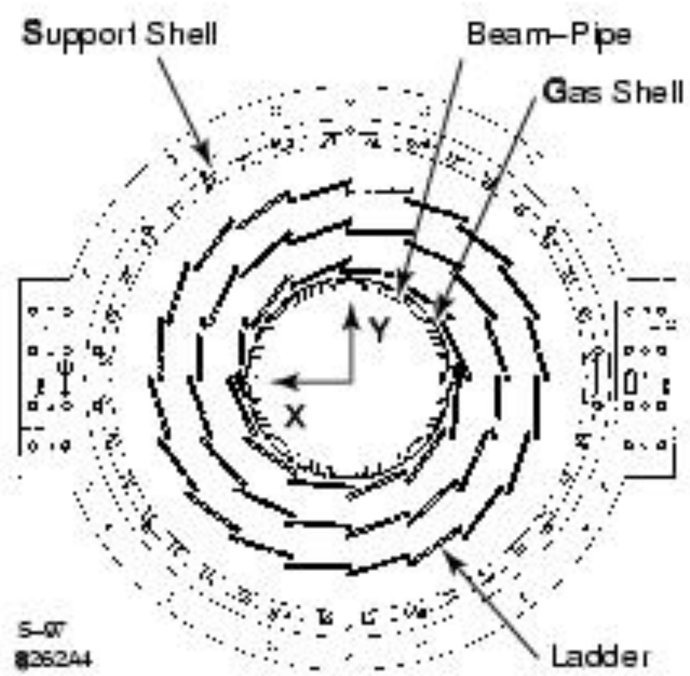

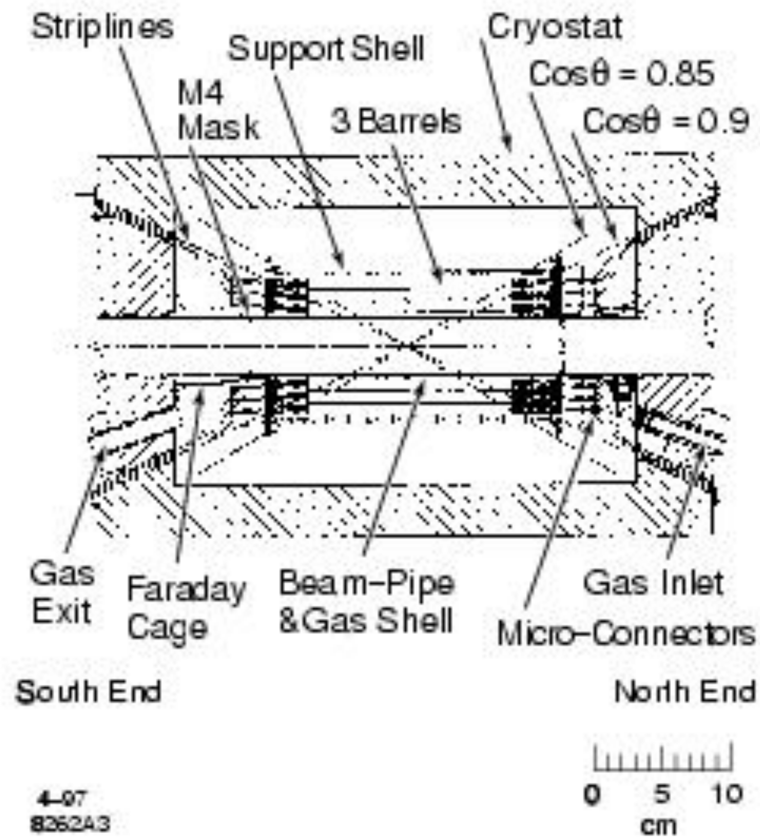

Survey Results

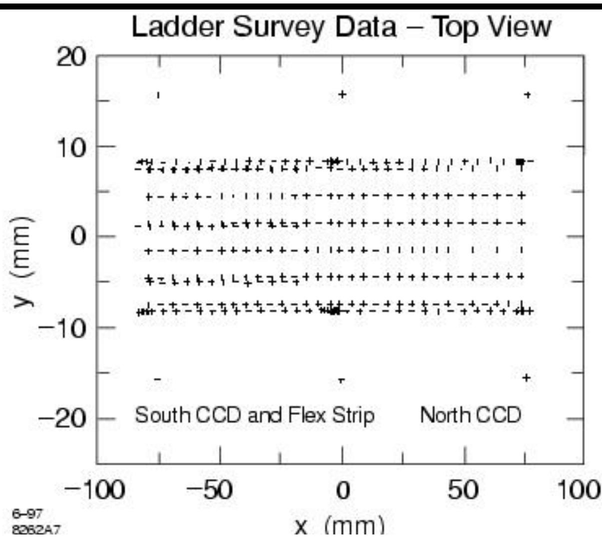

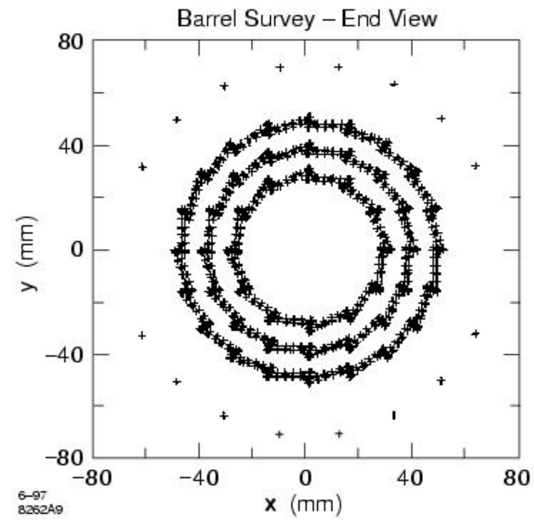

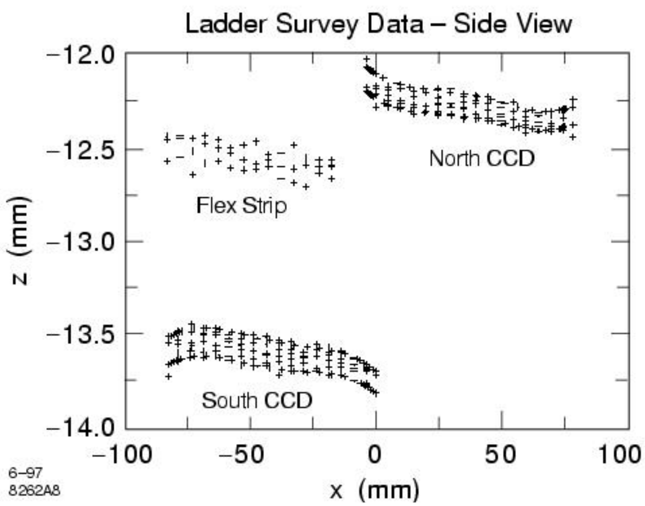

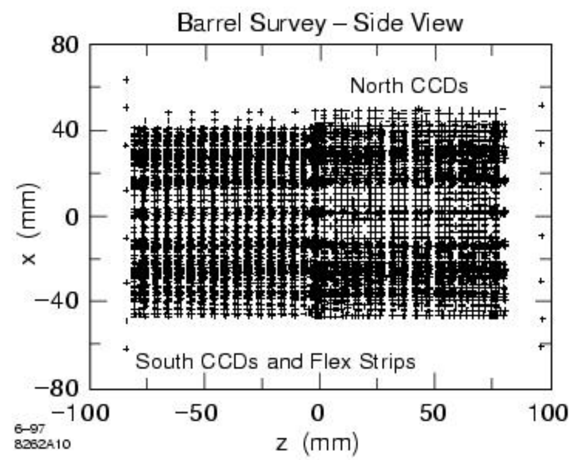

CCD shape

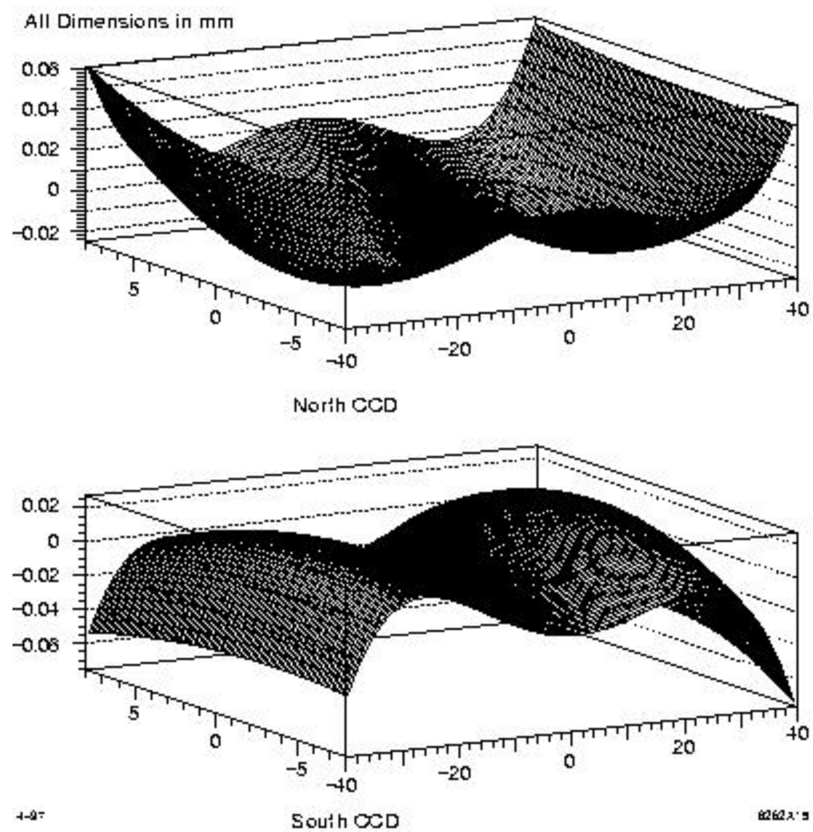
All Dimensions in mm
0.06
0.04
0.02
0
−0.02
5
0
−5
−40
−20
0
20
40
North CCD
0.02
0
−0.02
−0.04
−0.06
5
0
−5
−40
−20
0
20
40
South CCD

Internal Alignment

start from optical survey 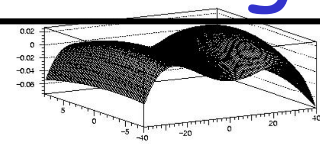 ~ 20 micron precision

1. Doublets 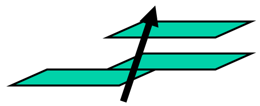 connects North and South

2. Shingles 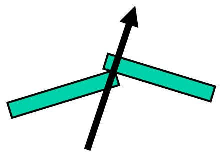 connects CCDs within layer

3. Triplets 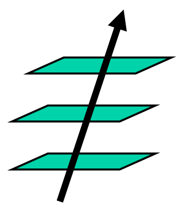 connects 3 layers

4. Z → μμ, ee (back-to-back) connects opposite regions

96 CCDs, 9 parameters each (3 translation, 3 rotation, 3 shape) plus two additional parameters ⇒ total of 856 parameters

Survey and Alignment

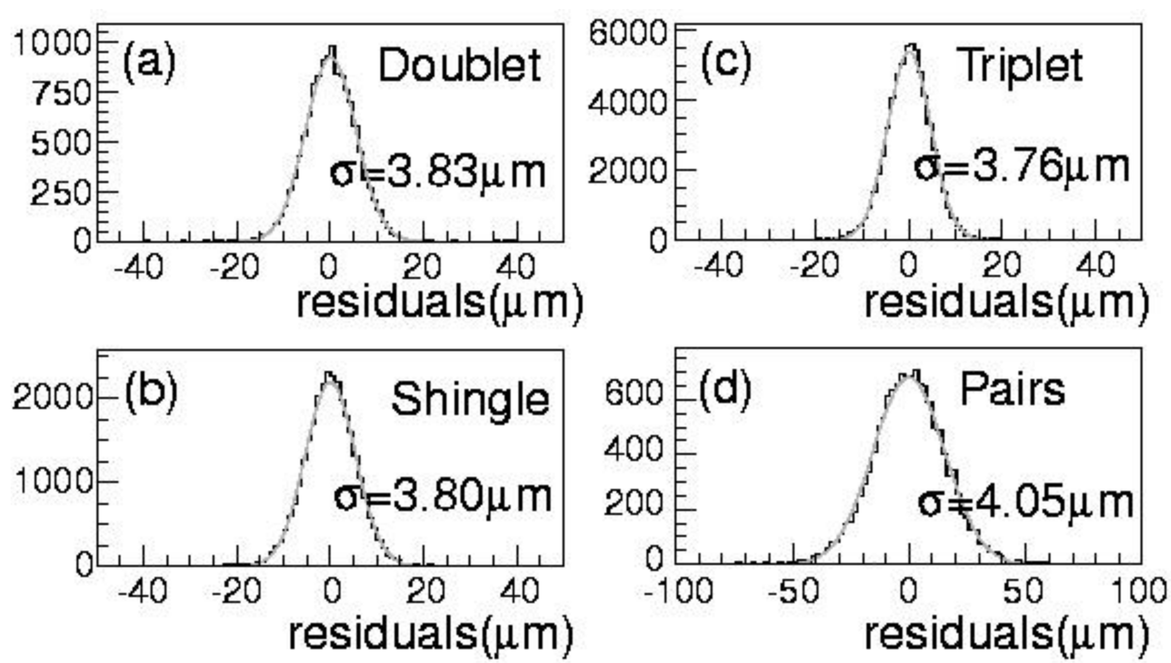

2 Prong Miss Distance

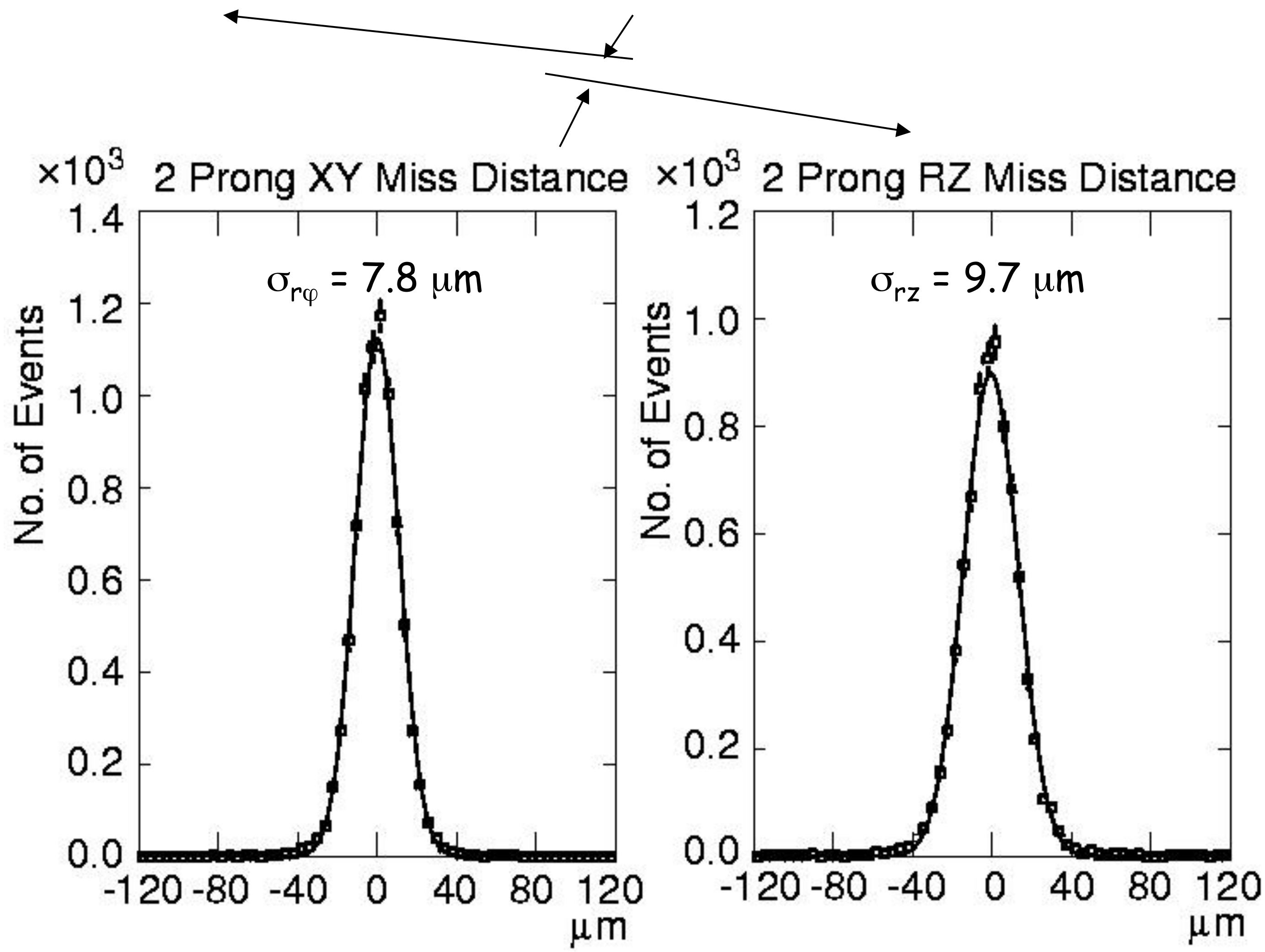

VXD3 Impact Parameter

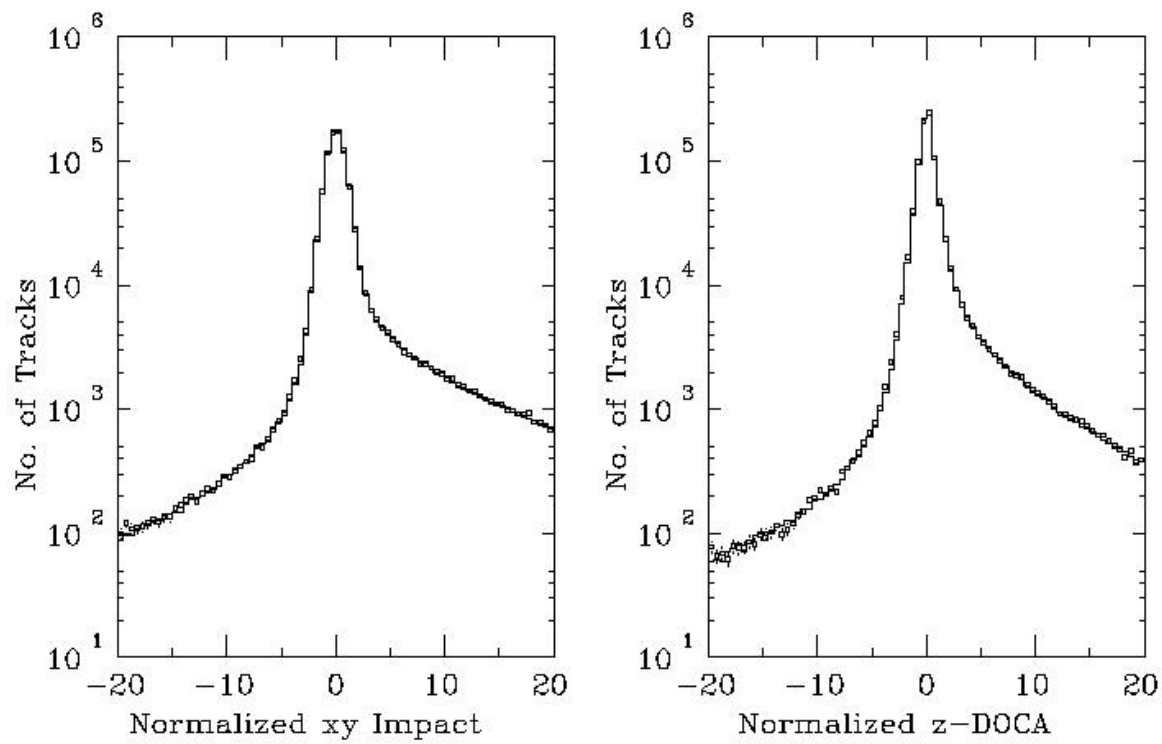

$\sigma_{r\varphi}$ (μm)= $7.8 \oplus 33/p \sin^{3/2}\theta$

σ_{rz} (μm)= $9.7 \oplus 33/p \sin^{3/2}\theta$

T. Abe, NIM A447, 90 (2000)

Topological Vertexing

- Parametrize tracks as Gaussian tubes in 3D
- Search 3D space for regions of high "tube overlap"

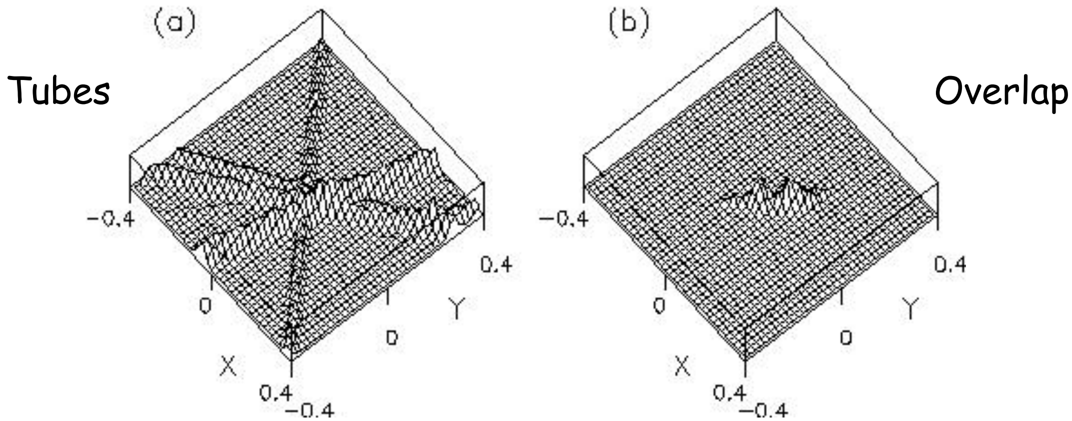

- Since B→D, multiple vertices
- Find "seed" vertex
- Attach tracks to "seed",
  if T < 1mm, L > 1 mm,
  and L/D > 0.25

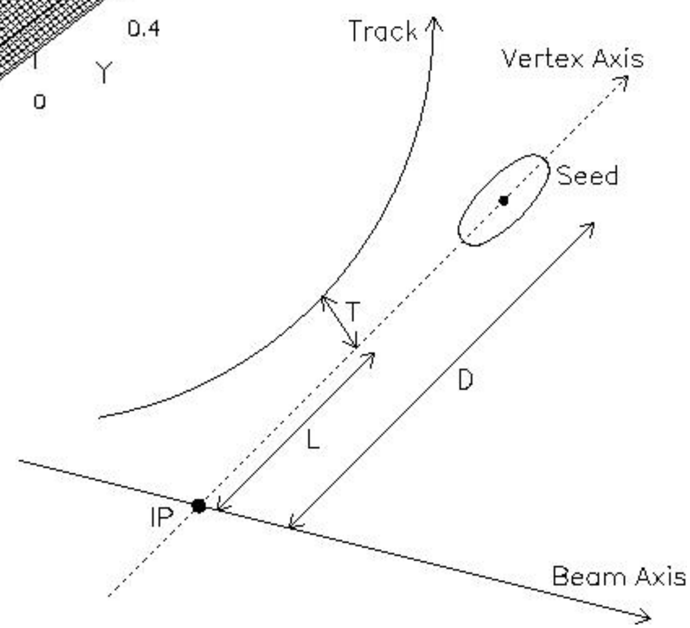

D. Jackson, NIM A388, 247 (1997)

Pt Corrected Mass

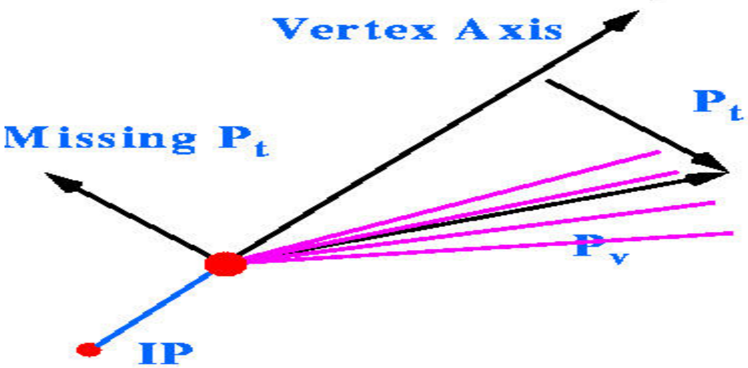

$$M = p_T + \sqrt{M_V^2 + p_T^2}$$

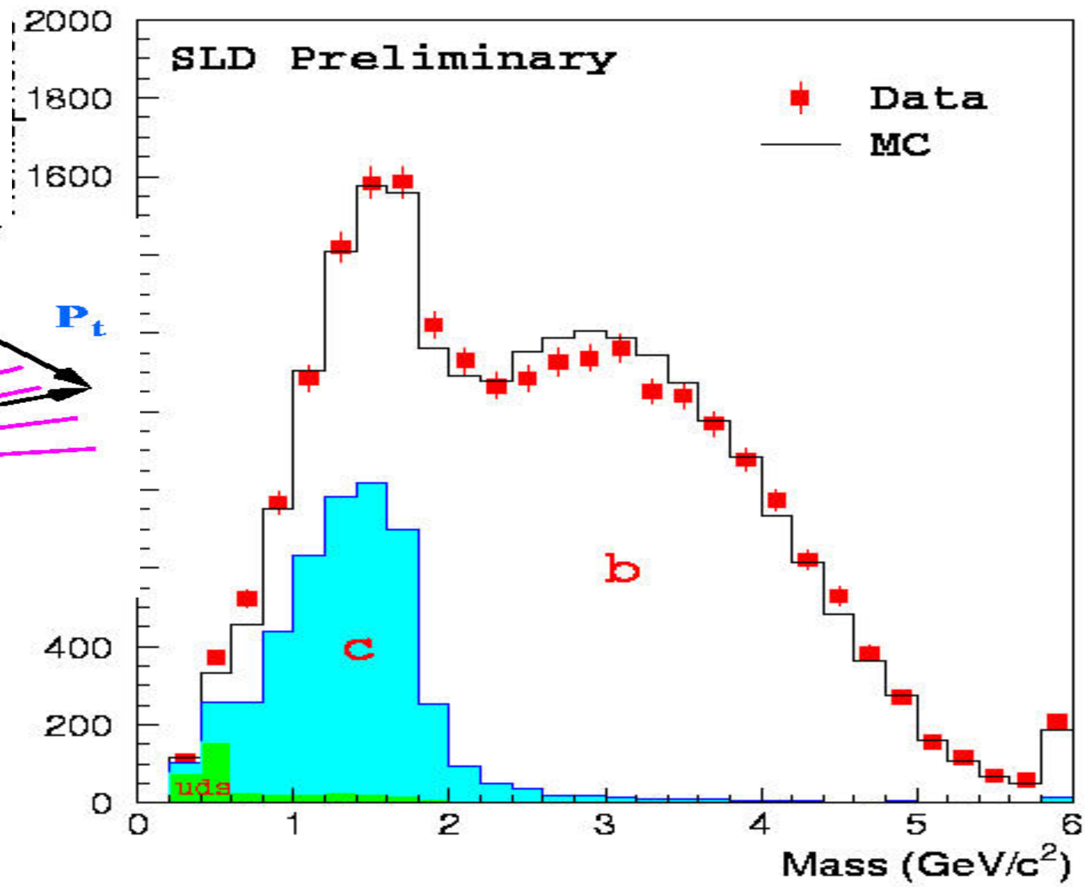

D. Jackson, NIM A388, 247 (1997)

VXD3 Purity and Efficiency

b tagging efficiency and purity

includes two layer tracks

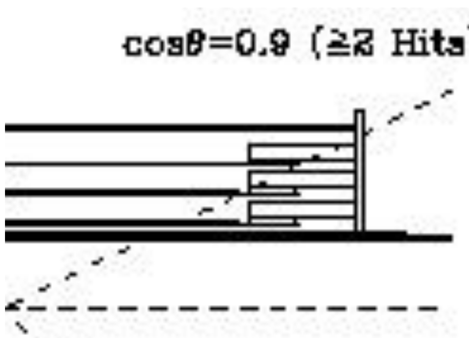

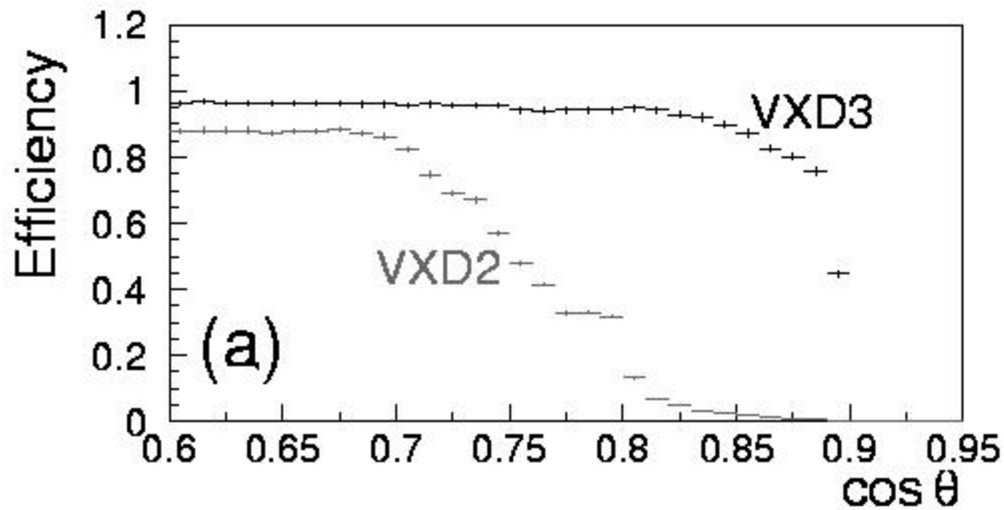

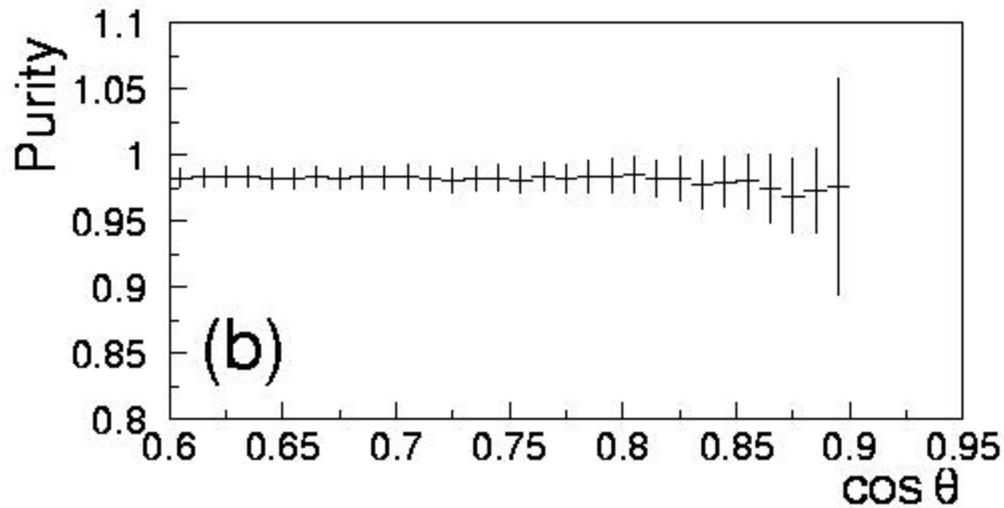

Dipole Charge

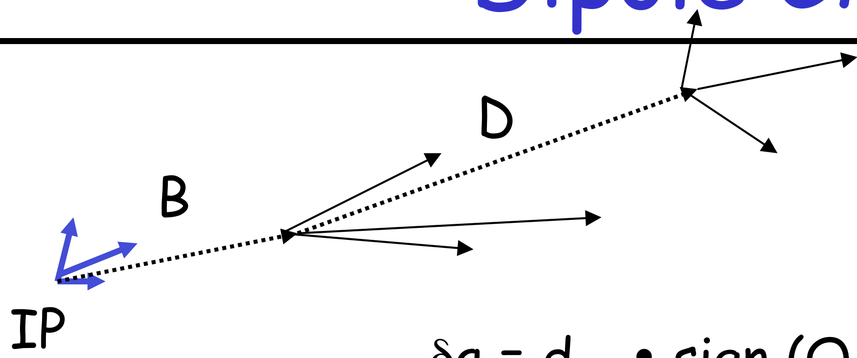

dipole charge separates B from $\bar{B}$

$$\delta q = d_{BD} \bullet \text{sign}\,(Q_D - Q_B)$$

$b \rightarrow c$ (dq positive)
$\bar{b} \rightarrow \bar{c}$ (dq negative)

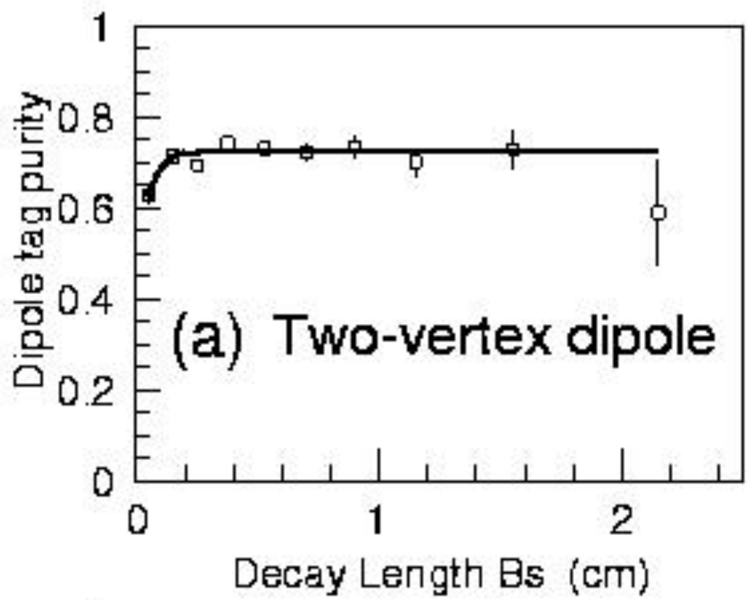

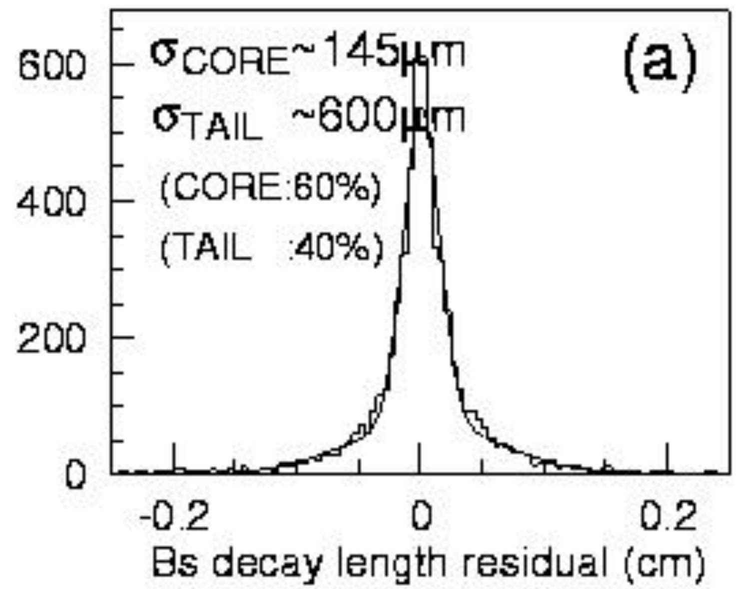

Ghost Track

Resurrecting
the Ghost Track!

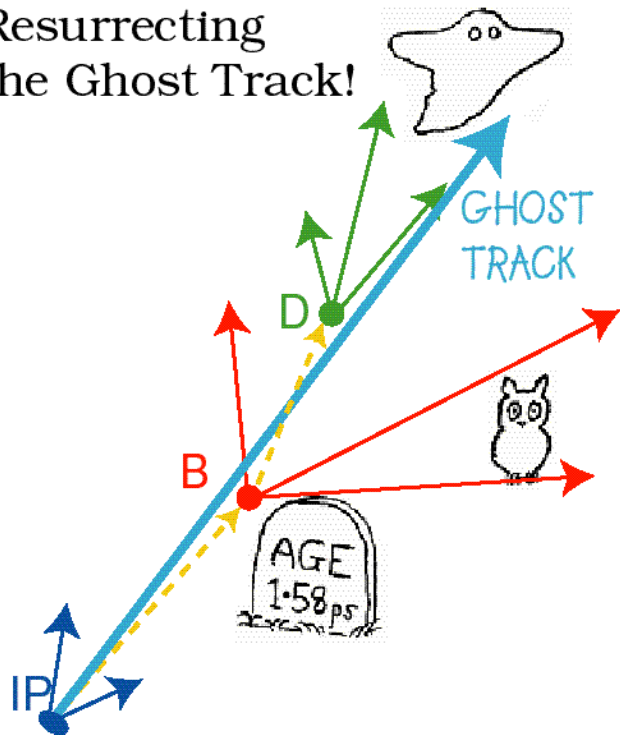

T. Abe

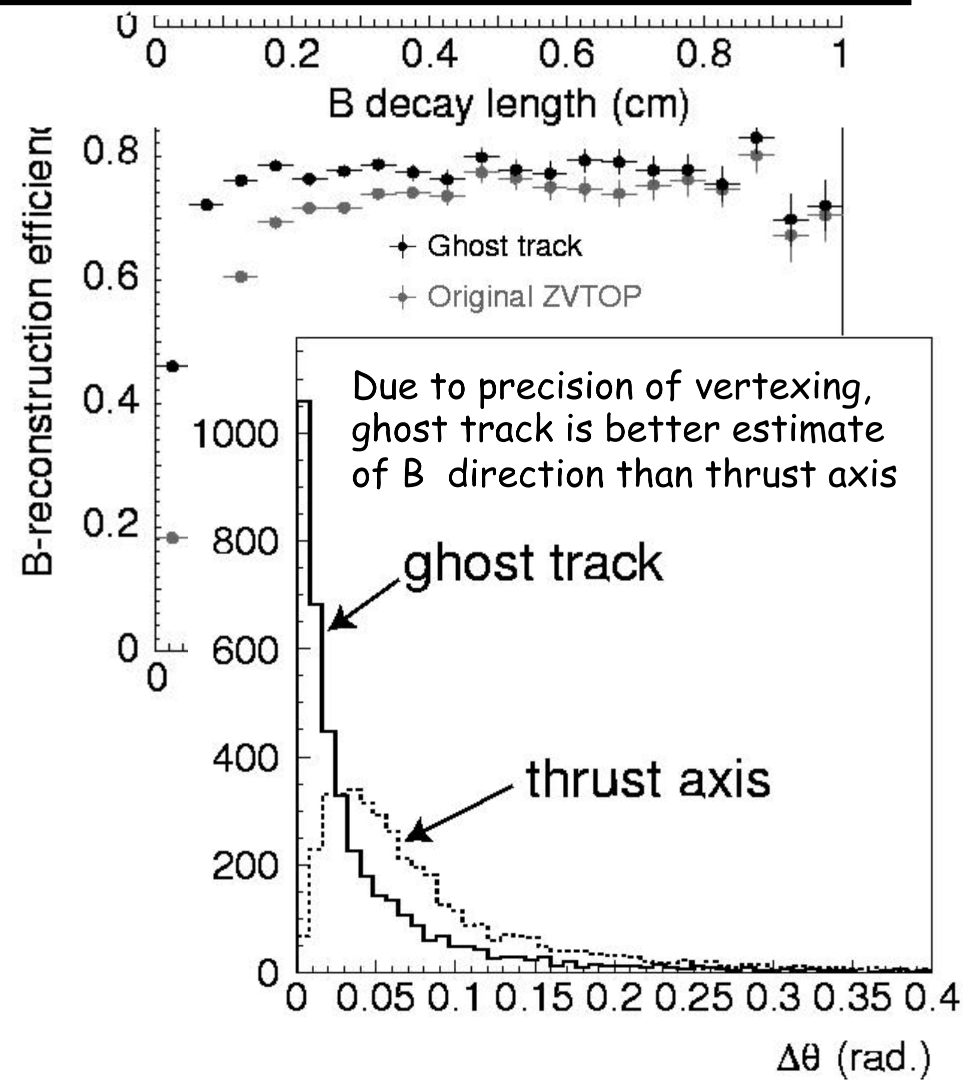

Charge Efficiency and Decay Length Resolution

Ghost track method improves dipole charge tag and decay length resolution

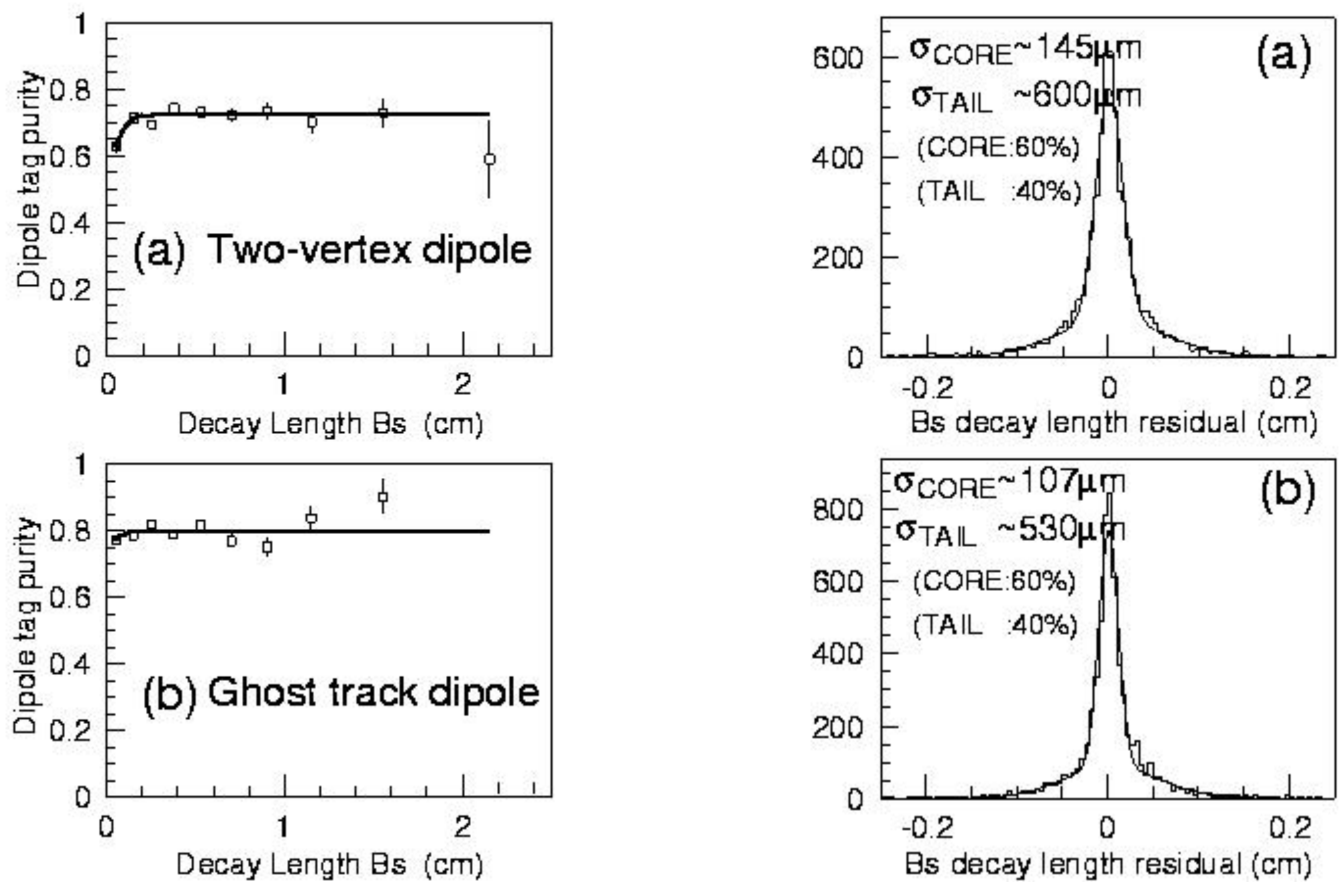

Recap of CCD Advantages

High granularity

20 x 20 x 20 μm^3 pixels (Intrinsically 3-dimensional)

superb spatial resolution (< 4 μm achieved at SLD)

Thin

0.4% X_0 at SLD (0.1% forseen)

low multiple scattering

Large detectors

80 x 16 mm^2 at SLD

facilitates ease of geometry

Exceptional system-level performance demonstrated

well matched to Linear Collider

CMOS Detectors

- **Complementary metal-oxide-semiconductor (CMOS)**
- Commercial fab processes
  - High noise immunity and low static power consumption.
- Directly addressed pixels

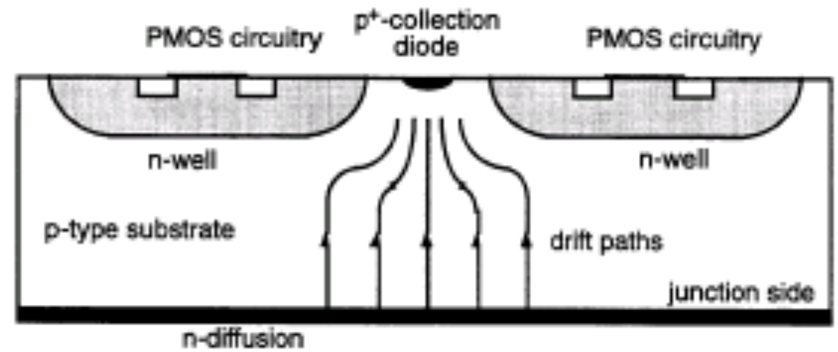

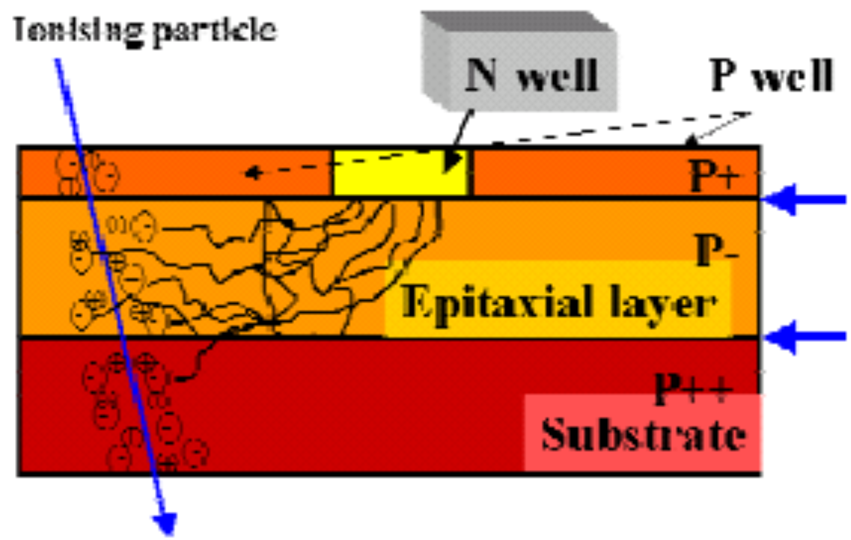

Chronopixel

- Under development by Oregon/Yale
- Time stamped readout

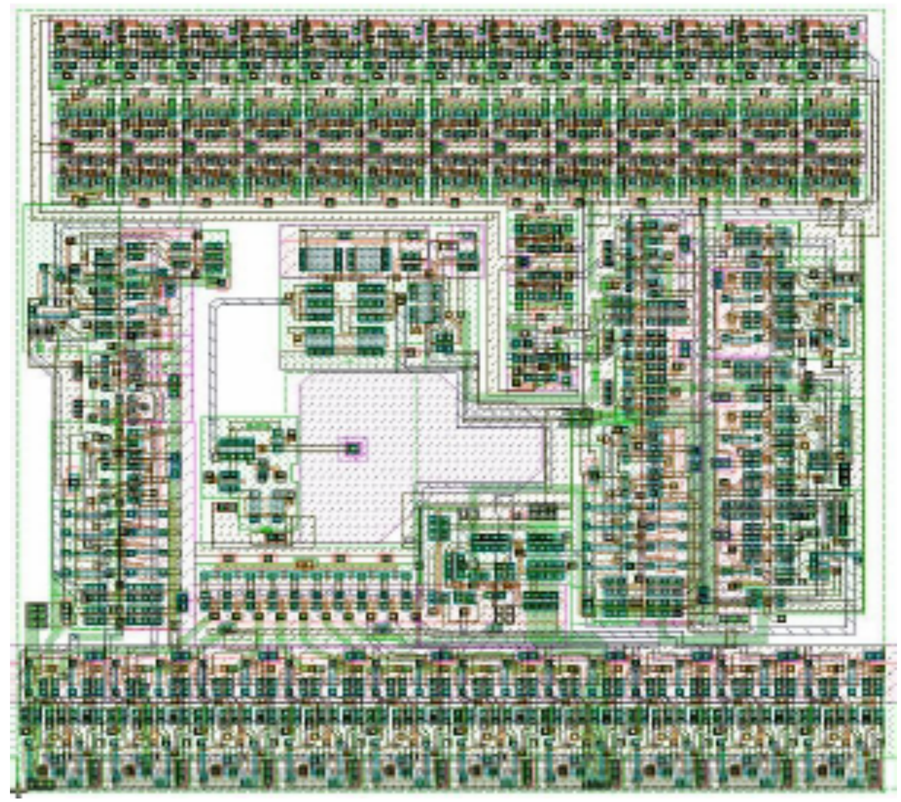

One pixel – 20 x 20 um^2

Diamond Detectors

- The susceptibility of silicon detectors to radiation damage has motivated the development of diamond detectors
  - 3 orders of magnitude more radiation tolerant than silicon
  - New techniques make synthetic production practical
    - Chemical Vapor Deposition (CVD)

Comparison of different active materials
Diamond - Silicon - Ga As at 293 K

	Diamond	Silicon	GaAs
Band Gap [eV]	5.5	1.12	1.43
Breakdown field [V/cm]	10^{+7}	$3 \times 10^{+5}$	$4 \times 10^{+5}$
Resistivity [Ω x cm]	10^{+13} - 10^{+16}	$1.5 \times 10^{+5}$	10^{+8}
Electron mobility [$cm^2/V/s$]	1800	1350	8500
Hole mobility [$cm^2/V/s$]	1200	480	400
Saturation velocity [km/s]	220	82	80
Density [gm/cm^3]	3.5	2.33	5.23
Atomic charge	6	14	31
Cohesive energy [eV]	7.37	4.63	
Dielectric constant	5.7	11.9	13.1
Energy (e- hole) [eV]	13	3.6	4.2
Radiaton length [cm]	12	9.4	2.3
dE/dX [MeV/cm]	4.69	3.21	5.6
Average e- holes / 100 µm	3600	8900	13000

Small dielectric constant i.e. small capacitance

high mobility i.e. fast signal collection

high resistivity i.e. low leakage current

Shower Detectors and Calorimeters

- Particle energies can be measured by absorbing the energy of an incident particle and measuring the signals generating in the absorber
- The absorbed energy appears as ionization, excitation, radiation, or other signals proportional to the total absorbed energy
- Examples:
  - ionization in liquid argon
  - Cerenkov radiation in lead glass
  - scintillation light in scintillating plastic
- Such devices are important method of detection of neutral particles, such as
  - gammas
  - K^0_L
  - neutrons

Shower Detectors and Calorimeters

- Typical tracking detectors have resolutions that deteriorate with increasing energy since the bending in a magnetic field is reduced

- Absorption detectors, on the contrary, improve with increased energy, often improving as $E^{-1/2}$

- Total absorption detectors also provide very fast signals, which are often employed as fast triggers for experiments

Electromagnetic Cascades

- Electromagnetic cascades are the basis for electromagnetic shower detectors
- High-energy electrons and photons incident on an absorber initiate electromagnetic cascades as pair production and bremsstrahlung generate more electrons and photons with lower energy
- Longitudinal development is governed by the high-energy part of the cascade, and scales as the radiation length in the material
- Electron energies eventually fall below the critical energy, and then dissipate their energy by ionization and excitation rather than by the generation of more shower particles.
- In describing shower behavior, it is therefore convenient to introduce the scale variables

$$t = x/X_0$$

$$y = E/E_c$$

so distance is measured in units of radiation length and energy in units of critical energy.

Electromagnetic Cascades

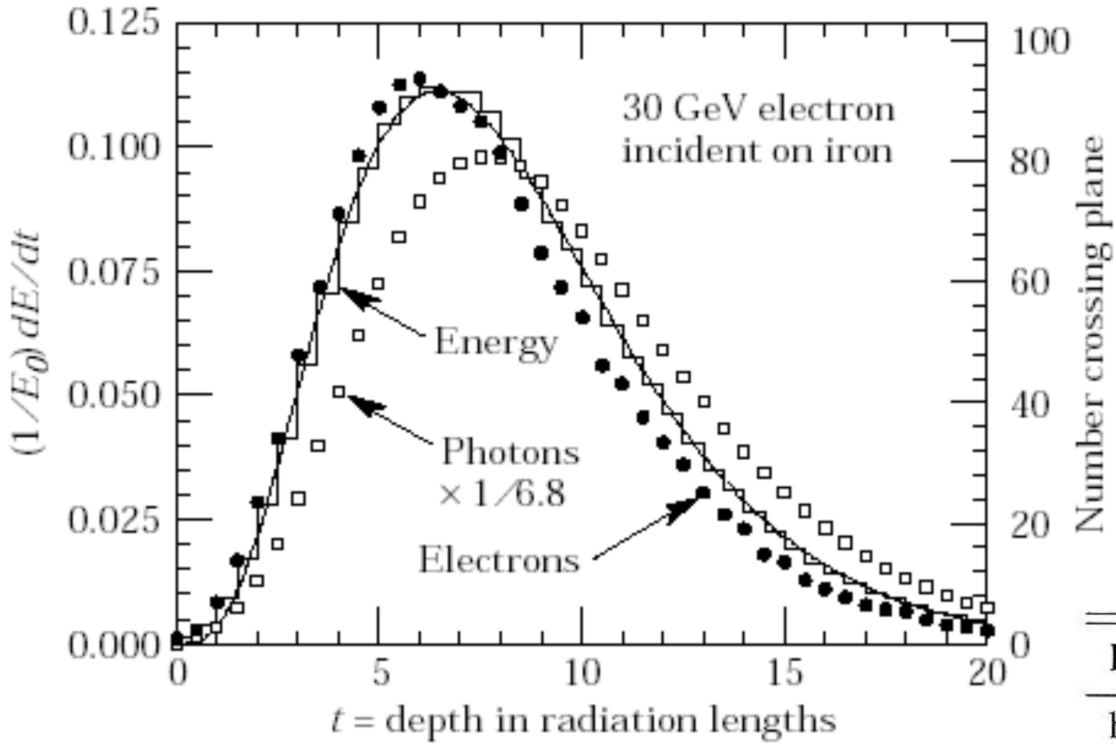

$$\frac{dE}{dt} = E_0\, b\, \frac{(bt)^{a-1} e^{-bt}}{\Gamma(a)}$$

Element	Z	E_c, MeV	X_0, g cm^{-2}
hydrogen	1	340	63.1
helium	2	220	94.3
carbon	6	103	42.7
aluminium	11	47	24.0
iron	26	24	13.8
lead	82	6.9	6.4

Electromagnetic Cascades

$$\frac{dE}{dt} = E_0\, b\, \frac{(bt)^{a-1} e^{-bt}}{\Gamma(a)}$$

$$t_{\max} = (a-1)/b = 1.0 \times (\ln y + C_j)$$

C_e = -0.5
$C\gamma$ = +0.5

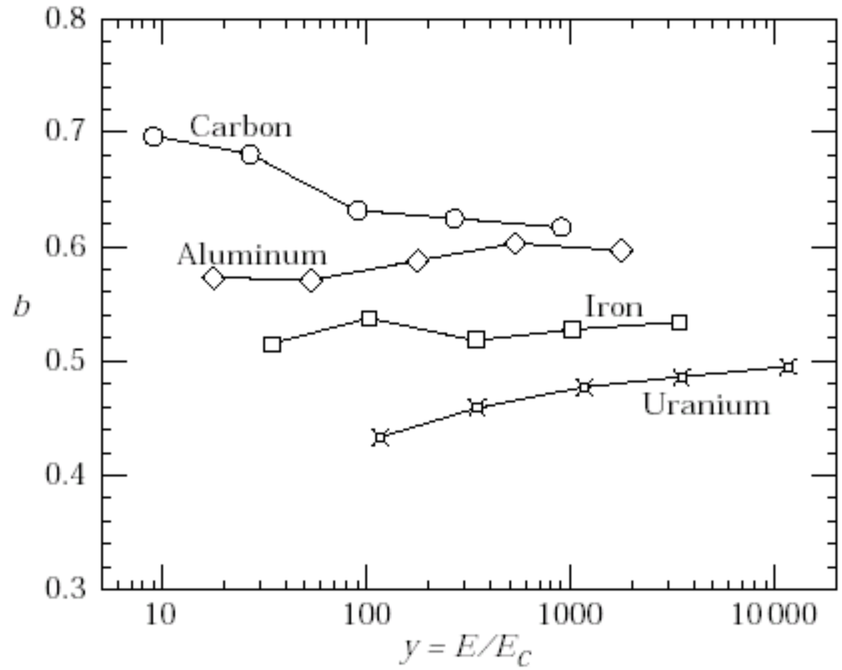

Electromagnetic Cascades

Transverse Profiles

- The transverse profiles of electromagnetic cascades are nicely represented by the Moliere radius (R_M)

$$R_M = X_0 E_s / E_c \quad (E_s = 21 \text{ MeV})$$

Element	Z	E_c, MeV	X_0, g cm^{-2}
hydrogen	1	340	63.1
helium	2	220	94.3
carbon	6	103	42.7
aluminium	11	47	24.0
iron	26	24	13.8
lead	82	6.9	6.4

- Typical relations
  - ~ 10% of energy outside R_M
  - ~ 99% of energy within 3.5 R_M
  - shower characterized by narrow core that broadens as the shower develops

$$f(r) = \frac{2r\,R^2}{(r^2 + R^2)^2}$$

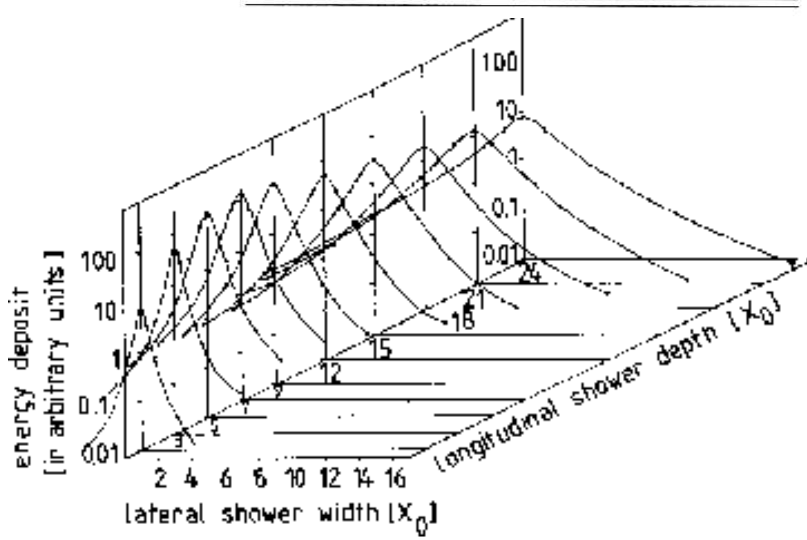

Electromagnetic Cascades

Lengths of showers

- The lengths of showers scale as $1/E_c$
  - this results from the fact that when the particles of the shower reach the critical energy, radiation ceases and the energy is deposited as ionization.

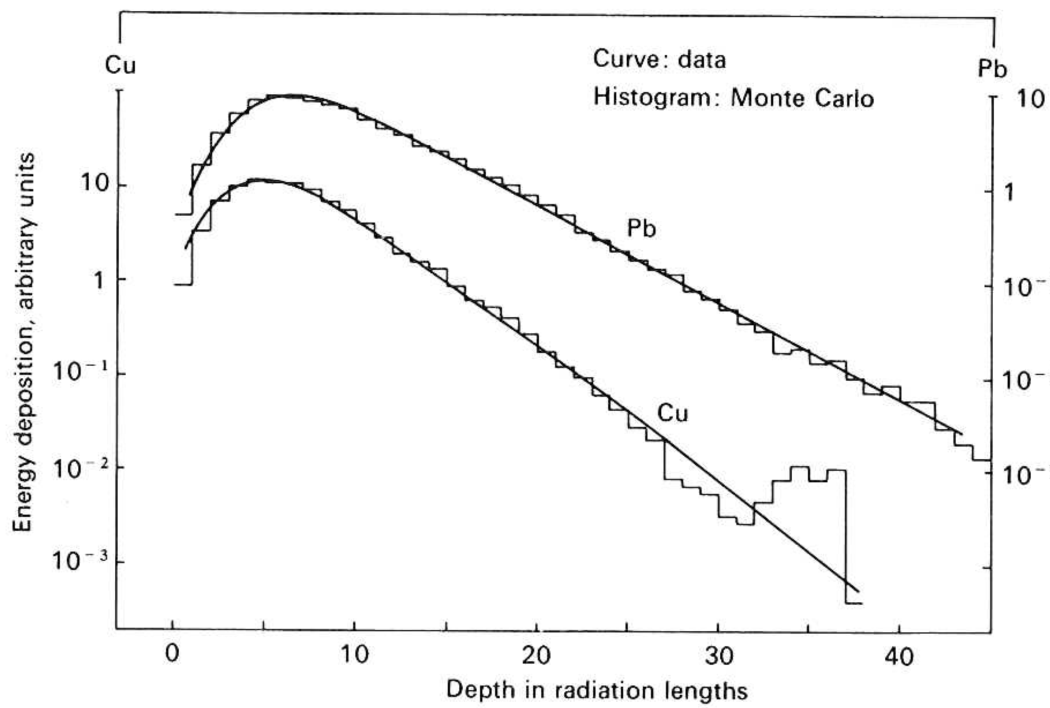

Electromagnetic Cascades

Review of Main Qualitative Features

- Maximum occurs at a depth that increases logarithmically with primary energy
- The number of shower particles at the maximum is proportional to the primary energy
- the total track-length integral is proportional to the primary energy
- Fluctuations in the total energy deposited about the average varies inversely with the square root of the number of particles in the shower, or inversely as the square root of the primary energy

Electromagnetic-shower Detectors

- Each calorimeter will detect a specific response which is proportional to the shower development, but may vary from technique to technique
  - energy deposition
  - track length
  - threshold energy

Note: at very high energy these resolutions will be limited by the size of the constant term

Table 24.5: Resolution of typical electromagnetic calorimeters. E is in GeV.

Detector	Resolution
NaI(Tl) (Crystal Ball [72]; 20 X_0)	$2.7\%/E^{1/4}$
Lead glass (OPAL [73])	$5\%/\sqrt{E}$
Lead-liquid argon (NA31 [74]; 80 cells: 27 X_0, 1.5 mm Pb + 0.6 mm Al + 0.8 mm G10 + 4 mm LA)	$7.5\%/\sqrt{E}$
Lead-scintillator sandwich (ARGUS [75], LAPP-LAL [76])	$9\%/\sqrt{E}$
Lead-scintillator spaghetti (CERN test module) [77]	$13\%/\sqrt{E}$
Proportional wire chamber (MAC; 32 cells: 13 X_0, 2.5 mm typemetal + 1.6 mm Al) [78]	$23\%/\sqrt{E}$

Electromagnetic-shower Detectors

Homogeneous Calorimeters

- Lead Glass
- NaI
- BGO
- BaF_2
- CeF_3
- CsI

- eg BaBar, 5760 crystals the barrel
  - 820 in the endcap

BaBar CsI(Tl) ECAL and Resolution

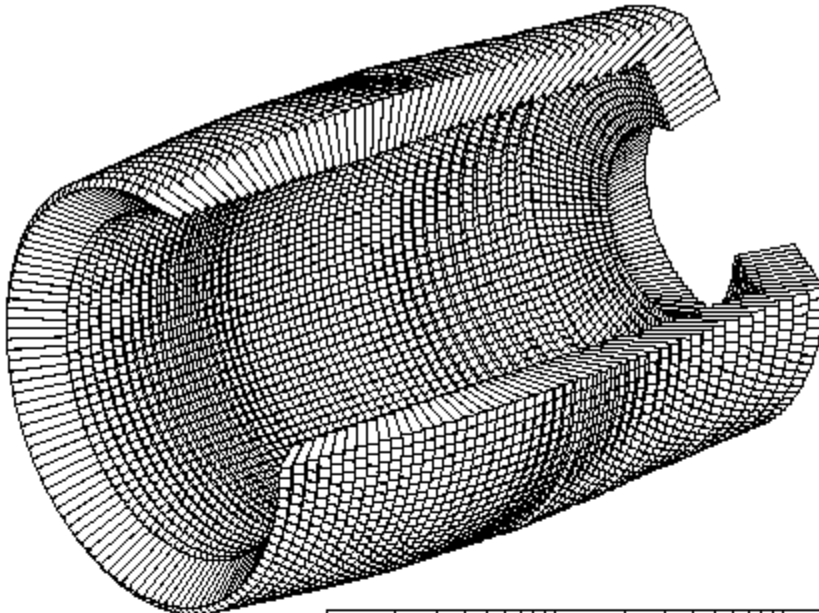

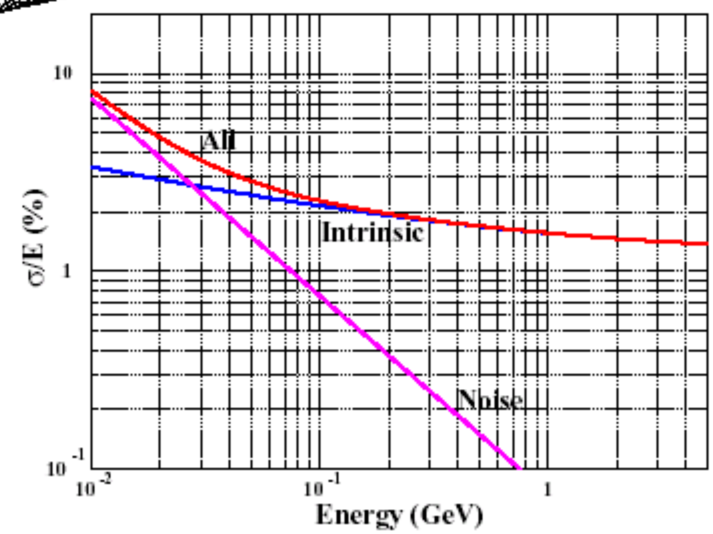

Electromagnetic-shower Detectors

Sampling Calorimeters

- Examples:
  - lead-scintillator
  - lead-liquid argon
  - silicon-tungsten

Electromagnetic-shower Detectors

Lead- scintillator

- Example: CDF barrel
  - 0.5 cm thick scintillator
  - 0.32 cm Pb absorber
  - 31 layers = 18 X_0

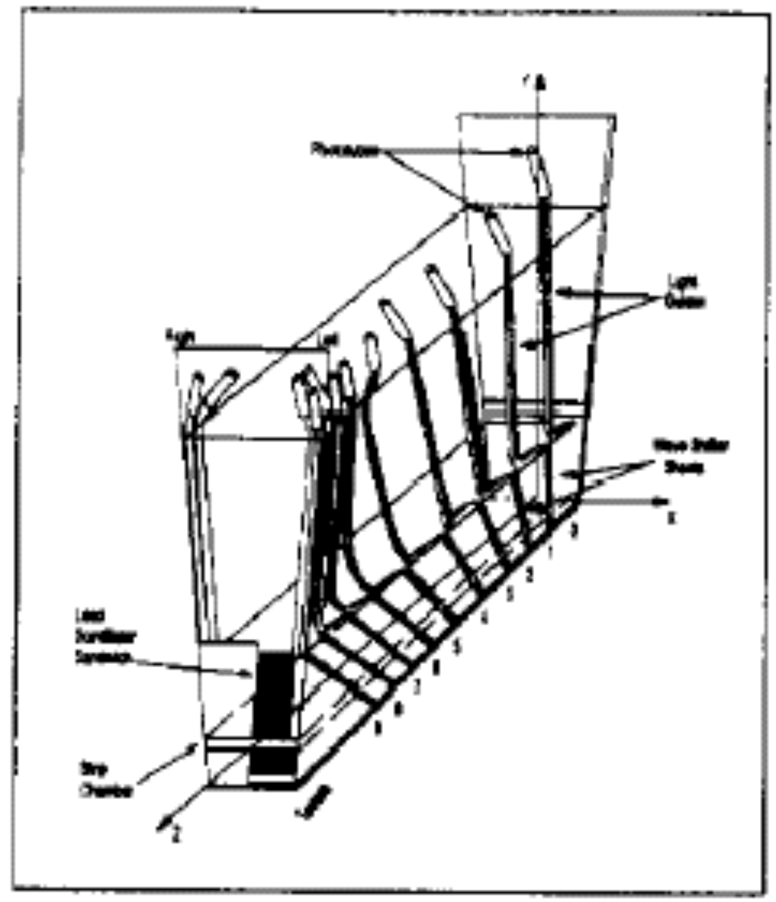

Electromagnetic-shower Detectors

Lead- liquid argon

- Example: SLD Calorimeter
  - 2 mm Pb
  - 2.75 mm Argon
  - 56 layers = 21 X_0

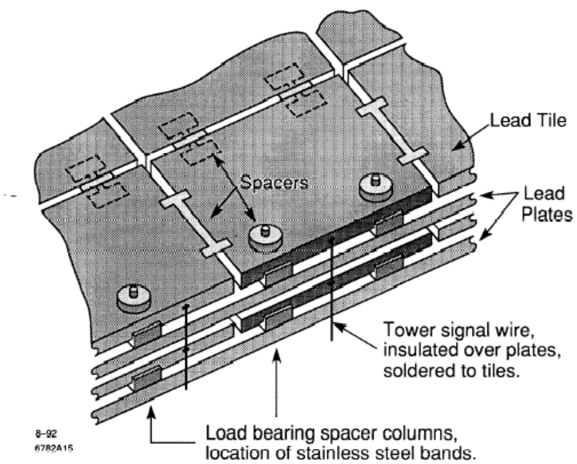

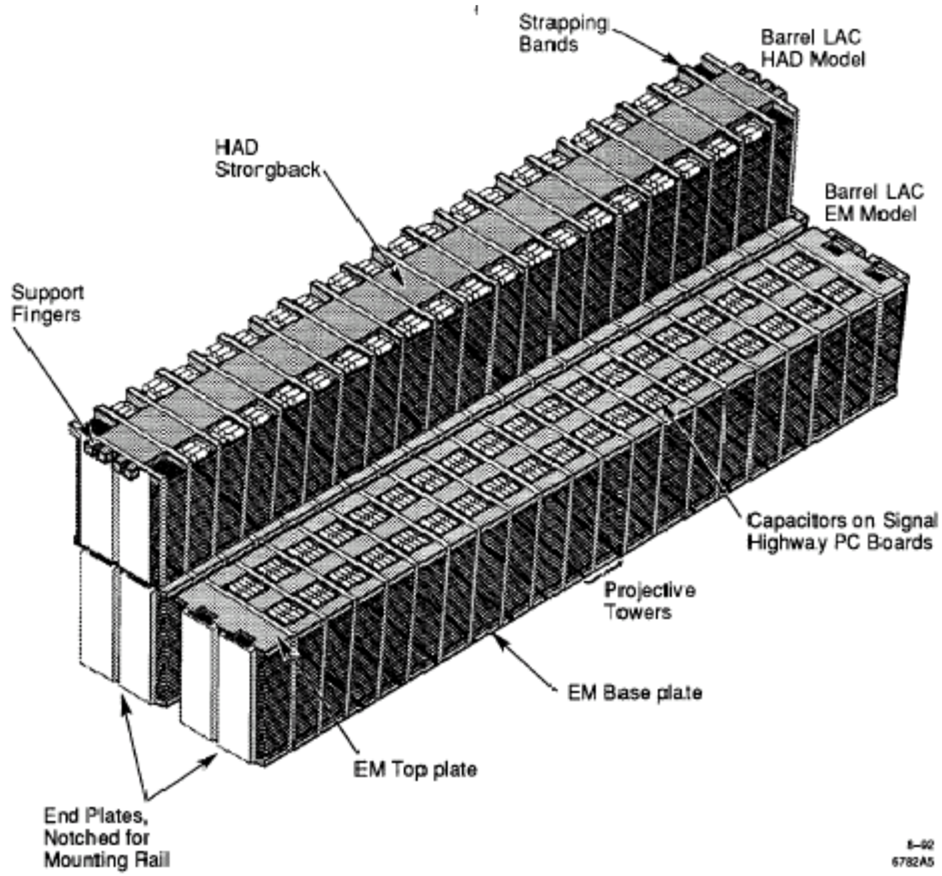

Electromagnetic-shower Detectors

Silicon- tungsten

- SLD Luminosity Monitor
  - 3.5 mm tungsten
  - 3.5 mm gaps for insertion of silicon diode detectors
  - 23 layers = 21 X_0

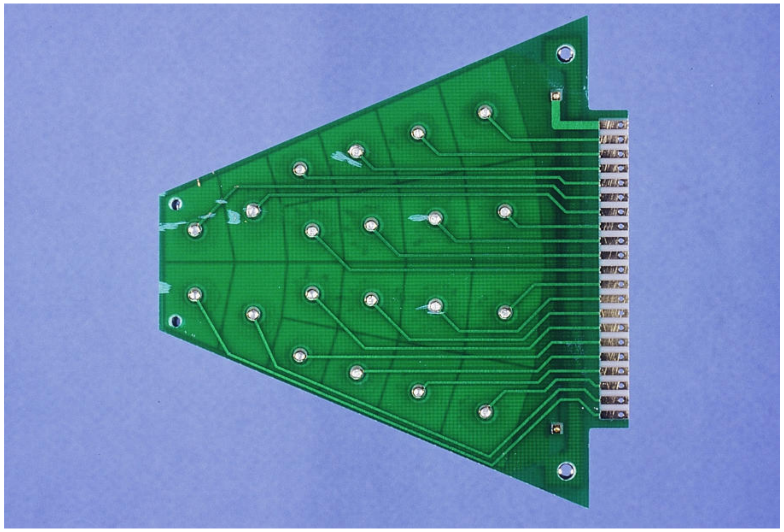

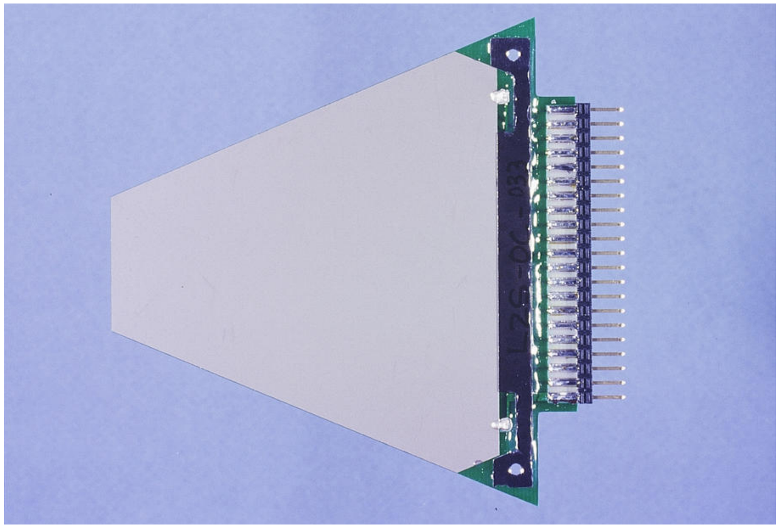

Electromagnetic-shower Detectors

Silicon- tungsten

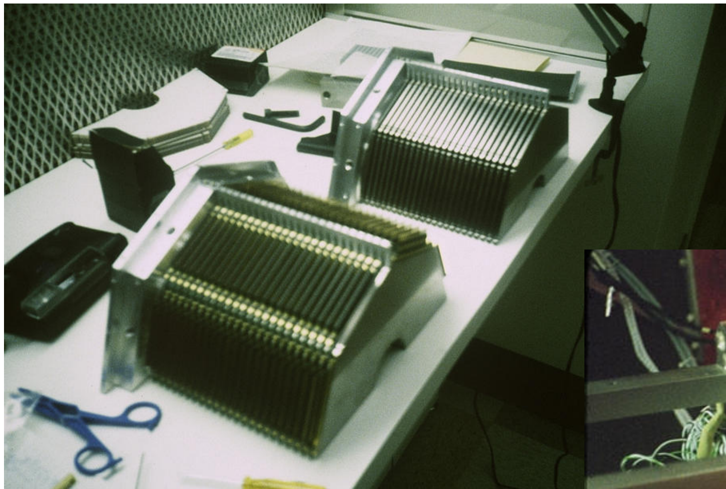

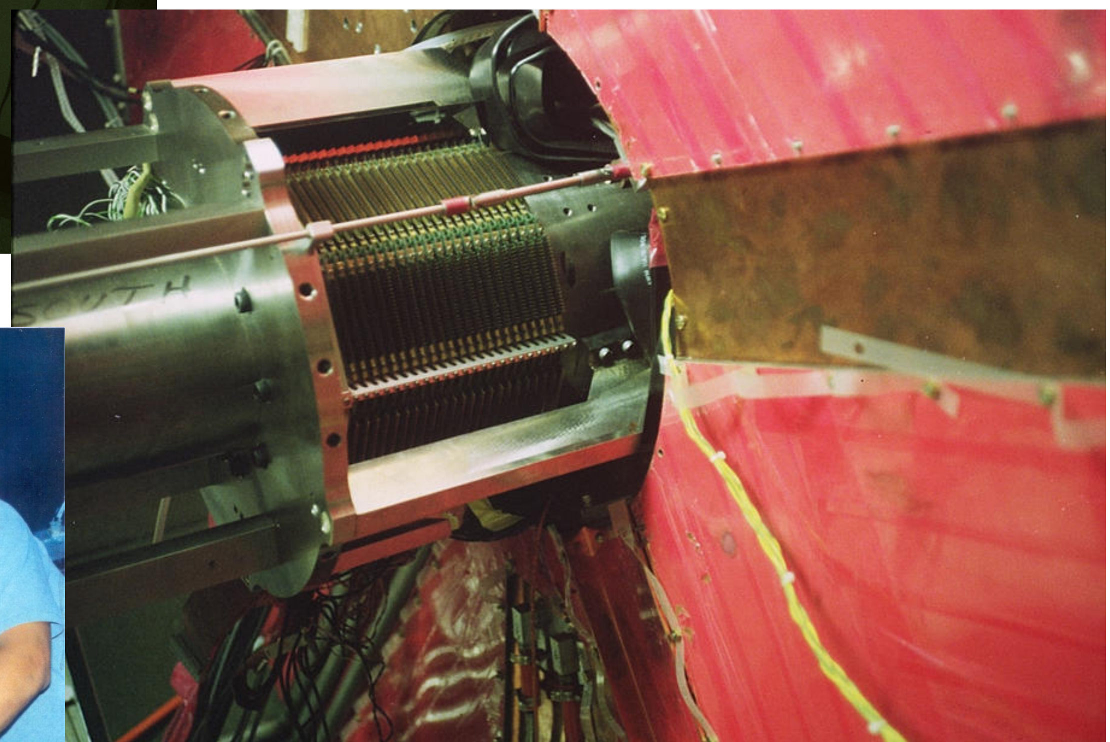

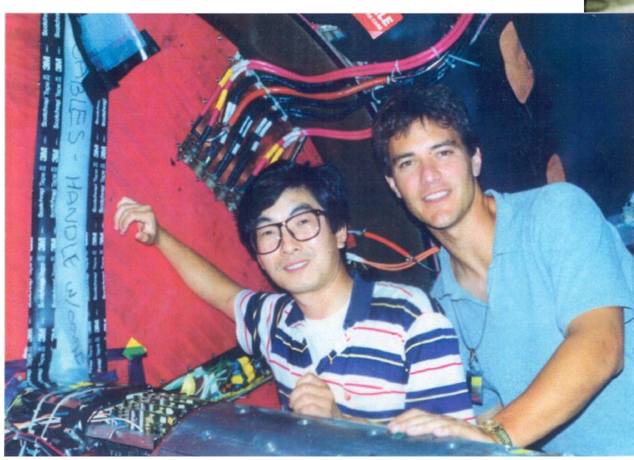

Hadron-shower Development

- Hadron showers are more complicated
  - nuclear interactions absorb energy from the shower
  - this loss of energy typically removes 30% of the incident particle energy, but fluctuations in the number and nature of the nuclear interactions give this loss large fluctuation
  - therefore, the energy resolution is much worse than for electromagnetic calorimeters
    - the best is about 35% / √E
    - many of the best calorimeters achieve only 50-70% / √E
    - note: an additional constant term can be large (see compensation)

- Scale length: $\lambda_I \approx 35 \text{ g cm}^{-2} A^{1/3}$

- Shower maximum:

$$x/\lambda_I \equiv t_{\text{max}} \approx 0.2 \ln(E/1 \text{ GeV}) + 0.7$$

Hadron-shower Development

- *Average shower profiles*
- Fluctuations about the average are very large

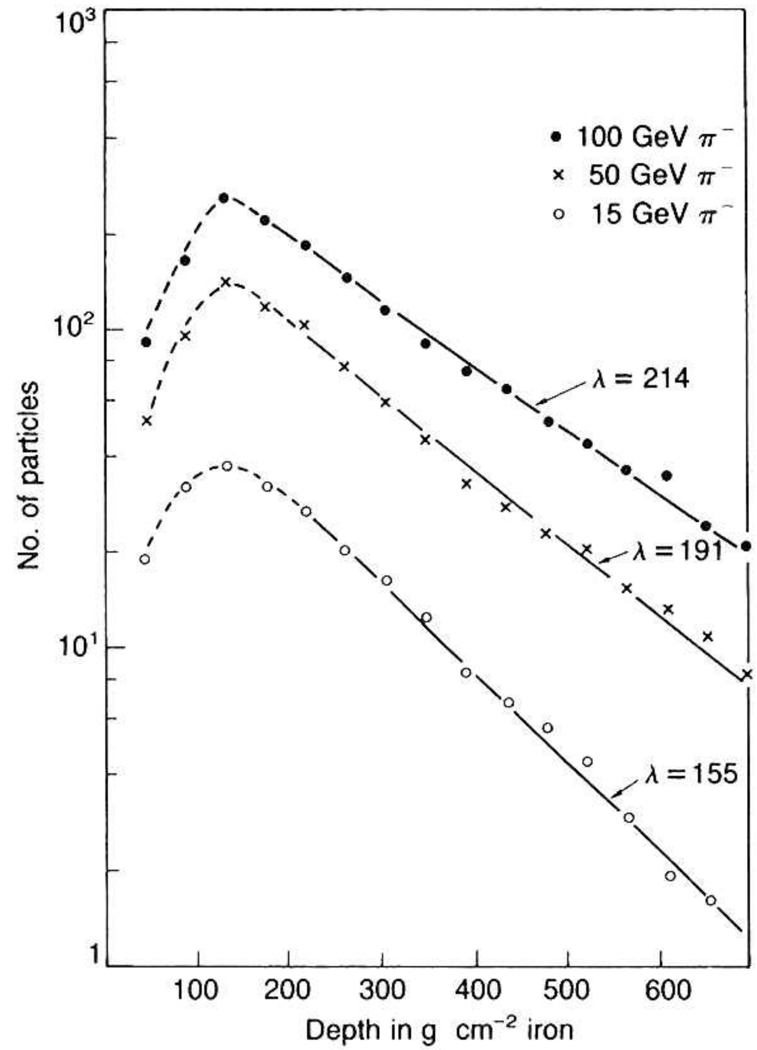

Hadron-shower Development

- Shower containment

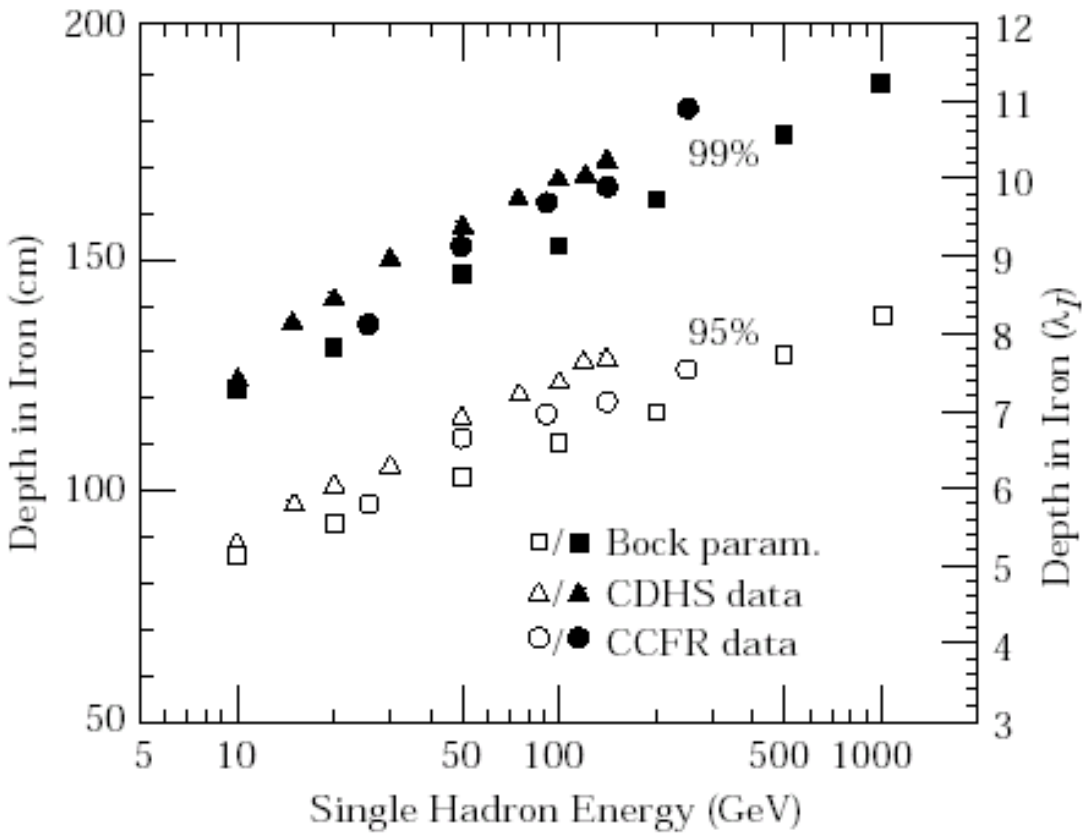

Hadron-shower Development

- The reponse of a calorimeter to the electromagnetic component (primarily from π^0 s) is much different than the response to the charge hadrons. Fluctuations from shower to shower in the fraction of energy deposited electromagnectically translates into energy resolution fluctuations, unless the calorimeter is "compensating"
- Compensating refers to the restoring of a balance in the calorimeter response to EM and charged energy deposition
  - this can be achieved by boosting the signal when energy is lost through nuclear breakup - the original technique of Uranium calorimetry (Willis et al)
  - or by suppressing the response when energy is deposited by electromagnetic sub-showers

Hadron-shower Development

- The hadronic component showers have been shown to be well described by $(E/E_0)^{m-1}$
  - $0.80 < m < 0.85$
  - $E_0 \sim 1$ GeV for pions
  - $E >$ few tens of GeV

- Then the ratio of the response of the calorimeter to the two components is

$$\text{“}\pi/e\text{”} = 1 - (1 - h/e)(E/E_0)^{m-1}$$

- where e/h is the intrinsic response

- Calorimeters with e/h close to one are then “compensating” and tend to have the best energy performance

Hadron-shower Detectors

- It was discovered in the 1980's that the proper combination of scintillator and uranium achieved the best compensating calorimeter.
  - J.E. Brau and T. A. Gabriel, "Monte Carlo Studies of Uranium Calorimetry," Nucl. Inst. and Methods, A238, 489 (1985).

- This was implemented by ZEUS at HERA
  - 3.3 mm U, 2.6 mm scintillator

$35\% / \sqrt{E} + 1\%$ for hadrons

$17\% / \sqrt{E} + 1\%$ for electrons

Hadron-shower Detectors

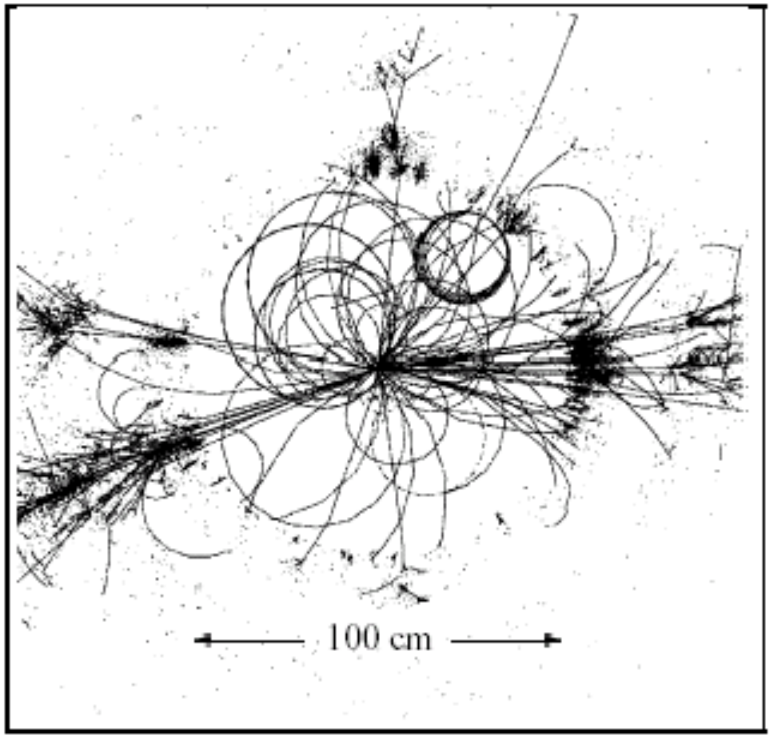

Figure 4: GEANT simulation of $e^+e^- \rightarrow Z^0h(120\ GeV)$ event. The inner region of this figure corresponds to the tracker and the inner surface of the electromagnetic calorimeter is evident from the onset of photon conversions[9].

Hadron-shower Detectors

Particle flow calorimeters

- Since the tracker of a detector is more precise than the calorimeter in detecting charged particles, a measurement of jet energies based on the "particle flow" can give better jet energy measurements than a calorimeter alone measurement.

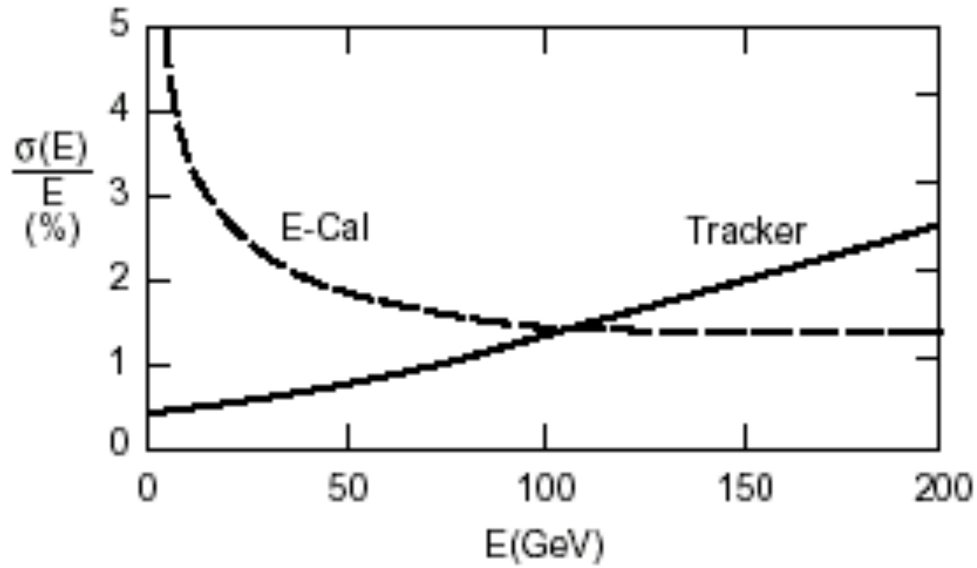

Hadron-shower Detectors

Particle flow calorimeters

- To do this well requires a separation of the signals in the calorimeter from charged and neutral particles

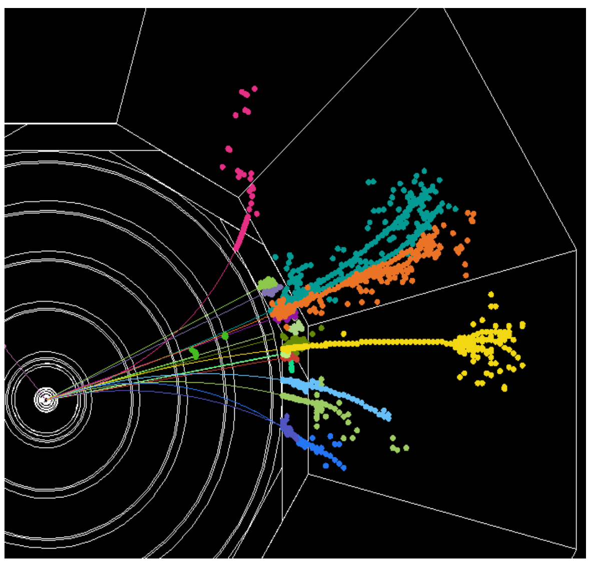

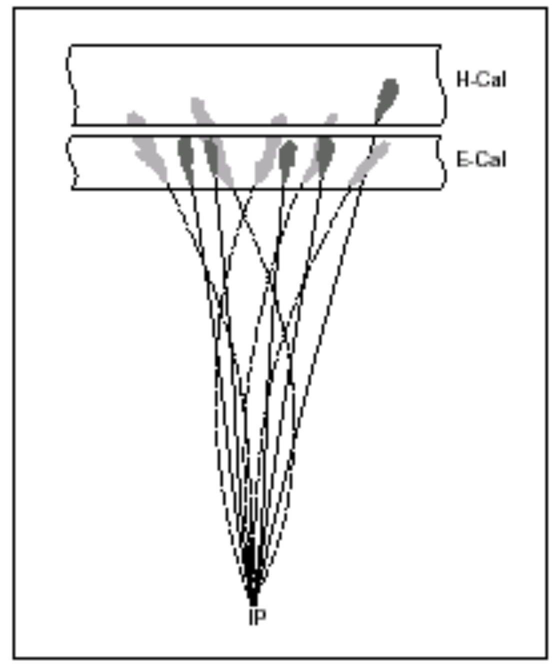

Fig. 3 Separation of charged and neutral particles in calorimeters

Particle Flow Calorimetry for ILC

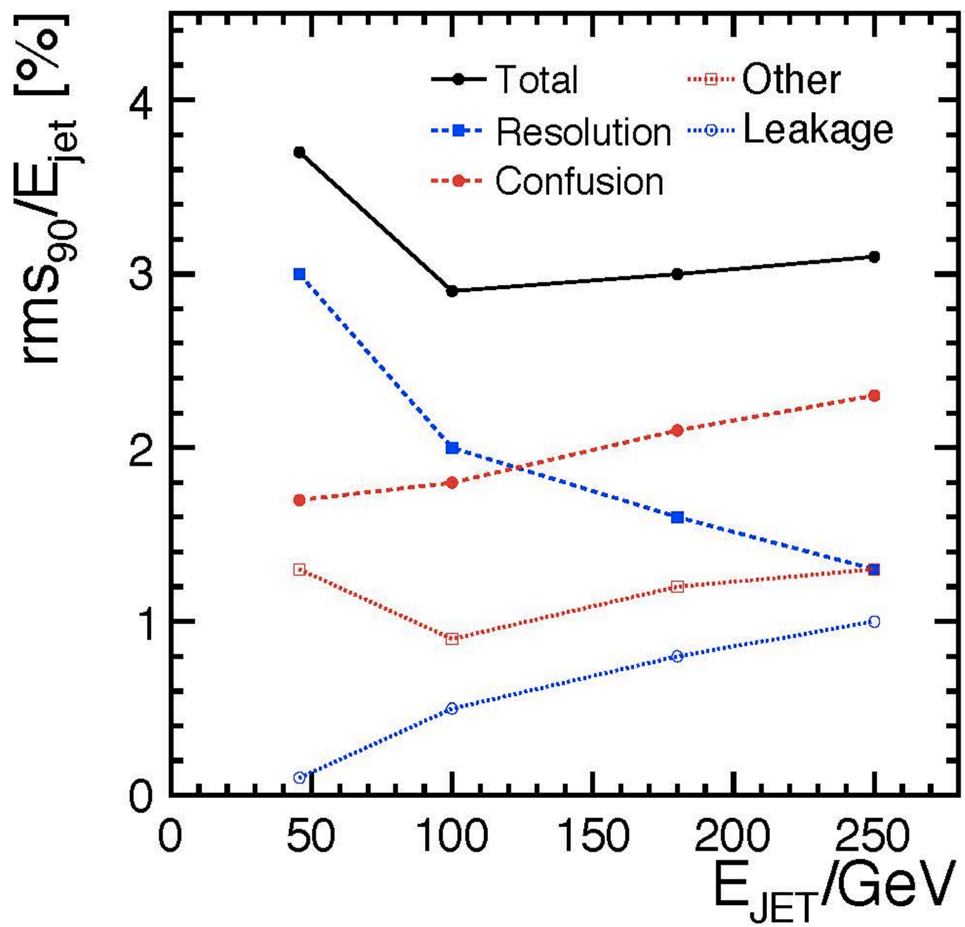

Hadron-shower Detectors

Particle flow calorimeters

- The linear collider projects are studying a silicon-tungsten calorimeter for this:
  - densest calorimeter
    - confines showers
  - most granular segmentation
    - allows readout of details
  - builds on experience with silicon calorimeters at SLD and LEP